Preparation and growth of solid supported phospholipid membrane: effect of cholesterol and nanoparticle

Thesis submitted to the Jadavpur University for the degree of Doctor of Philosophy (Science)

By

Amrita Basu

Supervisor: Prof. Sanat Karmakar

2022

DEPARTMENT OF PHYSICS
JADAVPUR UNIVERSITY

Dedicated To My Family

Prof. (Dr.) Sanat Karmakar
Professor
Department of Physics

যাদবপুর বিশ্ববিদ্যালয়
JADAVPUR UNIVERSITY

CERTIFICATE FROM THE SUPERVISOR

This is to certify that the thesis entitled "**Preparation and growth of solid supported phospholipid membrane: effect of cholesterol and nanoparticle**" submitted by Amrita Basu who got her name registered on 02.05.2014 for the award of Ph.D. (science) degree of Jadavpur University, is absolutely based upon his own work under the supervision of Prof. Sanat Karmakar and that neither this thesis nor any part of it has been submitted for either any degree/diploma or any other academic award anywhere before.

Sanat Karmakar

(Prof. Sanat Karmakar) 14/06/22

Prof. Sanat Karmakar
Department of Physics
Jadavpur University
Kolkata-700032, India

DECLARATION

I hereby declare that the work reported in this thesis is entirely original. I have developed this thesis independently at Jadavpur University under the supervision of Prof. Sanat Karmakar and all the literature has been properly cited. The work presented in this thesis has not been used previously for the award of any degree, diploma, membership, associate-ship, fellowship or any other similar title of any university or institution.

Prof. Sanat Karmakar 14/6/2022

Soft Matter and Biophysics Laboratory

Department of Physics

Jadavpur University

Kolkata700032

(Amrita Basu)

ACKNOWLEDGEMENT

CONTENTS

Chapter 5: Effect of anionic silver nanoparticle (AgNP) on the formation of solid supported phospholipid bilayer

Chapter 6: Preparation of giant unilamellar vesicles from large unilamellar vesicles (LUV) and characterization by Zeta potential and Dynamic light scattering

List of publications

Reprints of Papers

PREFACE

Lipid bilayer is the basic building block of all biological membranes. Many cellular events and biochemical reactions occurring on the cell surface are complex and regulated by various proteins and other bio molecules. Interactions of these biomolecules are also difficult to study in vivo as their interactions are governed by various appropriate conditions and signaling on the cell surface. Therefore, it is often useful to study model membrane in order to unravel mechanisms of more complex cellular events as well as interactions with some biomolecules such as cholesterol, proteins etc. In the present thesis I have prepared solid supported lipid bilayer and giant unilamellar vesicles which are excellent model system for studying many cellular events. Phospholipid structures can even serve as templates for nanostructure fabrication by imparting controlled positioning and growth of nanoparticle embedded bilayers. It has been well established that phospholipid membranes are held in place above a solid support by a combination of Van der Waals, Electrostatic, hydration and steric forces. The main advantage in using solid support is to increase robustness and stability of the phospholipid membrane. Another important advantage of solid lipid bilayer is that the interactions occur on the membrane surface can be probed by powerful surface specific analytical technique like atomic force microscopy (AFM). The advantage of AFM is that it can directly image label-free surface topography of the sample. Further, Peak-Force Quantitative Nanomechanical microscopy (PF-QNM) is another specialized version of AFM which acquires the data for nanomechanical properties like elasticity, viscosity, deformation, and dissipation of the sample. I have used PF-QNM for the measurement of nanomechanical properties of solid lipid bilayer with varying amount of cholesterol and nanoparticle in it.

Objectives:

1) To study the formation of solid supported lipid bilayer and multilayer with simple methodology of self organisation and physisorption of lipid molecules.

2) To study the nanomechanical properties of solid supported lipid bilayer with varying amount of cholesterol.

3) To study the interaction of solid supported lipid bilayer with anionic silver nanoparticle.

4) To prepare giant unilamellar vesicles from large unilamellar vesicles, measurement of zeta potential of lipid membranes prepared from different lipids, and to study the incorporation of antimicrobial peptide on it.

Methodology:

I have prepared solid supported lipid bilayer on mica surface by simple vesicle fusion method. In this method small or large unilamellar vesicles are added to the substrate, where they spontaneously adsorb, rupture and fuse to form supported bilayer. The unilamellar vesicles are prepared from multilamellar vesicles by extrusion technique. These supported bilayers can withstand the lateral forces imparted by the tip of AFM. Therefore, I can easily monitor the characteristics followed by the interaction of solid supported bilayers.

One disadvantage of solid supported bilayer is that the effect of substrate cannot be ignored completely. To overcome the limitation, GUV s are prepared from a simpler technique using LUV by electroformation technique. Owing to their large diameter (10-100 µm) they have been studied under phase contrast microscope.

Summary of the thesis:

In chapter1, I describe a general introduction on the topic in connection with the thesis. Sample preparation and all experimental techniques, used in this thesis work, are described in chapter 2. I primarily employed atomic force microscope to study solid supported lipid bilayer. Therefore, more detailed description of AFM is illustrated.

Chapter 3 reveals the growth of single as well as multiple bilayers of DOPC vesicle on highly hydrophilic mica surface by simple vesicle fusion method without any complex preparation of the substrate or incorporation of external reagent. The direct observation of co-existence of single, double and triple lipid bilayer by quantitative AFM measurement shows excellent prospect not only for easy preparation of single and multiple lipid bilayer but also for the study of the interaction of proteins or drugs with single and multiple DOPC bilayers in a single system.

In Chapter 4, we investigate the influence of different cholesterol levels (1–40 mol %) on the morphology   and   nanomechanical   stability   of   dioleoylphosphatidylcholine/cholesterol

(DOPC//Chol) membrane by means of atomic force microscopy (PF-AFM QNM) imaging. Cholesterol-containing bilayers with greater rigidity are found in comparison to the surrounding region. The tubular protrusion, a generic phenomenon of the natural cell membrane, is also noticed successfully at low cholesterol concentrations.

In Chapter 5, we explore that AgNP has the ability to induce defects in DOPC lipid bilayer. it is found that the AgNP cannot produce many defects on the cholesterol mediated DOPC lipid bilayer in comparison to pure DOPC lipid bilayer. The nanoparticle trapped bilayer regions show height elevation and increased rigidity. The silver nanoparticle is observed to induce cell membrane permeability which is reflected in the change of elastic modulus, adhesion and energy dissipation at the adhering site of nanoparticle with the lipid bilayer.

 In chapter 6, a simple method is described regarding the formation of GUV from LUV. The Zeta potential of phospholipid membranes, made of different lipids, is measured. Incorporation of antimicrobial peptide is also studied in this chapter.

Conclusion

The study of solid supported lipid bilayer and GUV is of great importance due to their biological significance. I have prepared and studied the growth of solid supported bilayer and multilayer system of phospholipids. The effect of cholesterol on the formation, growth and nano-mechanical properties are systematically investigated using AFM along with Peak-Force Quantitative Nanomechanical microscopy. The present study reveals that the cholesterol induces the formation of cholesterol rich domains in purely unsaturated lipid bilayer which resembles with the formation of liquid ordered (lo) phase in ternary system made up of saturated lipid, unsaturated lipid and cholesterol. Lateral asymmetric distribution of lipids plays an important role in trans-membrane signal transduction. Observed asymmetric distribution of membrane lipids leaves a scope for further research in revealing signaling process through purely unsaturated lipid membrane. Further, investigation of interaction of solid supported lipid bilayer with silver nanoparticle has potent bio medicinal applications. It is well known that silver nanoparticle shows antimicrobial effect due to its cytotoxic nature. My investigation reveals that cholesterol mediated solid lipid bilayer bears less effect than pure lipid bilayer during interaction of anionic citrate coated silver nanoparticle. It may be a reason that mammalian cell is more resistant to pore formation by silver

nanoparticle in comparison to other microbial cells. It is also revealed during investigation that larger zeta potential obtained from PC-PE mixture as compared to pure DOPC. It could be a consequence of increasing the rigidity in the presence of DOPE. A preliminary study shows that the implantation of antimicrobial peptide NK-2 exhibits pores in GUV which is, indeed, an important finding as pore formation is precursor to disruption of cell membrane.

Chapter 1

Introduction

Nature with all its diversities enables itself to survive because of its unique trick to fabricate cell membrane. The cell membrane is a selectively semi-permeable barrier which compartmentalizes the inner part of the cell from the outer world. It has distinctive quality to exchange selective materials between inner and outer world for the cell to stay alive.

There are wide varieties of lipids present in the bilayer membrane, among them, phospholipids, non-phospholipids and sterols are important constituents of mammalian cell membrane. There are four major phospholipids found in mammalian cell membrane, namely phosphatidylcholine (PC), phosphatidylethanolamine (PE), phosphatidylserine (PS) and sphingomyelin (SM). The outer leaflet mainly consists of Phosphatidylcholine (PCs) sphingomyelin (SM) whereas phosphatidylserine (PS) and phosphatidylethanolamines (PE) are the main constituents of the inner leaflet. In most of the bio membranes, only 10% lipids are charged and the remaining lipid fraction is either zwitterionic or neutral. Among them, PC-s, PE-s, SM-s are zwitterionic, PS-s are anionic in nature. There is no positively charged membrane lipid found in nature. The specificity of membrane lipid organization monitors many cellular functions such as cell trafficking, cell signaling, cell growth even the entry of various foreign particles i.e., viruses, bacteria or nanoparticles. Cholesterol is another molecule, abundantly found in mammalian cell membrane, is non-phospholipid by composition [1]. Its presence in the membrane changes the physical behaviour such as fluidity, permeability and phase. Further, the concept of the lateral organization of the lipid membrane is changed with the introduction of lipid raft theory [2, 3]. Lipid rafts, are heterogeneous structure in the cell membrane which ensembles high amount of cholesterol and saturated lipids and are responsible for signal transduction, protein clustering like various multicomponent activities of the cell.
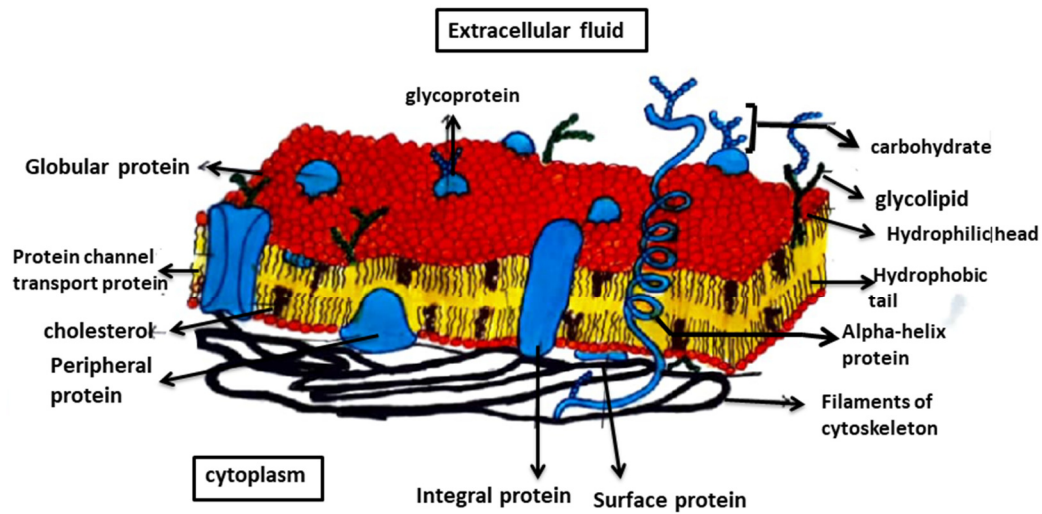
Figure 1.1: Schematic (hand sketch) presentation of cell membrane

The structure and dynamics of the lipid membrane (Fig.1.1) is highly complex and is dependent on various factors such as temperature, osmotic stress, pH, specific proteins, polymers, nanoparticle and other biomolecules. It is very challenging to extract meaningful data related with the cellular activities by isolating them in proper physiological condition. So, the researchers always try to find a simple model membrane system which is easy to breed and manipulate to track the various processes actually occur in real cell membrane. Model lipid membranes are prepared by the self-assembly of various type of lipids.

1.1. Lipid molecules: structure and function

Lipids are amphiphilic molecules which possess both hydrophilic and hydrophobic moieties. Amphiphilic molecules consist of two different covalently bonded segments. One component shows high affinity to polar solvent (hydrophilic) and another component shows affinity to nonpolar solvents like ethers, hydrocarbons and esters (hydrophobic). The head groups are usually charged or zwitterionic and contains negatively charged carboxylates: $-CO_2^-$, sulfonates $-SO_3^-$, phosphate $-PO_4^-$ along with positively charged amines $-NH_3^+$ or large number of polar uncharged hydroxyl group etc. The head group is linked with one or more hydrophobic hydrocarbon chains. A schematic of simplified lipid structure is shown in figure 1.2.
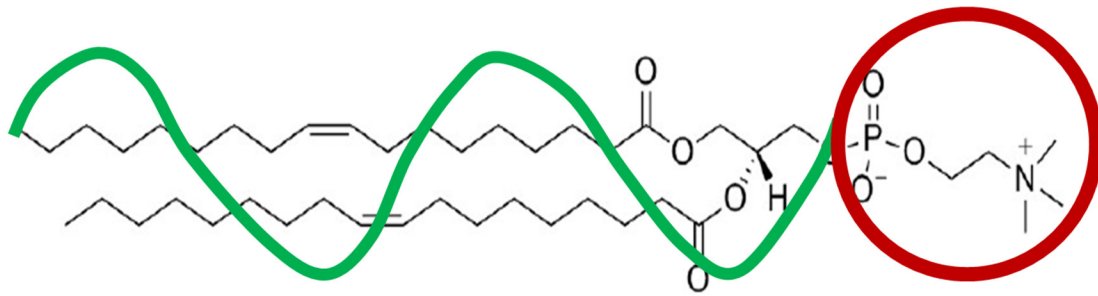
Figure 1.2: Schematic diagram of a lipid showing the hydrophilic head and the hydrophobic tail superimposed onto a lipid chemical structure

The lipid hydrocarbon chains can be fully saturated, monounsaturated with double bonds at different positions (cis and trans configuration) along the hydrocarbon chain or poly-unsaturated. The lipid molecule may be asymmetric in terms of chain length of two hydrocarbon chains also. The structures of lipids in terms of saturation are shown figure 1.3.

(a)

(b)

(c)
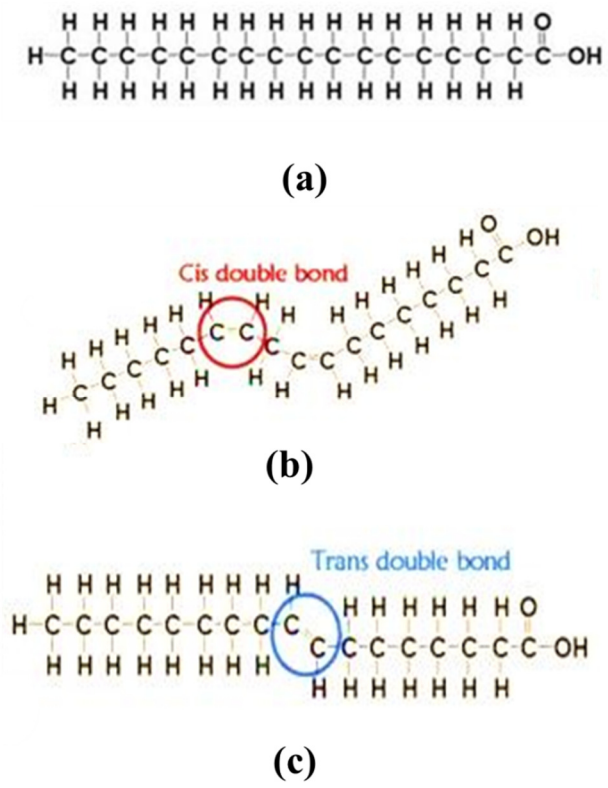
Figure 1.3: Structure of different types of lipids (a) saturated (b) unsaturated with *cis* configuration (c) unsaturated with t*rans* configuration

In the *cis* configuration, two hydrogen atoms are connected with the bond reside on the same side. It produces a kink or bend in the fatty acid chain as shown in Fig.1.3(b). In the *trans* configuration, hydrogen atoms are at the opposite sides of the double bond (Fig1.3(c)). The lipid chains with *cis* double bond (DOPC) have relatively low melting point than the saturated lipid. The lipid with *trans* double bond is rare in nature which is produced artificially by partial hydrogenation. *Trans* unsaturated fatty acids are packed tightly and tend to be solid at room temperature. Among all lipids, the main lipid used in this thesis is PCs which are abundant in the mammalian cell membrane.

1.1.1. Self- assembly of lipids

Owing to its amphiphilic character, the lipid molecules self- assemble in aqueous solution with the help of various forces such as hydrogen bonding, steric effects, hydrophobic and other electrostatic interactions. Generally, the head group forms a hydrogen bond with the water with an enthalpy gain, while the insertion of apolar tails lead to the hydrophobic effect with a gain in entropy of the bulk water. If a hydrophobic hydrocarbon chain is introduced in aqueous solution, it cannot form hydrogen bond. This is an entropically unfavourable phenomenon in which water molecule plays a decisive role. It forms a cage like structure around the non-polar tail part of the lipid molecule, which is more constrained. To avoid this strained condition, owing to hydrophobic forces, hydrophobic tails of amphiphilic molecules aggregate together, thus reduce entropy cost of the system [4]. Hydrophobic force not only plays a decisive role in self- assembly of amphiphiles but also shows a crucial role in protein folding or drug delivery in biomembrane. Although the individual forces involved in the aggregation of amphiphiles are mostly weak, the overall effect is strong enough to hold different amphiphiles together and provide the stability of the aggregation in the aqueous solution. The main requirement for a favourable aggregation of amphiphiles is the minimum energy condition at equilibrium. From thermodynamic point of view, self -assembly is driven by the competition between interfacial energy of the amphiphile head with solvent and the conformational distortion energy of hydrocarbon tails attached with the head. In this respect, critical micellar concentration is important for (CMC) self-assembling process. The thermodynamic equilibrium satisfies the criteria that the chemical potential (μ) of all identical amphiphiles is same in all aggregates, i.e., $\mu_1 = \mu_2 = \mu_3 = ... = \mu_N$. It can be written as,

$$\mu = \mu_1^0 + K_BT \log X_1 = \mu_2^0 + \frac{KT}{2}\log\frac{X_2}{2} = \mu_3^0 + \frac{KT}{3}\log\frac{X_3}{3} = \cdots \qquad (1)$$

or
$$\mu_N = \mu_N^0 + \frac{KT}{N}\log\left(\frac{X_N}{N}\right) = \text{Constant} \qquad (2)$$

Where, N = 1, 2, 3..... represent monomers, dimers etc., μ_N is the mean chemical potential of a molecule in an aggregate of aggregation number N, μ_N^0 is the standard chemical potential corresponds to the interaction free energy per molecule in N, K is the Boltzmann's constant which relates the average kinetic energy for each degree of freedom of the amphiphile in equilibrium to its temperature T. X_N is the total concentration of molecules in aggregate N. The second term in the equation (2) arises from entropy of mixing [5] . If the total concentration (X) of the system is considered to be small, then,

$$X = \sum_{N=1}^{\alpha} X_N \ll 1 \qquad (3)$$

For $\mu_N = \mu_1$, we get

$$X_N = N\left[X_1 exp\{(\mu_1^0 - \mu_N^0)/KT\}\right]^N = N(X_1 e^\alpha)^N \qquad (4)$$

Where, $\alpha = \frac{\mu_1^0 - \mu_N^0}{KT}$. The necessary condition for the formation of aggregates of size N is $\mu_N^0 < \mu_1^0$. When $X_1 \ll 1, X_1 e^\alpha < 1$, then we must have $X_N \ll X_1$ for sufficiently low monomer concentrations. Most of the molecules will be in favourable monomer state. As X_1 is increased, $X_1 e^\alpha$ approaches unity. Since $X_N < 1$, X_1 should not exceed a value of $e^{-\alpha}$. Therefore, the aggregation starts after monomer concentration crosses the value of the order of $e^{-\alpha}$. This concentration is called the critical micellar concentration (CMC). It is given by

$$CMC = (X)_C \approx (X_1)_C \approx e^{-(\mu_1^0 - \mu_N^0)/KT} \qquad (5)$$

At very low concentration, amphiphilic lipid molecules form a monolayer at air water interface. Above the critical micellar concentration (CMC), they aggregate into a variety of structures. The typical value of CMC of a lipid, such as DOPC, is ~ 50 µM at room temperature. Usually, the CMC decreases with increasing the hydrocarbon chain length due to greater hydrophobicity [6].
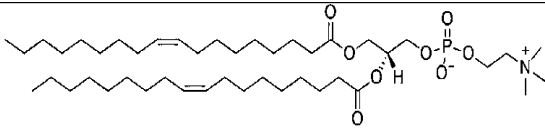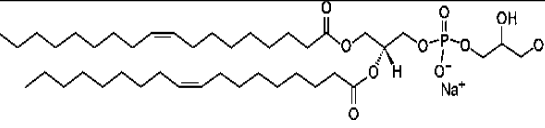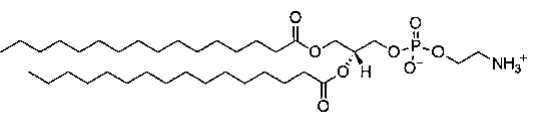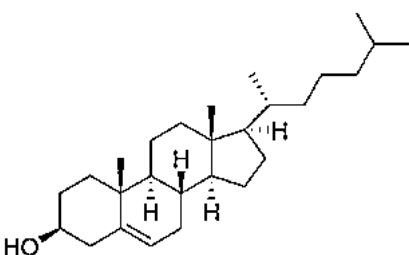
The shape and size of the aggregates depend on the geometry of the amphiphile and the solution conditions such as concentration of amphiphiles, temperature, pH and ionic strength. The

packing parameter (p) is also an important parameter that determines the different shape of the self-assemble lipid depending on the geometry of amphiphile. The dimensionless parameter (p) is defined as the ratio of the hydrocarbon volume (v) to the product of the area of the polar head group (a_0) and the critical acyl chain length (l_c).

$$p = \frac{v}{a_0 l_c}$$

Thus, larger head group lipids, such as, DOPC, DOPG generally form vesicles at a sufficient concentration above CMC in aqueous solution.

Table 1: List of lipids used in the present work

Lipids	Structure	Charge
1, 2-dioleoyl-sn-glycero-3-phosphocholine **(DOPC)**		Zwitterionic
1,2-dioleoyl-sn-glycero-3-phospho-(1'-rac-glycerol) (sodium salt)**(DOPG)**		Negative
1,2-dioleoyl-sn-glycero-3-phosphoethanolamine **(DOPE)**		Zwitterionic
Cholesterol		Negative

1.1.2. Model Lipid Membranes:

Lipid vesicles [7], solid supported lipid bilayers (SLB) [8] and Langmuir-Blodgett lipid film (LB film) [9] are good model systems of all biological membranes. Lipid vesicles are spherical lipid bilayers with an aqueous chamber inside it. As model systems, unilamellar vesicles are widely used for studying structure and function of membrane at physiological condition. Vesicles are widely utilized as carriers of bioactive agents, including drugs, vaccines and cosmetics also [10]. Apart from the model systems of biological membrane, these vesicles can be used as micro reactors for enzymatic RNA synthesis [11] and also to form nanoparticle of control size distributions [12]. They are found in different sizes, i) small unilamellar vesicles (SUV of 10-100 nm), ii) large unilamellar vesicles (LUV;100-500 nm), and iii) giant unilamellar vesicles (GUV;10-100 um). (fig 1.4)
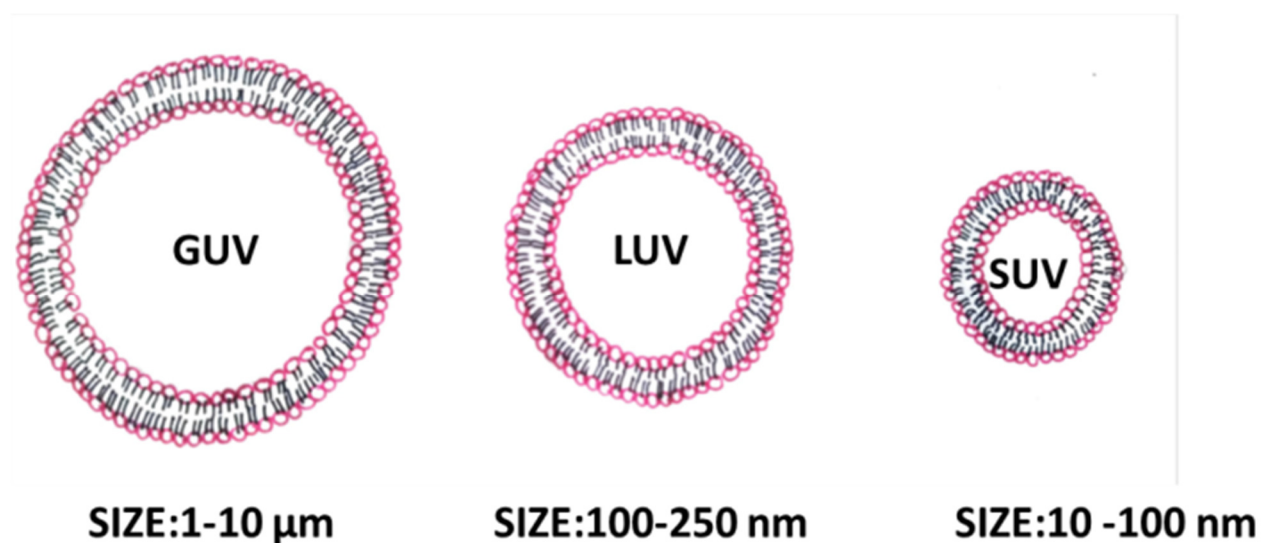
Figure 1.4: Schematic diagram of unilamellar vesicles according to their average size

Among them, GUVs are closest to actual cell size. The GUVs are useful in investigating the phase behaviour as well as to track many cellular processes like cell to cell recognition, cellular fusion, cell trafficking etc. [13] [14] [15]. GUVs are also easy to detect in optical microscopic techniques such as confocal or fluorescence microscopy [16]. However, the disadvantage of using vesicles is their metastable structure and poor longevity. In addition, it is not a suitable system to study the molecular label interaction using high resolution techniques.

1.1.3. Solid Lipid Bilayer (SLB) and its importance:

Mc Connell and co-workers did a ground breaking job in the year 1981.They discovered a process where a vesicular membrane could assemble on a planar surface. SLB is more stable model membrane system than vesicles [17].

Generally, two methods are used for the preparation of solid supported lipid bilayers, 1) Langmuir trough deposition 2) vesicle fusion method. These methods are used separately or in conjunction to produce symmetric or asymmetric lipid bilayer in controlled condition. Recently another method is used by spin coating the solvent on the substrate.

The Langmuir trough deposition (Langmuir - Blodgett/Langmuir- Schaefer methods):

Langmuir reported the formation of organized monolayers of amphiphilic molecules at the air-water interface which is referred as Langmuir film [18]. This film can be transferred to a substrate. Katharine Blodgett observed a systematic study on transferring this monolayer on the substrate in controlled condition. She adopted a method of transferring by lowering the substrate vertically into the trough, this method is mentioned as Langmuir – Blodgett film. Later, Langmuir and Schaefer invented a new process of transfer by lowering the substrate horizontally on the Langmuir-Blodgett trough. This process is named as Langmuir- Schaefer method. Multiple layers can be formed on the substrate by pushing the substrate back down through air-water interface required number of times.
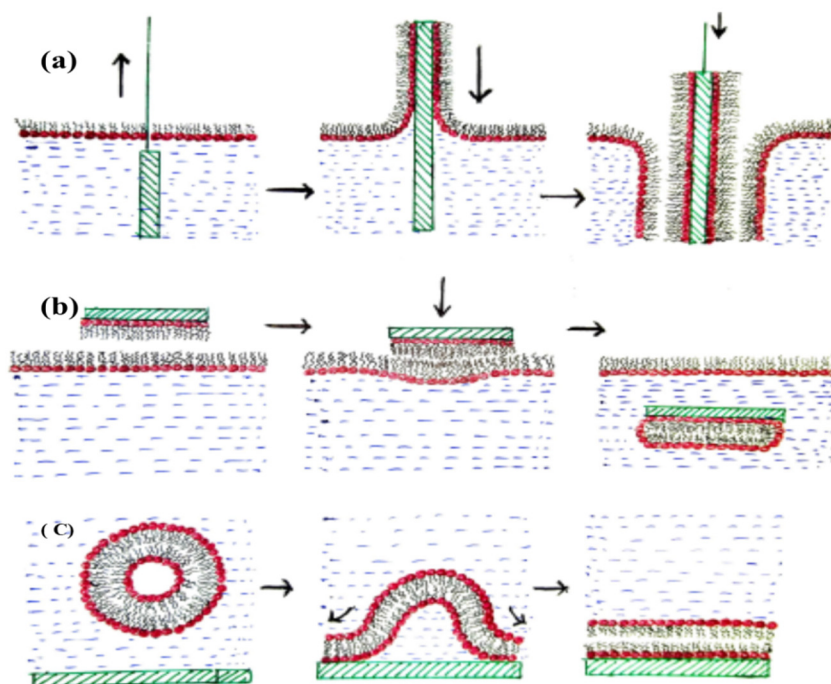
Figure 2.6. Schematic diagram of the formation of solid lipid bilayer (a) Langmuir-Blodgett method (b) Langmuir-Schaefer method (c) vesicle fusion method

Good quality of LB film depends on many factors such as the quality of substrate surface, the transfer speed, waiting time of the substrate in air between the deposition cycles in case of more than one layer deposition. This Langmuir Blodgett lipid film deposition on solid substrate gives very accurate thickness of lipid bilayer although huge amount of lipid is necessary for the proper deposition of lipid bilayer on the substrate.

Vesicle fusion method:

Vesicle fusion method for the preparation of solid lipid bilayer is much easier and more cost effective. Small or large unilamellar vesicles prepared from different lipids are needed to deposit on a hydrophilic clean substrate to create solid lipid bilayer patches. For this reason, we have used vesicle fusion method to prepare solid lipid bilayer. Vesicle fusion method produces discrete bilayer patches which are advantageous for us to utilize the edges of adjacent isolated bilayer fragments. The detail process of preparation is mentioned in chapter 2.

This solid supported bilayer system (SLB) is used to study the surface chemistry, morphology and various structural changes with the incorporation of different relevant biomolecules by X ray scattering [19], Scanning Electron Microscopy [8], Transmission Electron Microscopy [20], Neutron Reflection method [21] Atomic Force Microscopy [22] with high resolution. Two conventional and mostly used methods are i) Quartz Cristal Microbalance with Dissipation [23] and ii) Atomic Force Microscopy. The advantage of using AFM is that it can image label-free surface topography of the sample directly. Peak-Force Quantitative Nanomechanical microscopy (PF-QNM) is another specialized version of AFM which uses the tapping operating mode with a minimum tip force to acquire the data for nanomechanical properties like elasticity, viscosity, deformation, dissipation of the sample [24]. For accurate measurement, sample preparation is an important criterion. The process of preparing vesicles and solid supported bilayers has become well-structured after the discovery of various experimental as well as simulation studies. One disadvantage of single SLB is that many transmembrane proteins which have extra cellular domains and have a larger dimension cannot be accommodated in a single bilayer of thickness ~5 nm. Fundamental requirement of a transmembrane protein is to be surrounded by water on both sides of the membrane in order to function properly. So, there is a need for multilayer formation on solid surfaces or adding spacer groups between solid support and supported bilayer. Spin-coating is a useful method for producing stack of homogeneous lipid bilayers on solid surface. With the advancement in the fields of lipid multilayer fabrication, a tethered biomembrane were produced by Lech's lab in 1998, a stable stratified polymer-lipid composite films were introduced by Tanaka and Sackmann in the year 2000. Soft polymers are useful to ease the stress-free mobilization of molecules through bilayer surfaces. Self-organization and physisorption of amphiphilic molecules also lead to lipid multilayer formation [25]. In addition to this, nanoparticle supported lipid bilayer are very potent agents for biomedical imaging, drug delivery, targeting therapy and bio-sensing. They are created by adsorbing lipid vesicles in silica or gold or other nanoparticles embedded surface for tracking.

1.1.4. Role of substrate in SLB:

Under appropriate experimental conditions, a variety of substrates, such as fused silica, borosilicate glass, mica and oxidized silicon are used for the formation of stable supporting phospholipid bilayers. However, for a defect free high quality membrane, the surface needs to be

smooth, clean and hydrophilic [26]. We have chosen mica as a substrate for its various advantages. It does not need any complicated method of preparation before using it as a substrate. Freshly cleaved mica surface is extremely hydrophilic and clean.

1.2. Phase behaviour of lipid water system:

The response of individual lipid molecules in the lipid bilayer in terms of relative mobility is known as the phase [27]. In a single component system, lipids exist in solid or liquid phase at a given temperature. The solid phase is also called the gel phase. All lipids have a characteristic temperature above which they transit from solid (gel) to liquid phase. This temperature is called transition temperature (T_m). T_m depends on hydrocarbon chain length, number of unsaturated bonds in hydrocarbon chain and also on the nature of head group. Above this temperature, the hydrocarbon chains of lipid changes into fluid phase, it is known as l_α phase. Below T_m, fluid phase transforms into a gel phase where hydrocarbon chains show higher molecular ordering and low lateral mobility. There are two types of gel phases found in lipids, known as L_β phase and $L_{\beta'}$ phase. In the L_β phase, the hydrocarbon chains are aligned parallel to the bilayer normal. Some lipids with larger head group exhibit the $L_{\beta'}$ phase where chains are tilted with respect to bilayer normal. Fully saturated DPPC forms L_β phase whereas DOPC with double unsaturated hydrocarbon chains shows L_d phase at room temperature. However, in a multicomponent system, two or more phases may co-exist in the bilayer at the same temperature. This phase separation plays a vital role in various biochemical phenomena like intracellular compartmentalization of different proteins, stress adaptations, genomic regulation etc. line tension also acts at the interface of different lipids due to their different hydrocarbon chain lengths. This causes unfavourable interaction between tails and leads to phase separation to reduce the high energy interface between them. The presence of cholesterol in the lipid bilayer influences the phase behaviour of the system. Liquid ordered (l_0) phase is exhibited by the bilayer which coexists with the gel phase (($L_{\beta'}/L_\beta$) at a particular concentration of cholesterol below T_m [28]. Above T_m, Liquid ordered (l_0) phase changes into liquid disordered phase (l_d) which begins to coexist with the gel phase [29]. The gel phase completely disappears and Liquid ordered (l_0) is predominant with the increasing amount of cholesterol [30]. Ripple $P_{\beta'}$ phase is formed in between L_α and $L_{\beta'}$ with the presence of higher

amount of water in the bilayer [31]. A schematic diagram is presented in the figure showing all phases of lipid bilayer.
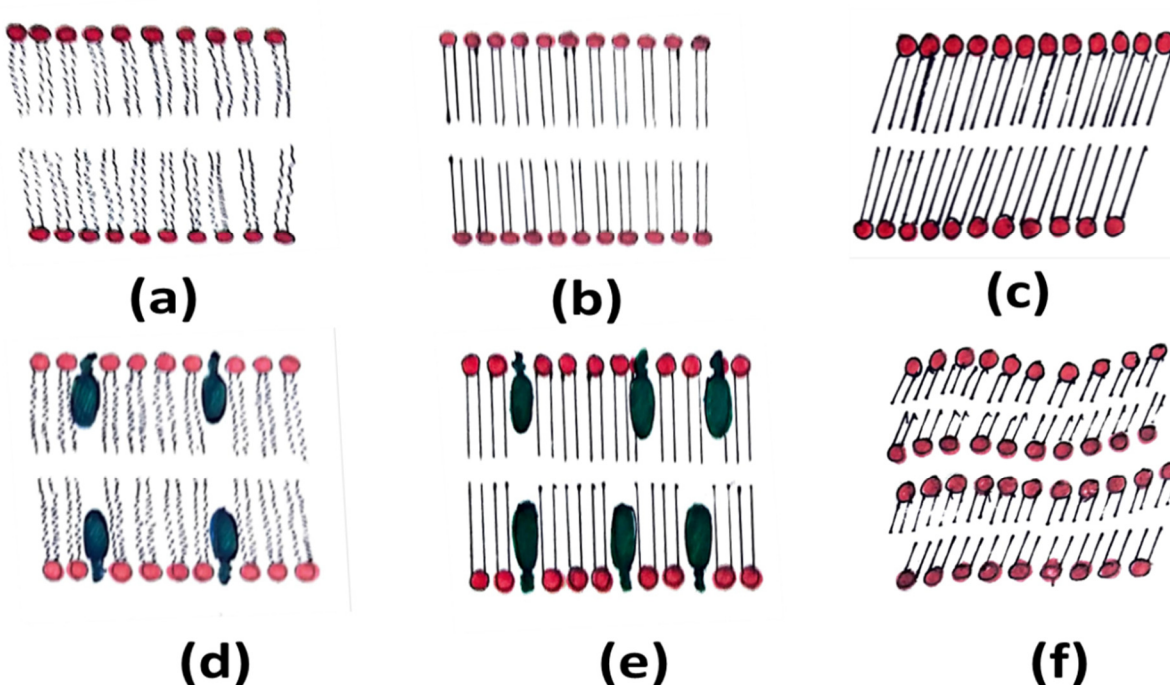
Figure 1.6: Schematic representation of different bilayer phases. (a) L_α phase, (b) L_β phase, (c) $L_{\beta'}$ phase, (d) l_d phase, (e) l_o phase, (f) $P_{\beta'}$ phase.

1.2.1 Effect of cholesterol on the phase behavior and mechanical properties of the membranes:

The cholesterol is an amphiphilic molecule with a different structure in comparison to phospholipids.it has a small hydrophilic –OH head group which helps the molecule to orient itself to lipid bilayer-water interface. But the rest of the part being apolar due to the presence of four fused hydrocarbon rings and hydrophobic 8 carbon aliphatic tail, it is deeply immersed in the lipid bilayer. The ring structure considerably reduces the disordering of the phopholipid tails and makes it ordered. This ordering is accompanied by the diminution of lateral phospholipid cross section area in presence of cholesterol. It is called the condensing effect of cholesterol. Many multicomponent phospholipid-cholesterol model membrane systems are studied in order to have a view on the influence of cholesterol in the real cellular membrane. One of the mostly used lipid

12

mixture is a saturated lipid of high T_m, an unsaturated lipid of low T_m and cholesterol. Wide angle X-ray scattering and NMR measurements reveal an increase in orientation order parameter on addition of cholesterol [32, 33]. On the basis of Differential Scanning Calorimetric studies, it is proposed than a gel phase is stabilized for the lipids of carbon chain length <17, and fluid phase is stabilized for >18 carbon chain length of the lipid[34]. This behaviour is observed due to the mismatch of the size of cholesterol (~17Å) with the hydrocarbon chain of the phospholipid. The phase state is affected by the insertion of cholesterol. The cholesterol has a unique nature to produce cholesterol rich liquid ordered phase (L_o) by increasing the conformational order of the lipid molecules in L_α phase above T_m. A generic phase diagram is shown in the figure 1.7 based on recent studies of cholesterol and phospholipid mixture. Above transition temperature a two phase area consisting of liquid ordered phase(lo) and liquid disorered phase (ld) is observed at excess water content.
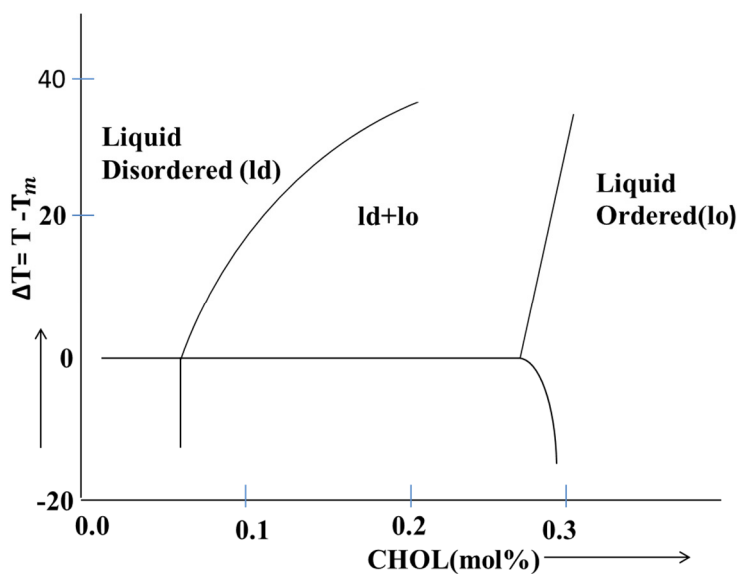
Figure 1.7: Generic phase diagram for phospholipid, cholesterol and water system [35].

Pan et al. [36] demonstrated that perturbation of cholesterol on the lipid bilayer is non- specific in nature. Cholesterol also induces non-lamellar phases in PEs and unsaturated PCs. In this thesis we presented the influence of cholesterol in a simple binary system of unsaturated phospholipid and cholesterol in presence of water. We observed cholesterol rich domain in the solid supported DOPC lipid bilayer with varying amount of cholesterol intercalation. We also measured the variation of nanomechanical properties of DOPC lipid bilayer with the incorporation of cholesterol

13

by PF-QNM. We believe that the present study will provide some insight into the structural and functional characterization of unsaturated phospholipids.

1.3. The interaction of lipid bilayer with Nanoparticle:

The use of nanoparticles in various fields of research as well as in daily life is expanding nowadays. With the advancement of technology, engineered nanoparticles are greatly used in targeted drug and gene delivery, bio sensing, diagnosis therapeutics imaging. Gold nanoparticles and superparamagnetic iron oxide are used in cancer therapy. Imaging for medical diagnosis has been greatly improved with the use of semiconducting nanocrystals. Introduction of nanoparticles in the field of biology arises some specific questions like their interaction and compatibility with the cell. It is reported that many engineered nano particles bear a pronounced effect on damaging the cell in various ways. A better understanding regarding cytotoxic activity of nanoparticle with bio membrane is necessary before its application in numerous biomedical fields. It is a challenge for the researchers to investigate the interactions of nanoparticles with the cell. Nanoparticles are observed to bind to cell membrane and cause a local change in the membrane curvature [37] [38] [39][40]. This change in membrane curvature may induce lipid redistribution and increase permeability of cell membrane. It is also revealed that cytotoxicity as well as microbial activity mostly depends on the physicochemical properties of nanoparticle i.e. particle size, shape, chemical composition, surface chemistry and porosity [41-43]. Roiter et al. [44] showed that silica nanoparticle of size 1.2 nm to 22 nm are capable to form pores in DMPC bilayers. Chan and coworkers [45] detected that 50 nm nanoparticles show highest cellular uptake by HeLa cells among a set of GNPs that ranged from 10 nm to 100 nm. Again, it is observed that HeLa cells accumulate more spherical nanoparticles in comparison to rod shape nanoparticles. Thus the size, shape and other chemical parameters are crucial for consideration of cytotoxicity of nanoparticles. [45-47]. Guarnieri et al. demonstrated that the accumulation of metal nanoparticles in the lysosome of the cell is responsible for their cytotoxic behaviour [48]. Silver nanoparticle (AgNP) is an important engineered metal nanoparticle which is widely used in bio medicinal applications. It shows enormous microbial activity owing to the size as well as its large surface-to-volume ratio even at low concentration [49]. A number of investigations show that AgNP is cytotoxic in nature [50-52]. Silver nanoparticles are able to release silver ions, which are considered to kill microbes [53]. Silver ions can adhere to the cell wall and cytoplasmic membrane through electrostatic

14

attraction. The adhered ions increase the permeability of the cytoplasmic membrane and eventually lead to disruption of the bacterial envelope [53]. With the rapid development of synthesis techniques, silver NPs can be functionalized differently with various coating materials. Chemical properties and the relative arrangements of the coating material on the nanoparticle surface play a vital role in the functionalization and the cellular uptake of nanoparticles [54-56]. The coating stabilizes silver nanoparticles through electro steric forces and reduces their agglomeration [57]. AgNP s are coated with organic (polymers, proteins, polysaccharides etc.) and inorganic materials (sulfides, chlorides etc.). The coating thickness and chemical composition play an important role in defining the cytotoxic behaviour of nanoparticle. Poly vinyl pyrrolidone (PVP) coated AgNP produces antigenic factor [58]. Chitosan-coated triangular silver nanoparticles can act as photo thermal agents. Chitosan-coated triangular silver nanoparticles can act as photo thermal agents against human non-small lung cancer cells [59]. AgNPs modified with oligonucleotides can heal wounds without any side effects [60].
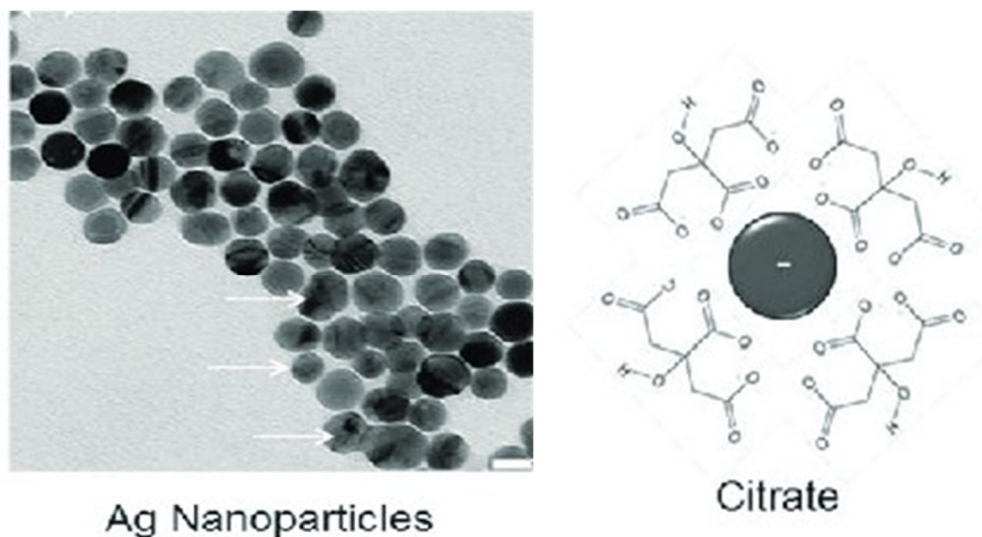
Figure 1.8: A TEM image of citrate coated Silver nano particle [61].

Here, I have used citrate coated silver nano particles (figure 1.8) for experimentation and studied the effect of nanoparticle on phospholipid bilayer. I observe that the insertion of citrate coated nanoparticle in solid supported pure and cholesterol mediated lipid bilayer shows variation in nanomechanical properties.

1.4. Main objectives of the thesis:

The general objectives of this thesis are to study the growth of solid supported bilayers by vesicle rupture and to investigate the interaction of biomolecules & inorganic nanoparticle with the lipid bilayer. The specific objectives are,

1) Single and multiple bilayer formation by DOPC small unilamellar vesicles (SUV) rupture and to study the growth mechanism.

2) To study the nanomechanical properties of cholesterol rich domains in mica supported unsaturated lipid bilayer.

3) To study the interaction of citrate coated anionic silver nanoparticle (AgNP) with pure and cholesterol mediated DOPC lipid bilayer.

4) Preparation of Giant Unilamellar Vesicles (GUV) from Large unilamellar vesicles (LUV) and to study the implantation of an antimicrobial peptide NK-2 on GUV by Phase Contrast Microscopy.

Although, the topics are quite vast, a general introduction has been conversed only in the framework of this thesis.

References:

[1]   E.L. Crockett, AMER. ZOOL 38 (1998) 291-304.

[2]   K. Simons and D. Toomre, Nature Reviews Molecular Cell Biology 1 (2000) 31-39.

[3]   E. London and D.A. Brown, Biochim Biophys Acta 1508(1-2) (2000) 182-95.

[4]   J.N. Israelachvili, Academic Press London (1991).

[5]   E. Ikonen, Nat. Rev. Mol. Cell Biol. 9 (2008) 125.

[6]   C.J. Marzzacco and B. Peterson, The Chemical Educator 12 (2007) 80-84.

[7]   J. Wilschut and D. Hoekstra, Chemistry and Physics of Lipids 40 (1986) 145-166.

[8]   R. Richter, R. Berat and A.R. Brisson, Langmuir 22 (2006) 3497.

[9]   A.P.Girard-Egrot and L.J.Blum, Nanobiotechnology of Biomimetic Membranes 1 (2007) 23-74.

[10]   V.P. Torchilin, Nature Reviews Drug Discovery 4 (2005) 145–160.

[11]   A. Fischer, A. Franco and T. Oberholzer, Chembiochem 3(5) (2002) 409-17.

[12]   P. Yang, R. Lipowsky and R. Dimova, Nano.Micro.Small 5 (2009) 2033-2037.

[13]   B. Kubsch, T. Robinson, J. Steinkühler and R. Dimova, J Vis Exp.. 128 (2017) 56034.

[14]   N. Stuhr-Hansen, C.-D. Vagianou and O. Blixt, Bioconjugate Chem. 30,8 (2019) 2156–2164.

[15]   R.B. Lira, T. Robinson, R. Dimova and K.A. Riske, Biophysical Journal 116 (2019) 79–91.

[16]   O. Wesołowska, K. Michalak, J. Maniewska and A.B. Hendrich, Acta Biochimica Polonica 56 (2009) 33–39.

[17]   T.K. Lind, H. Wacklin, J. Schiller, M. Moulin, M. Haertlein, T.G. Pomorski and M. Cárdenas, PLoS ONE 10 (2015) 0144671.

[18]   I. Langmuir, J. Am. Chem. Soc 39 (1917) 1848-1906.

[19]   Y. Xu, J. Kuhlmann, M. Brennich, K. Komorowski, R. Jahn, C. Steinem and T. Salditt, Biochim Biophys Acta Biomembr 1860(2) (2018) 566-578.

[20]   L.E. Franken, E.J. Boekema and M.C.A. Stuart, Advanced Science 4 (2017) 1600476.

[21]   T. Soranzo, D.K. Martin, J.-L. Lenormand and E.B. Watkins, Scientific Reports 7 (2017) 3399.

[22]   S.J. Attwood, Y. Choi and Z. Leonenko, Int. J. Mol. Sci. 14 (2013) 3514.

[23]   N. Yousefi and N. Tufenkji, Front. Chem. (2016).

[24]   M. Majewska, D. Mrdenovic, I.S. Pieta, R. Nowakowski and P. Pieta, Biochim Biophys Acta Biomembr 1862(9) (2020) 183347.

[25]   A. Basu, P. Karmakar and S. Karmakar, The Journal of Membrane Biology 253(03) (2020) 205-219.

[26]   C. Scomparin, S. Lecuyer, M. Ferreira, T. Charitat and B. Tinland, Eur Phys J E Soft Matter 28(2) (2009) 211-20.

[27]   F.A.Heberle and G.W.Feigenson, Cold Spring Harb. Perspect. Biol. 3 (2011) 1–13.

[28]   K. Mortensen, W. Pfeiffer, E. Sackmann and W. Knoll, Biochim Biophys Acta 945(2) (1988) 221-45.

[29]   M.B. Sankaram and T.E. Thompson, Biochemistry 29(47) (1990) 10670-5.

[30]   Q. Waheed, R. Tjörnhammar and O. Edholm, Biophys J. 103(10) (2012) 2125–2133.

[31]   O. Lenz and F. Schmid, Physical Review Letters 98(5) (2007) 058104.

[32]   T.T. Mills, G.E.S. Toombes, S. Tristram-Nagle, D.-M. Smilgies, G.W. Feigenson and J.F. Nagle, Biophys J. 95(2): (2008) 669–681.

[33]   L.S. Vermeer, B.L.d. Groot, V.r. Reat, A. Milon and J. Czaplicki, Eur Biophys 36 (2007) 919–931.

[34]   T.P.W. McMullen, R.N.A.H. Lewis and R.N. McElhaney, Biophysical Journal 79 (2000) 2056-2065.

[35]   G. Oradd and G. Lindblom, Magn. Reson. Chem. 2004; 42: 42 (2004) 123–131.

[36]   J. Pan, T.T. Mills, S. Tristram-Nagle and J.F. Nagle, Phys. Rev. Lett 100 (2008) 198103.

[37]   R.A. Sperling, P.R. Gil, F. Zhang, M. Zanella and W.J. Parak, Chem. Soc. Rev. 37 (2008) 1896–1908.

[38]   B.D. Chithrani, A.A. Ghazani and W.C.W. Chan, Nano Lett. 4 (2006) 662–668.

[39]   E. Boisselier and D. Astruc, Chem Soc Rev 38(6) (2009) 1759-82.

[40]   A. Verma and F. Stellacci, Small (2009) 1-10.

[41]   K. Kettler, K. Veltman, D.v.d. Meent, A.v. Wezel and A.J. Hendriks, Environ Toxicol Chem 33(3) (2014) 481-92.

[42]   M. Zhu, G. Nie, H. Meng, T. Xia, A. Nel and Y. Zhao, Acc Chem Res. 46(3) (2013) 622–631.

[43]   W. Wang, K. Gaus, R.D. Tilley and J.J. Gooding, Mater. Horiz. 6 (2019) 1538-1547.

18

[44] Y. Roiter, M. Ornatska, A.R. Rammohan, J. Balakrishnan, D.R. Heine and S. Minko, Nano Lett. 8(3) (2008) 941.

[45] B.D.Chithrani, A.A.Ghazani and W.C.Chan, Nano Lett 6 (2006) 662–68.

[46] B.D.Chithrani and W.C.Chan, Nano Lett 7(6) (2007) 1542-1550.

[47] A.E.Nel, L.Madler, D.Velegol, T.Xia, E.M.V.Hoek, P.Somasundaran, F.Klaessig, V.Castranova and M.Thompson, Nat. Mater 8(7) (.2009) 543-557.

[48] D.Guarnieri, S.Sabella, O.Muscetti, V.Belli, M.A.Malvindi, S.Fusco, E.D.E.D. Luca, P.P.Ponda and P.A.Netti, Nanoscale 6(17) (2014) 10264-10273.

[49] I.X. Yin, J. Zhang, I.S. Zhao, M.L. Mei, Q. Li and C.H. Chu, Int J Nanomedicine 15 (2020) 2555-2562.

[50] T. Zhang, L. Wang, Q. Chen and C. Chen, Yonsei Med J. 55(2) (2014) 283–291.

[51] C. Liao, Y. Li and S.C. Tjong, Int J Mol Sci. 20(2) (2019) 449.

[52] S. Gurunathan, J.W. Han, V. Eppakayala, M. Jeyaraj and J.-H. Kim, BioMed Research International (2013) Article ID 535796

[53] S.-T. Yang, A.J.B. Kreutzberger, J.L. 1, V. Kiessling and L.K. Tamm, Chem Phys Lipids. 199 (2016) 136-143.

[54] A. Verma, O. Uzun, Y. Hu, H.S.Han, N. watson, S.Chen, D.J.Irvine and F.Stellacci, Nat. Mater 7(7) (2008) 588–595.

[55] H.Gao, Journal of the Mechanics and Physics of Solid 62(1) (2014) 312–339.

[56] D.D. Jurašin, M. Ćurlin, I. Capjak, T. Crnković, M. Lovrić, M. Babič, D. Horák, I.V. Vrček and S. Gajović, Beilstein J. Nanotechnol. 7 (2016) 246-262.

[57] H.M. Fahmy, A.M. Mosleh, A.A. Elghany, E. Shams-Eldin, E.S.A. Serea, S.A. Alia and A.E. Shalan, RSC Adv 9 (2019) 20118-20136.

[58] K. Kang, D.-H. Lim, I.-H. Choi, T. Kang, K. Lee, Eun-YiMoon, YoungYang, M.-S. Lee and J.-S. Lim, Toxicology Letters 205 (2011) 227-234.

[59] S. C.Boca, M. Potara, A.-M. Gabudean, A. Juhem, P. L.Baldeck and S. Astilean, Cancer Letters 311 (2011) 131-140.

[60] S. Keleştemur, E. Kilic, Ü. Uslu, A. Cumbul, M. Ugur, S. Akman and M. Culha, Nano Biomed. Eng. 4(4) (2012) 160-176

[61] D. Radziuk, R. Schütz, A. Masic and H. Moehwald, Physical Chemistry Chemical Physics 16 (2014).

Chapter 2

Experimental Techniques

2.1   Introduction:

In this chapter, I have described briefly the experimental techniques which are used to study the formation of bilayer and multilayer of phospholipid membrane as well as to study the interaction of solid supported phospholipid bilayer with cholesterol, nanoparticle and other biomolecules, such as peptide.

Extrusion technique [1] was used to prepare unilamellar vesicles described in section 2.2. The size distribution of the lipid vesicles and zeta potential were determined by dynamic light scattering measurement which will be discussed in section 2.3. In section 2.4 I have discussed the technique used to prepare solid supported phospholipid bilayer by vesicle fusion method [2]. In section 2.5 I described the methodology used in Atomic Force Microscopy in contact and tapping mode. I have employed Nanoscope V controller and Peak Force Quantitative Nanomechanical (PF-QNM) contact and tapping mode for the detection of various interaction with solid supported phospholipid bilayer.

2.2. Preparation of small and large unilamellar vesicles:

Several techniques are reported in the literature for the preparation of large unilamellar vesicles [3]. However, extrusion method is widely used and popular method to prepare large unilamellar vesicles. During the preparation of vesicles, it is important to keep the temperature above the chain melting transition temperature (T_m) of lipid i.e., vesicles form only in the fluid lamellar phase of the hydrated lipid film. In the gel phase, the membranes are rigid and stiff. It costs more energy to bend the bilayer and hence it prevents the formation of vesicles. Large unilamellar vesicles were prepared using an extrusion technique as described by Hope et al. [1]. An appropriate amount of

lipid in chloroform (concentration of stock solution is 25 mg/ml) was transferred to a 5 ml glass bottle. Organic solvent was gently removed by passing dry nitrogen gas. The sample was put in a desiccator connected to a vacuum overnight to remove the trace amount of solvent.
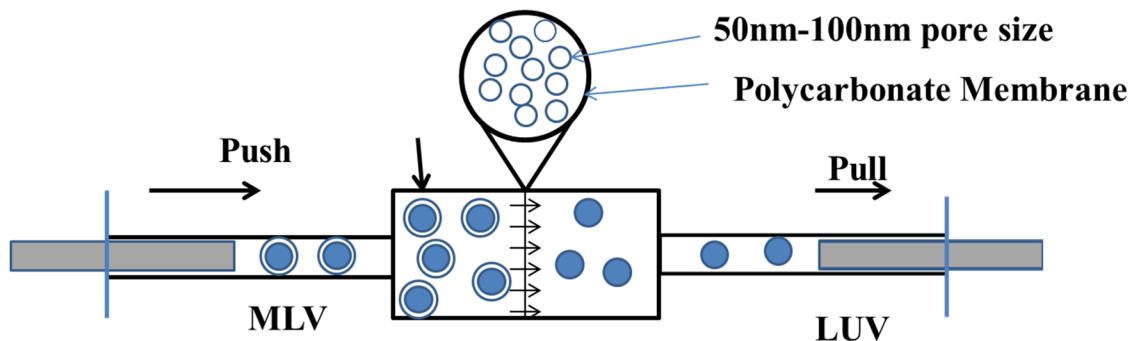
Figure .2.1. Schematic diagram of extruder showing the formation of SUV and LUV from MLV.

After that, dried lipid film was hydrated with required volume of millipore water so that the final desired concentration (1 mg/ml) was obtained. Hydrated lipid film was vortexed for about 30 minutes to produce multilamellar vesicles (MLV). LUVs and SUVs were prepared by extruding the MLV with LiposoFast from AVESTIN (Canada). MLV suspensions were extruded through polycarbonate membranes of different pore diameters (100 nm and 50 nm) to produce LUVs and SUVs. This resulted in a formation of well-defined size of LUVs (average diameter ~ 100 nm) and SUVs (average diameter ~ 60 nm) depending on the membranes of different pore size used. Size distribution of vesicles was confirmed by dynamic light scattering (DLS). Before DLS measurement, vesicle solution was degassed each time in order to avoid the artifact caused by air bubbles.

2.3   Dynamic Light Scattering (DLS)

2.3.1   Working principle of dynamic light scattering:

Unilamellar vesicles (LUVs and SUVs) are categorized by average size measured through DLS [4] [5]. When a monochromatic light of wavelength λ is incident on a vesicle solution, light is scattered. When light scatters from molecules executing Brownian motion, the motion imparts randomness to the phase of the scattered light. A change in the destructive or constructive

interference occurs when the scattered light from more than one particle are added together. This leads to time dependent fluctuation in the intensity of the scattered light. The fluctuation in the scattered intensity is measured by the detector fixed at scattering angle θ. This fluctuation is directly related to the rate of diffusion of the molecule through the solvent. This, in turn, is directly related with the hydrodynamic radius of the particle. In a typical experimental setup, scattered light can be detected at both 90⁰ as well as 173⁰ scattering angle as shown in Fig. 2.3(a). Usually, unwanted particles scatter light in forward direction [6]. Thus, backscattered light intensity (173⁰) is better than 90⁰ scattered in case of size measurement of vesicles. The rotational diffusion coefficient can be ignored during backscattered intensity measurement. The back scattered light is sent to digital signal processing correlator. The scattering wave vector ($\vec{q}$) is defined as $|\vec{q}| = |\vec{k}_s - \vec{k}_i| = \frac{4\pi n \sin{\theta}/2}{\lambda}$, where $\vec{k}_i$ and $\vec{k}_s$ are the incident and scattering wave vector respectively as shown in Fig. 2.2(b) and n is the refractive index of the solvent.
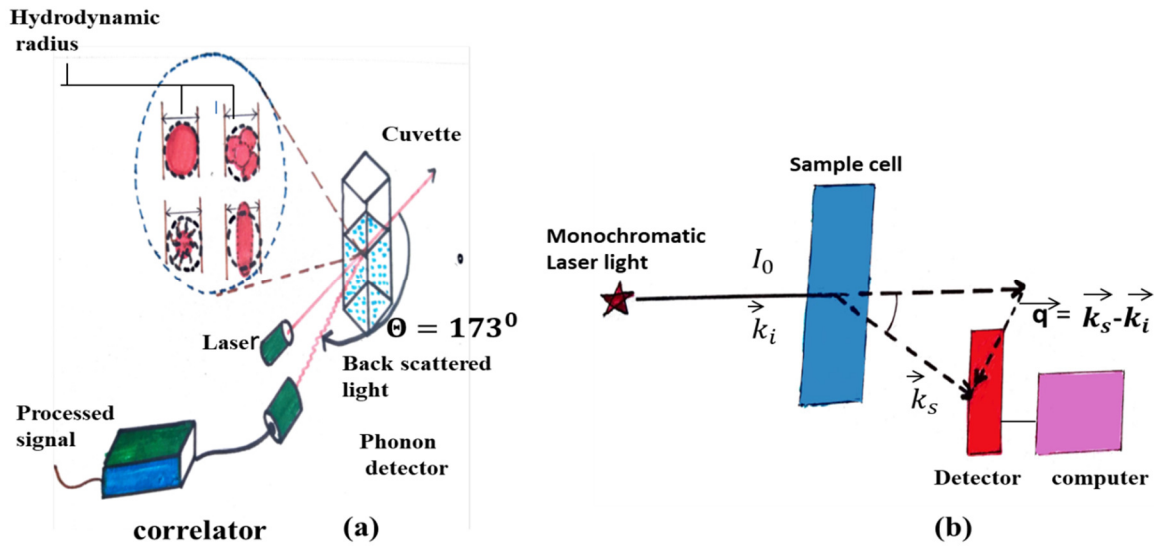
Figure.2.2. (a) Key components of Dynamic Light Scattering which uses back scattering mode at an angle 173^0 (b) represents basic light scattering geometry.

Intensity autocorrelation function obtained from digital correlator when fitted to exponential decay function gives the diffusion constant D. Knowing D, the hydrodynamic radius (R_h) of the vesicles can be obtained by using the Stokes-Einstein relation.

$$R_h = kT/6\pi\eta D$$

Here, k is Boltzmann constant, kT is the thermal energy, η be the viscosity of the medium. Hydrodynamic radius (R_h) refers to the radius of the sphere that diffuses with the same velocity as that of the particle. In DLS measurement, the vesicle shape is assumed to spherical in all respect [7].

Polydispersity index (PDI) indicates the extent of polydispersity of the size distribution determined from the width of the Gaussian curve of particle size distribution. The value of PDI > 0.7 usually treated the distribution as polydisperse. However, PDI < 0.7, system is referred to mono dispersive in nature. PDI < 0.05 is purely monodisperse.

In our experiments, the size distribution was measured with Zetasizer Nano ZS (Malvern Instruments, UK) at room temperature (~ 25^0C). Zetasizer Nano uses 4 mW He-Ne Laser of wavelength 632.8 nm. In each measurement, we have performed 10-100 consecutive runs. A transparent quartz cuvette was used for the measurement of vesicle size. The disposable zeta cuvette is also used to measure both size distribution and zeta potential. Typical size distribution of LUV has been shown in Fig. 2.3.
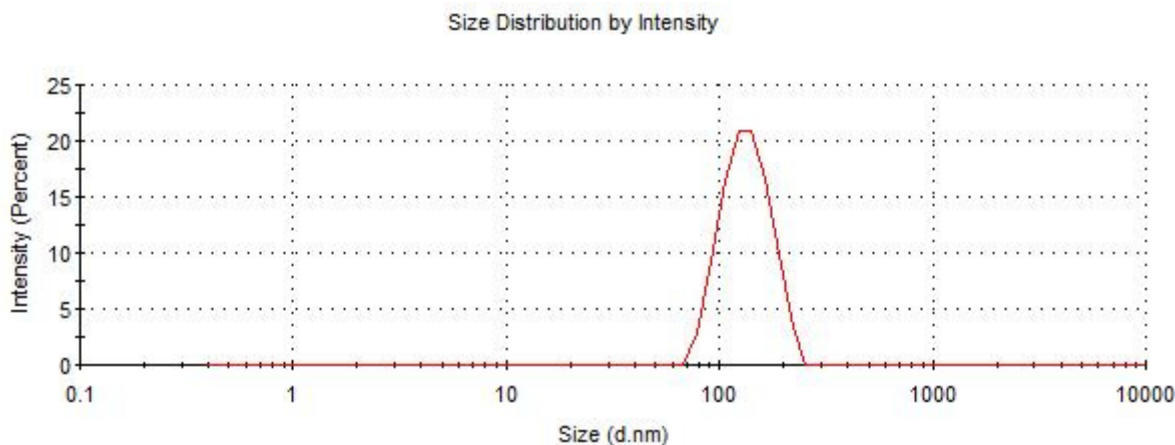
Figure .2.3. Size distribution of LUV made from DOPC.

2.3.2 Theory of Zeta potential:

Electrophoresis:

The technique of zeta potential is widely used to investigate the stability of colloidal dispersion, estimate the surface charge and surface potential of the vesicles of a system. When charged LUVs

are embedded in aqueous solution, the oppositely charged ions form electrostatic double layer around the LUV. This electrostatic double layer exists around each vesicle. Inner layer is called Stern layer.
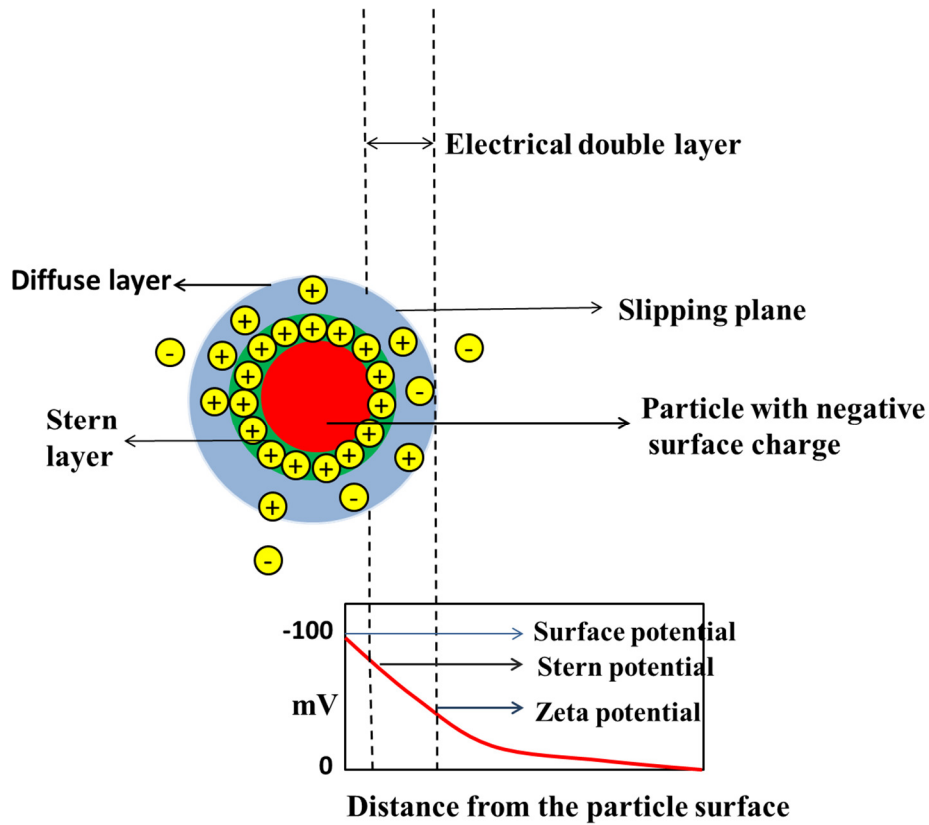
Figure 2.4: Formation of electric double layer on the charged vesicles and measurement of zeta potential at the slipping plane.

Ions are strongly bound with the vesicles. The outer region is called diffuse layer where the ions are loosely bound. The boundary of the diffuse layer is called shear or slipping plane. When the vesicle moves, ions within the boundary of slipping plane move with it. The electrostatic potential that exists in the shear or slipping plane is known as zeta potential. Therefore, zeta potential can be a good approximation of the surface potential at low and moderate electrolyte concentrations up to 0.1 M. Zeta potential is measured from the electrophoretic mobility μ using a model described by the Smoluchowski and Hückel equation [8] [9].

$$\zeta = \frac{3\mu\eta}{2\varepsilon f(\kappa a)}$$

24

Where, η is the coefficient of viscosity of the aqueous solution or the medium of dispersion, ε is the dielectric constant, $f(\kappa a)$ is the Henry function where κ inverse Debye length and a is the effective radius of the vesicle including Stern layer measured from DLS.

2.4. Preparation of solid supported lipid bilayer:

2.4.1 Substrate preparation:

Naturally available high grade muscovite mica from Jharkhand, India was used for experiment. For consistency, a single 200 mm-150 mm mica was cut into pieces of 12 mm-12 mm. For PF-QNM, 12 mm mica circular disks from Agar Scientific were used. Mica substrates were glued to 12 mm magnetic AFM stubs by epoxy. They were freshly cleaved by scotch tape and used directly for sample preparation without further processing.

2.4.2. Supported bilayer formation:

In comparison to lipid vesicles, solid supported lipid bilayer is more stable and its fixed and well-defined structure enables it to be an excellent model membrane to study by using various surface sensitive techniques like Atomic Force Microscopy. This model membrane is easy to form under definite experimental condition by vesicle fusion method. 30-50 µl vesicle solution (SUV or LUV) was taken in a micropipette and deposited on freshly cleaved mica. The sample was incubated for 15 to 45 minutes to grow the bilayer structures. After incubation the sample was thoroughly rinsed and used for imaging. A schematic diagram of supported lipid bilayer formation is depicted in the figure 2.5. Deposited vesicles are first adsorbed by the mica surface. Adsorbed vesicles are distorted due to the adhesion force between the vesicle and surface. Finally, distorted vesicles are ruptured and form bilayer patches on the surface as shown in the figure 2.5.
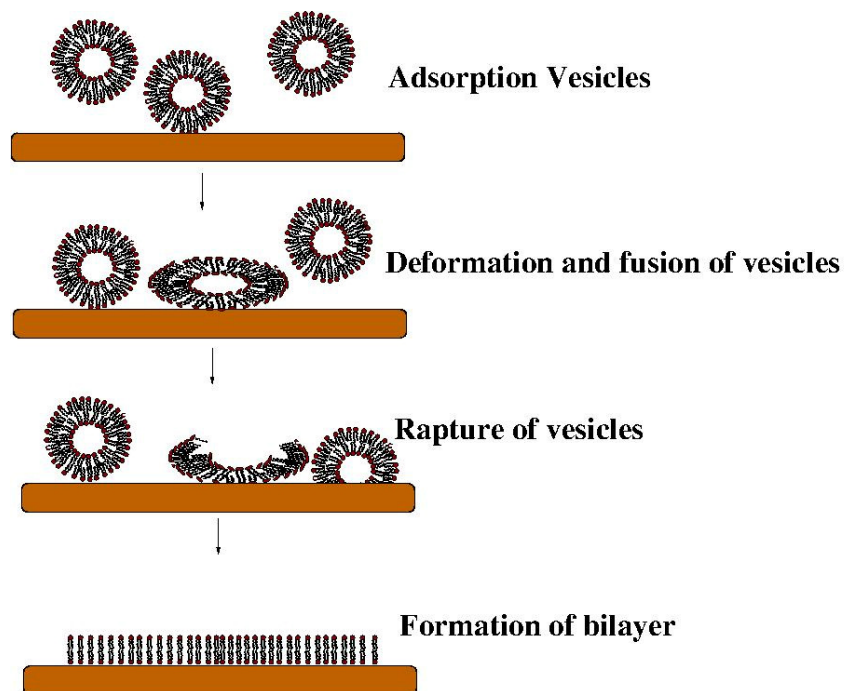
Figure 2.5: schematic diagram of the formation of solid supported bilayer by vesicle fusion method

2.5. Atomic Force Microscopy:

Atomic Force Microscopy (AFM) belongs to Scanning Probe Microscopy where a probe with a tip raster scans across a surface and monitors the probe–surface interactions. A 3-D topographic map is obtained with angstrom level resolution in Z direction. It is a good technique in probing surfaces of biological sample in air as well as in aqueous medium. At first Scanning Tunneling Microscope was developed by Binnig and Rohrer[10]. However, STM was limited to a conducting sample. Further , Binnig demonstrated the use of AFM for imaging insulator samples for the first time [11].With continuous development, nowadays AFM is routinely used to obtain images in real time with several frames per second. A basic set up of AFM is shown in the figure 2.6.
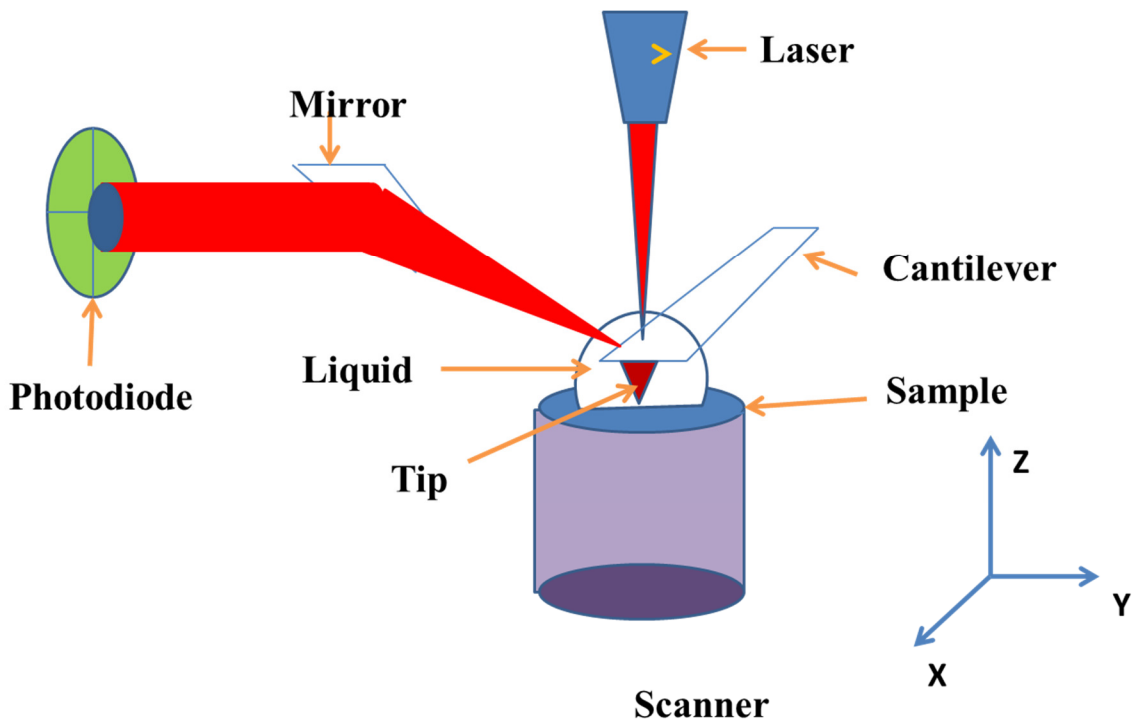
Figure 2.6: Schematic diagram of AFM operated in fluid.

Some key features of AFM are discussed below.

2.5.1. AFM probes

The term in AFM, experiment probe, tip, cantilever, are often pronounced synonymously though they have specific aspects. Generally, a probe is a silicon/silicon nitride wafer chip with a base to hold into AFM tip holder, a cantilever and a tip (figure 2.7). Cantilever is a mechanical lever that protrudes from the probe base and deflects when the tip scans different features of the sample.
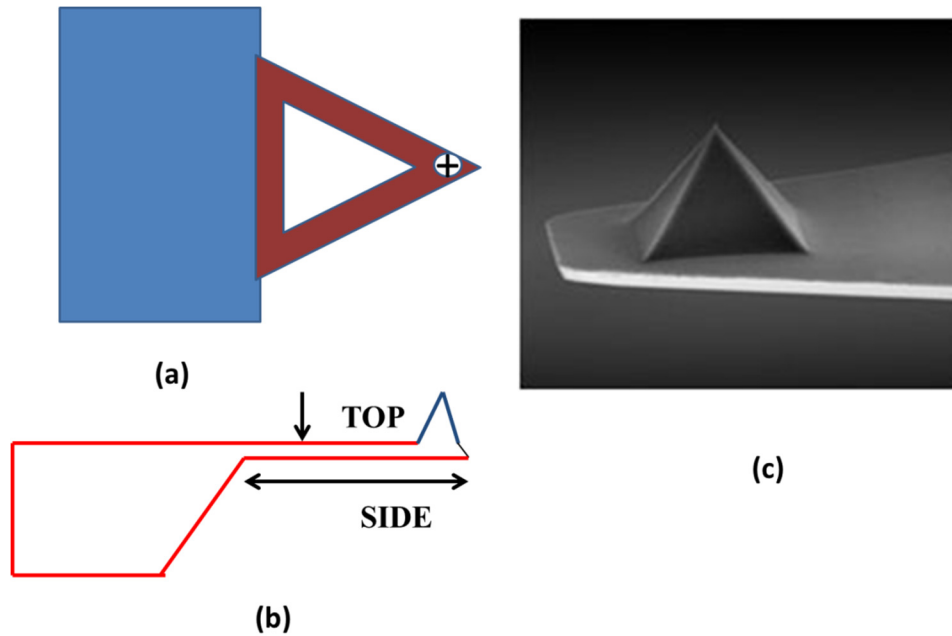
Figure 2.7: a) Schematic diagram of AFM probe showing cantilever protruding from the probe, (b) diagram showing the tip protruding from the cantilever, (c) electron microscopic image of AFM tip protruding from the cantilever.

Cantilevers come in a variety of shapes although the standard shape is triangular as shown in the figure. Usual cantilever dimensions are 20-150 μm in length and 5- 25 μm in width. Cantilever spring constant (k) values can vary from 0.1 N/m for the study of soft samples to 100-200 N/m for the study of hard samples. A pyramidal shaped tip protrudes down from the cantilever which has typical radius of 5-50 nm. The sharper tips provide higher resolution.

2.5.2 Piezo Scanner:

Piezoelectric materials are vital for AFM as they enable voltage to be transformed into mechanical motion. When a voltage is applied to piezo, it changes its geometry. The expansion of piezo is around 1nm/voltage applied [12]. This property enables the controlled movement of tip or sample in a small scale which results in high resolution mapping and imaging. Two different types of piezo are used in AFM, one is responsible for moving the tip/sample in X-Y direction and another guides the movement of the tip/sample in Z direction.

2.5.3 Feedback control

Feedback control enables the force to be kept constant between the tip and surface. The force on the cantilever is fed into PID (proportional-integral derivative) controller which senses the change of force from the desired set point along with proportional gain and integral gain provided by the user and controls the piezo to move back to initial set point.

2.5.4 Imaging:

The probe, the piezo and the feedback, all together, control the scanning and imaging procedure of the sample all together. AFM probe acts as optical lever force sensor. A laser is aligned on the reflective top coating of the probe and is fed into photo detector. A set point or a set voltage relative to photo detector is defined by the user. The tip begins to scan the surface with the given set voltage. The tip deflects more when it is closer to the surface and deflects less when it is away from the surface. The deflection change of the cantilever is sensed by the photo detector through the reflected laser spot. This causes a change in voltage in the photo detector. The change is fed through the feedback loop. The feedback voltage along with proportional and integral gain feeds the cantilever with the initial set voltage by moving the Z-piezo in upward or downward direction. The movement of the Z piezo is thus recorded during the scan in X-Y direction and a three-dimensional image of the surface is obtained.
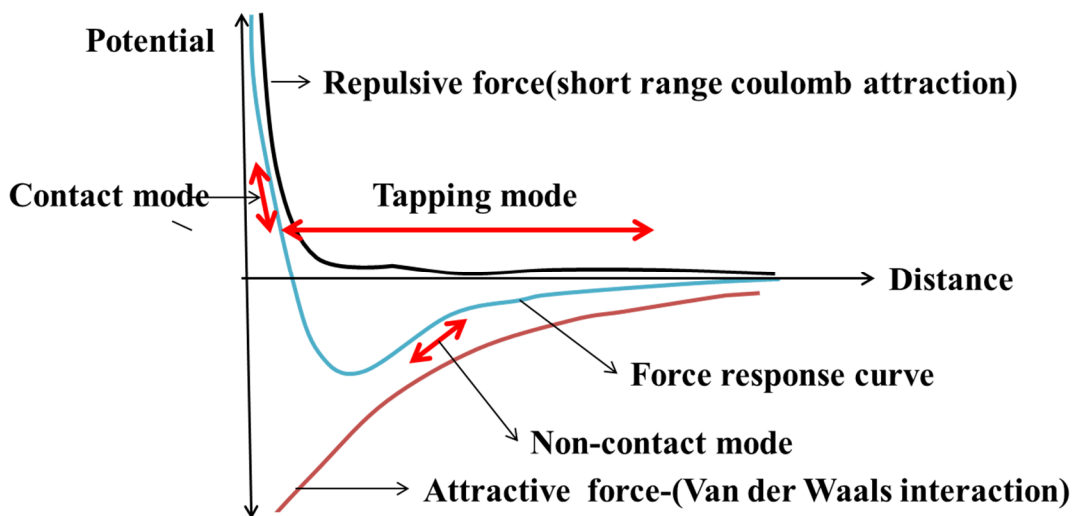
Figure 2.8: Lennard - Jones potential showing tip-sample forces in AFM**.**

2.5.5. Tip-sample forces:

The forces involved in the tip-sample interaction can be expressed using Lennard-Jones Potential,

$$U(r) = 4\varepsilon\left(\left(\frac{\sigma}{r}\right)^{12} - \left(\frac{\sigma}{r}\right)^{6}\right)$$

U(r) is the potential energy between the tip and the sample; r is the tip-sample distance, ε is the minimum potential, σ is the tip-sample separation at zero potential. When the tip approaches the sample, there is an attraction due to long range Van der Waals force, causing cantilever deflection towards the surface. However, with the reduction in tip sample separation within Angstrom range, there is repulsion due to short range Pauli's exclusion principle. When the repulsion overcomes the attractive force, the cantilever is deflected away from the sample. The tip sample interaction as a function of separation is used for operation of AFM in different modes [13].

2.5.6. Imaging modes:

Contact Mode-

AFM can be operated in various modes depending on the monitoring and manipulating tip –sample interactions. Contact mode is the basic imaging mode of AFM. Here, the cantilever tip is brought into contact with the sample to a set deflection point. As the tip raster scans the surface, the cantilever deflects according to the change in height on the surface. The feedback control maintains a constant deflection level by moving Z-piezo. This Z piezo motion produces an image of surface topography. The tip applies high lateral forces as it remains in constant contact with the surface. This high force is undesirable for soft biological samples as it can alter the surface topography. Another disadvantage of contact mode is the deflection of the cantilever will drift over time, even without contact of the sample. To maintain the set point, the applied imaging force is to be changed. Typical applied forces remain within a range of 100-500 pN, at scan rates of around a frame per minute, using cantilevers with spring constants of < 0.1 Nm [14].

Tapping mode:

In tapping mode, the tip makes intermittent contact instead of constant contact with the surface. This can be achieved by moving the cantilever at its resonant frequency at amplitude around 20 nm. During full cycle of oscillation, the tip gets in and out of attractive and repulsive regimes respectively. In tapping mode, the feedback control is tuned in fixed amplitude set point. When the tip interacts with high surface feature, the oscillation is damped, as a result z- piezo retracts the tip so that it gains initial amplitude set point. If the tip meets low surface the amplitude increases, this in turn pushes the tip to surface so that the damping feeds the tip with initial amplitude set point. As the tip makes intermittent contact with the surface, the lateral force is reduced significantly. Thus, the mode is safe for soft biological samples. In tapping mode, a phase image is obtained along with topographic image. The phase difference between the oscillation of driving piezo and the oscillation of the cantilever is reflected in the captured phase image. According to simple harmonic theory, this lag is 90^0 at the resonant frequency. Phase image gives an idea about the physical properties of the surface.

2.5.7. Peak Force Quantitative Nanomechanical Mapping (PF-QNM):

Peak Force Quantitative Nano mechanical Mapping in a recent development in AFM by Bruker where peak force tapping (PFT) mode is used to obtain force curves for each pixel of an AFM image and fits the curves in real time to get the image maps of modulus, adhesion, deformation and dissipation. To study the nanomechanical properties, some important calibration steps are to be followed.

Calibration steps for PF-QNM:

Cantilever calibration:

At first, we focus on cantilever calibration for optimizing deflection sensitivity. The deflection in photo detector measured in volts needs to be converted in terms of deflection of cantilever in nm. This can be calibrated by ramping the cantilever on a hard surface whose modulus is significantly higher than the tip. The deflection sensitivity of the cantilever is measured by the change in voltage

in the photo detector per unit distance of cantilever deflection ($\frac{V}{nm}$).The advantage of calibration is that deflection sensitivity is independent of the type of the surface.

Spring constant:

The cantilever deflection measured in nm is converted into force if the spring constant of the cantilever is known using Hooke's law.

$$F= - k.x$$

Where F is the applied force, x is the deflection of the cantilever and k is the spring constant. We have taken the value of tip radius and spring constant from the manufacturer's data.

Sync distance:

Sync distance is one of the important parameters in PF-QNM. It is a time constant between the start and the peak of the force curve which in turn gives the value of maximum piezo extension. This is the point where the approach part of the force curve changes to retract part. When the sync distance is calibrated properly, the peak force registered in the PF-QNM gives the exact value of maximum force imparted by the tip on the surface. For calibration, a force curve is generated by the scanning the tip on a hard surface. It is essential prior the measuring of the viscoelastic properties of a soft sample like bilayers. There can be a time dependent deformation while scanning a soft sample. If sync distance is properly calibrated, the time dependent response will also be measured perfectly to give exact values of physical parameters.
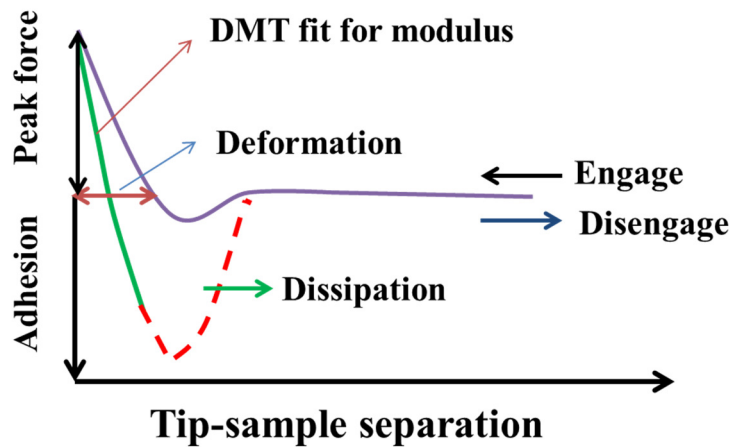
Figure 2.9: Force curve showing peak force and the position of different physical parameters where the data are extracted.

In our experiments, all images were captured in liquid cell by Bruker made multimode and catalyst scanning probe microscopes with Nanoscope V controller. Both tapping mode and contact modes were used to acquire the images of the surface topography of lipid bilayer. A liquid resistant 10 um scanner, a standard fluid cell with cantilever holder with liquid flow arrangement were used for AFM imaging in the multimode system. Peak Force Tapping mode was operated in the catalyst system using ScanAsyst-liquid probes and liquid cell for the measurement of nano-mechanical properties of supported lipid bilayer. Details of AFM measurement are described in the respective chapters.

2.6. Preparation of giant unilamellar vesicle (GUV)

Giant Unilamellar Vesicles (GUV) were prepared by electroformation method, first described by Angelova et al. [15]. Electroformation yields unilamellar vesicles of 10- 100 µm diameter and formation rate (95%) is high in comparison to other method discussed in the literature [6]. Owing to their large size these vesicles can be observed under phase contrast or fluorescence microscopy. Therefore, any morphological change can be visualized directly using optical microscopy.
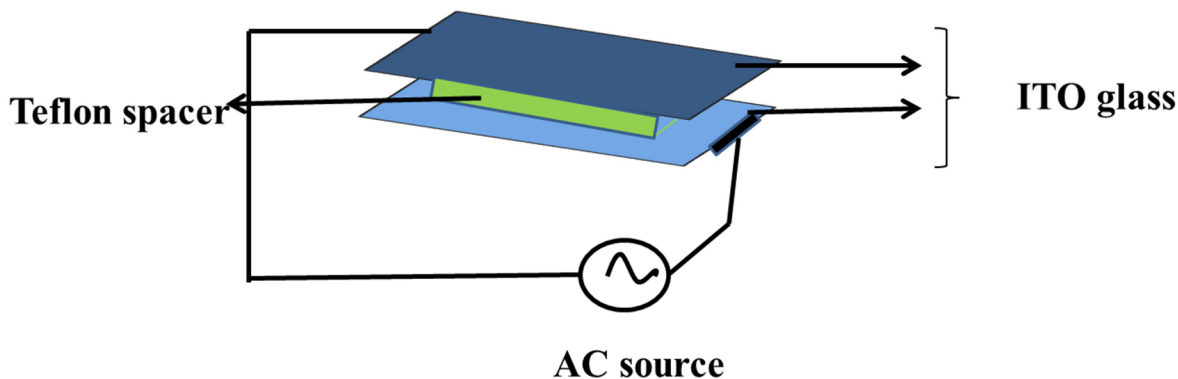
Figure 2.10. Schematic diagram of electroformation chamber where GUV s are produced

In electroformation method, two ITO coated glass plate separated by a very thin Teflon spacer (1 mm thick) were taken and ITO coated side was kept face to face to form electrode. Electric connections were made by either conducting tape or silver paste. 2-3 µl stock solution of the lipid or lipid mixtures (~ 0.5 mg/ml was taken out using Hamilton syringe and layered onto both ITO coated side of the electrode. The coated glasses were allowed to dry to evaporate solvent and a

thin lipid film was formed. The optimum thickness was allowed in the range 10-100 bilayers. Both the ITO glasses were kept overnight in vacuum desiccator to remove the traces of the solvent. Electroformation chamber was then prepared using Teflon spacer and the chamber was filled with millipore water or buffer with fixed pH. 1-3 volts 10-15 Hz frequency alternating voltage was applied across the ITO electrodes for a couple of hours. AC field was minimized gradually to zero so that GUV could detach from the surface. Aqueous solution of GUV was collected and stored in 5 ml glass bottle for further experiments.

References:

[1]   M.J. Hope, M.B. Bally, W. Webb and P.R. Cullis, Biochem. Biophys. Acta 55 (1985) 812.

[2]   H.M.McConnell, T.H. Watts, R.M. Weiss and A.A. Brian., Biochim. Biophys. Acta. 864 (1986) 95–106.

[3]   H.H. HUB, U. ZIMMERMANN and H. RINGSDORF, FEBS LETTERS 140 (1982) 254-256.

[4]   K.S. Schmitz, Academic press (1990).

[5]   B.J. Frisken, APPLIED OPTICS 40(24) (2001) 4087-4091.

[6]   V. Patravale, P. Dandekar and R. Jain, nanoparticulate drug delivary (2012) 87–121.

[7]   F.R. Hallett, J. Watton and P. Krygsman, Biophys. J 59 (1991) 357-362.

[8]   R.J. Hunter, Academic Press (1988).

[9]   A.K. Patri and J.D. Clogston, Characterization of Nanoparticles Intended for Drug Delivery 697 (2010) 63-70.

[10]   G.Binnig, H.Rohrer, C.Gerber and E.Weibel, Physical Review Letters (1982) 57–61.

[11]   G. Binnig, C.F. Quate and C. Gerber, Phys. Rev. Lett. 56 (9) (1986) 930–933.

[12]   P.Eaton and P.West, Oxford University Press (2010).

[13]   N. Chan, C. Lin, T. Jacobs, R.W. Carpick and P. Egberts, Beilstein J. Nanotechnol 11 (2020) 729–739.

[14]   M.C. Leake, Cambridge: Cambridge University Press (2013).

[15]   M.I.Angelova and D.S.Dimitrov, Faraday Discuss. Chem. Soc 81 (1986) 303.

Chapter 3

Formation of supported planar single and multiple bilayer by DOPC vesicle rupture on mica substrate:

3.1 Introduction:

A planar lipid bilayer on a solid support serves as model system that explains fundamental aspects of membrane biology and enables us to characterize wide range surface sensitive techniques including molecular engineering. Present chapter aims at understanding the process of single and multiple bilayer formation after the exposure of small unilamellar vesicles (SUV) of dioleoyl phosphatidylcholine (DOPC) to mica substrate. Isolated single bilayer formation and co-existence of double and triple lipid bilayers in the aqueous medium has been quantitatively measured by Atomic Force Microscopy and discussed the physicochemical mechanism. To the best of our knowledge, this is the first report of co-existence of single, double and triple bilayers in an aqueous medium by simple sequential addition of diluted DOPC vesicle solution on the highly hydrophilic mica surface. A large number of studies on the formation mechanism of solid supported lipid bilayer and multilayer have been employed due to their important role in studying the interaction of cell membrane with various biomolecules. These earlier studies are summarized in section 3.2. All experimental results have been elucidated in section 3.3. The results and the mechanism is discussed in section 3.4. We conclude this chapter in section 3.5.

3.2. Earlier studies:

As stated earlier, it is often useful to study model membrane in order to gain insight into the structure and functions of membranes which may be difficult to study *in vivo*. Unilamellar vesicles are excellent model systems to study. Besides unilamellar vesicles, solid supported bilayers (SLB) are useful for studying many biological processes, especially cell adhesion, fusion, signaling, adsorption of molecules, to name a few [1]. A variety of techniques, viz., Langmuir−Blodgett

deposition [2], vesicle fusion [3], lipid-detergent method [4] and many more have been applied to prepare SLB.   Among them, the vesicle fusion method is quite reliable and easy. However, mechanism of SLB formation by simple vesicle fusion is not yet adequately understood.

Various differing reports are present in hitherto published literature regarding the mechanism of SLB formation. Reviakine and Brisson[5] used the vesicle fusion method on mica to study the early stage of SLB formation and compared their results with available theoretical works. They observed that the SLB formation depends highly on vesicle size, lipid concentration and the presence of Ca^{+2} ions in the medium though Attwood et al. [6] noted that the SLB could be formed even in the absence of Ca^{+2} ion. Weirich et al. [7] revealed that the vesicles need rearrangement before rupture. Besides, Jass et al. [8] demonstrated that when liposomes are attached to a hydrophilic surface, they get flattened until two membrane bilayers stack on top of each other. Moreover, the authors reported that the upper layer of the stacked layers slides over the lower layer and forms a bilayer patch. In order to gain insights into the fundamental as well as the applied aspects of membrane, various experimental techniques, such as, atomic force microscopy (AFM), [3, 9, 10], dissipation-enhanced quartz crystal microbalance (QCM-D) [10, 11], ellipsometry [12], neutron reflection [10, 13, 14], interferometric scattering microscopy [15], fluorescence microscopy [10, 16] have been used.

In addition to the single bilayer, formation of multilayer model membrane is of great importance for studying its interaction with drugs, nanoparticles or membrane-embedded protein. For example, embedded proteins of larger dimension cannot be accommodated in a single solid lipid model bilayer due to their structural deformation [17]. The lipid multilayer model system can be an effective solution in the aforementioned scenario of structural deformation. Multilayer lipid membranes are also found in the natural environment, *e*.g., in mitochondrial cristae, in neuron, thylakoid, etc. Different procedures have been followed to form artificial lipid multilayers [18, 19] [20] [21] [22] [23]. Vogel et al. [22] reported the formation of lipid multilayer by depositing lipid solution dissolved in an organic solvent on silica and glass substrate by "spin coating" method. A "rock and roll" method for the construction of multilayer was followed where lipid solvent solution was deposited on different substrates [24]. Heath et al. [20] reported the formation of multiple bilayers by adding Poly-L-Lysine (PLL), an electrostatic linker, repeatedly in a controlled condition to the junction of two lipid bilayers. Single and double bilayers were also

observed by injecting dioleoylphosphatidylethanolamine (DOPE) liposome suspension diluted with MgCl$_2$ aqueous solution on mica surface [25]. Okamoto et al. [26] prepared a single and double bilayers by depositing DOPC in buffer solution on Graphene Oxide surface by vesicle fusion method. Sironi et al. [21] used a different procedure where aqueous liposome solution was drop cast on mica substrate and dried to form a large number of stacked anhydrated bilayers. In all these works, lipids were dissolved in an organic solvent and/or additional linker was added between the bilayers or the aqueous medium was dried to form the artificial multi bilayer structure. The native characteristics as well as fluid nature of such stacked bilayers may be lost due to incorporation of ligands and linkers. Therefore, spontaneously growing multiple bilayers in the aqueous medium without using additional interlayer or ligands is more desirable for the realistic model system.

Our objective in this chapter is to investigate the mechanism of DOPC vesicle rupture and consequent spontaneous single and multiple SLB formation on the freshly cleaved mica surface. For quantitative measurement of SLB fragments in liquid medium, along lateral and vertical directions, Atomic Force Microscope has been used.

3.3 Experimental:

Small unilamellar vesicles (SUV) were prepared by following the extrusion method described by Hope et al. [27] and the process is discussed elaborately in chapter 2. the final concentration of SUV solution is maintained at 0.05 mg /ml. The size distribution of extruded vesicles was measured by the dynamic light scattering (DLS) technique. The mechanism of DLS measurement is also discussed in chapter 2. Solid supported bilayers were prepared by vesicle fusion method on the highly hydrophilic mica substrate which is already discussed in chapter 2. In the first set of experiment 10, 20 and 30 µl of 0.05 mg/ml SUV solution was deposited on three freshly cleaved mica surfaces and incubated for 15 minutes. In the second set of experiment (case of sequential deposition), the 10 µl of the same DOPC solution was added successively on mica substrate every 15 minutes and incubated for a total time of 45 to 75 minutes (as indicated) in a closed container to avoid evaporation. In both the cases, after the incubation period, samples were rinsed gently with millipore water and immediately covered with pure water as well as placed on the AFM scanner for measurements in liquid mode. In third set of experiment, 10 microliter of 0.05 mg/ml

DOPC solution was deposited on freshly cleaved mica and incubated for 15 minutes like the first experiment of the first set but here the time lapse AFM images were recorded without rinsing the deposited solution. Mica surface covered with DOPC solution was imaged continuously for 15 minutes. Then additional 10 microliter 0.05 mg/ml DOPC solution was injected *in situ* in the liquid cell by a syringe without stopping the scan. Time lapse AFM images were recorded for another 70 min. Every full scan took around 9 minutes.

Here, I operated the AFM in tapping as well as scan asyst modes. I used super sharp silicon nitride (Bruker SNL10) probe with tip radius 2 nm and spring constant 0.12 N/m for tapping mode. A resonance frequency of the probe in pure water was manually selected at ~ 5.8 kHz and manually adjusted the amplitude set point for best imaging. For peak force scan asyst mode, high resolution probes (Bruker, SCAN ASYST- FLUID) with spring constant 0.35-1.4N/m were used, where scan parameters were controlled in auto mode. In all cases the images were acquired at scanning rate 1-2 Hz. I flattened the AFM images by "Flatten plus" of WSxM software to eliminate slopes, bows and/or bands in the images [31]. Using the same software, I presented the line profiles and statistical distribution of heights and lateral sizes. In figure 7, 9 and 10, contour plots of the AFM images were presented by the same software. By selecting the range of heights corresponding to the first, second and third bilayers, the height images were sliced to show single, double and triple bilayers separately.

3.3.1 Structural orientation of mica substrate:

The chemical property of the mica was investigated by X-ray Photoelectron Spectroscopy [28]. Contact angle measurement of freshly cleaved mica shows super hydrophilic nature with contact angle less than 5° [29]. Muscovite mica is a naturally available layered structured material where negatively charged aluminosilicate layers are interconnected by positively charged K^+ ions. Due to weak ionic bonding via K^+ ions, aluminosilicate layers are easily separable. During cleaving by scotch tape, K^+ ions are shared by the two newly generated surfaces [30]. As a result, the cleaved surface becomes negatively charged due to depletion of K^+ ions. With time the negative surface charge is compensated by the bulk positive charges. Immediate deposition of vesicle solution just after cleaving results in strong adhesion between mica and vesicle through attractive interaction

between negatively charged mica surface and zwitterionic DOPC vesicles. We have used muscovite mica substrate from MTI Corporation also.

3.4. Results and Discussion:

3.4.1 Formation of single SLB fragments on mica from DOPC SUV:

Size distribution of SUV obtained from extrusion method is shown in figure 3.1.
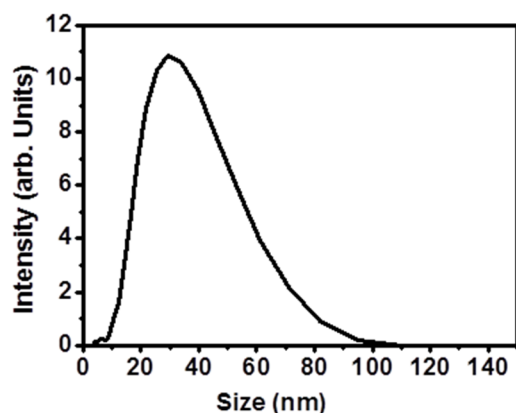
Figure 3.1. Size distribution of DOPC vesicles as measured by Dynamic Light Scattering (DLS)

The polydispersity index (0.07) clearly indicates that the vesicles are fairly monodispersed. Figure 3.2(a) shows the AFM image of bilayer fragments formed by rupture of uniform DOPC vesicles for 15 minutes incubation and subsequent rinse by millipore water. It is clearly evident from the one dimensional line profile (Figure 3.2 b) that the average height of the bilayer patches is ~3.0 nm. Height distribution of the entire surface is shown in figure 3.2 (c). It shows two peaks. The first one is from 0.5 to 2 nm, peaked at 1.2 nm for the bare mica surface with adsorbed ultrathin water layer and the other one is for single bilayer fragments with a broad peak maximum at 4.2 nm. Mornet et al. also reported an ultrathin water layer of thickness 0.5-1.5 nm between the substrate and lipid bilayer by Cryo-Transmission Electron Microscopy [32]. Typical bilayer thickness is around 4 - 5 nm [33] [34] but we observe lower average height of bilayer because some times higher tapping force could result in lowering the height of the bilayer [35]. The measured average height of the bilayer fragments is in agreement with the earlier reports [11] [36].

40

The distribution of the diameter of the bilayer patches is also shown in figure 3.2. (d), which shows the peak at around 50-60 nm. It is also evident that the patches of maximum size are found to be at 180 nm. Interestingly, the bilayer patch size distribution is consistent with the vesicle size distribution measured by DLS (figure 3.1). It shows the size distribution maxima at around 30 nm and sizes up to 90 nm (figure3.1). Therefore, it is conceivable that the individual vesicle of radius R_0 forms the isolated bilayer fragment of radius nearly equal to $2R_0$.
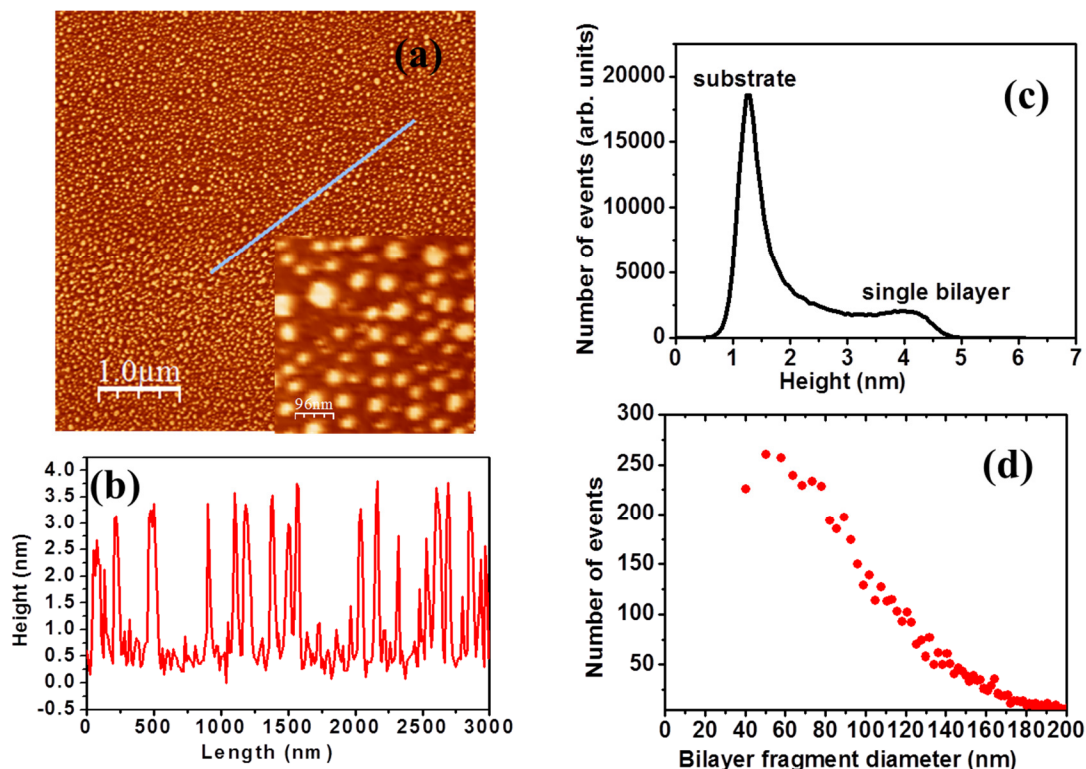
Figure 3.2. (a) AFM image of DOPC bilayer fragments on mica surface after 15 minute incubation with 10 micro liter solution and subsequent rinse with water, (b) line profile along the marked line, (c) height distribution of the surface, (d) lateral size distribution of the bilayer fragments.

When the SUV in the solution reaches randomly on the mica surface, it may rupture depending on the probability of the pore formation on the vesicle membrane and the interaction between the vesicle and mica surface [37][38]. At finite temperature, pores of a vesicle membrane appear stochastically and reseal transiently. The pore opening is driven by the membrane tension whereas its closure is guided by the pore's line tension [39]. We assumed that the vesicles in the solution

are spherical in shape. Mui et al. [40] showed that if contamination free Millipore water is used, the vesicles will swell to spherical shape after extrusion. When the vesicles are in contact with the flat hydrophilic surface, their shapes are deformed to maximize its contact area with the adhering surface [38].
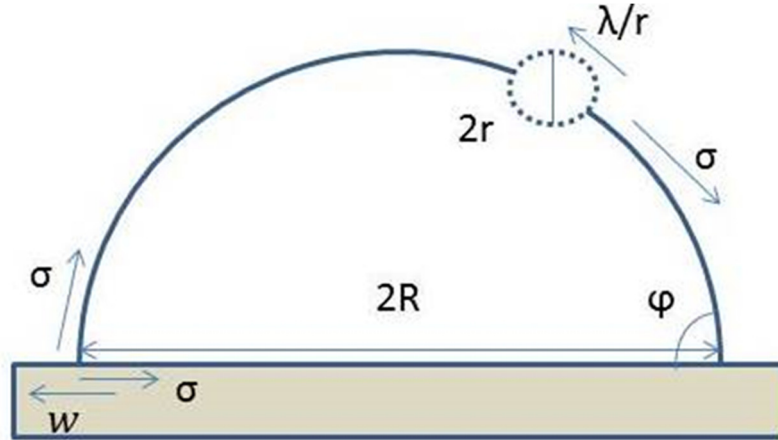
Figure 3.3. Schematic diagram of pore formation and adsorption of vesicle on a solid substrate

If we consider a cap-shaped deformed adsorbed vesicle on a mica surface (figure 3.3) as described by Takats et al. [38], the surface tension of the membrane can be described by the force balance equation of Young Dupre [41] in thermal equilibrium condition:

$$\sigma = \frac{w}{1+\cos\varphi} = w\frac{A_{\parallel}-\pi R^2}{2\pi R^2} \approx w\frac{A_0-\pi R^2}{2\pi R^2}$$

where w is the adhesion energy per unit area between the membrane and the surface, φ is the contact angle between surface and the vesicle, R is the radius of the contact area of the vesicle with the surface, $A_{\parallel}$ is the projected area of the vesicle when thermally induced undulations of the membrane are averaged, A_0 is the total area of the vesicle. A critical value of w for rupture of the vesicle of radius R_0 can be estimated by balancing the energy gain due to adhesion and the energy cost of the free edge of the final bilayer patch of radius $2R_0$,

i.e., $\qquad 4\pi R_0^2 w_{crit} = 4\pi R_0 \lambda,$

or $\quad w_{crit} = \lambda/R_0,$

where λ is the line tension of the bilayer edge. The w_{crit} obtained from this thermodynamic criterion does not guarantee the rupture of vesicle. It occurs only for significant larger value of w than w_{crit} [38]. This can be understood from the pore opening kinetics and the consequent change of surface tension.

Pore opening in the membrane is a stochastic process and can occur anywhere along the membrane. Pore formation leads to a decrease of energy $(-\pi r^2 \sigma)$ due to the relaxation of stress and increase of energy $(2\pi r\lambda)$ due to pore boundary formation [42] where r is the radius of pore and λ is the line tension. The energy of the pore can be written as

$$\Delta E \cong 2\pi r\lambda - \pi r^2 \sigma.$$

Now the maximum energy of the pore, $\Delta E_{max} = \frac{\pi\lambda^2}{\sigma}$ at $r = \frac{\lambda}{\sigma}$ which can be considered as the activation energy of pore formation. Thus, pore opening rate can be written as:

$$K_d = K_0 \frac{A_c}{a^2} exp\left[-\frac{\pi\lambda^2/\sigma}{K_B T}\right],$$

where $A_c = A_0 - \pi r^2$ is the non-adhering surface area of the vesicle, a^2 is the surface area of the lipid molecule of linear size $a \approx 0.8 \, nm$, K_0 is the local attempt rate of pore nucleation. $k_B T$ is the thermal energy. Thus, to open a pore on the membrane the value of surface tension has to exceed

$$\sigma_{crit} = \frac{\pi\lambda^2}{K_B T ln\left(\frac{K_0 A_c}{K_d a^2}\right)}.$$

At the initial stage of vesicle adsorption, the non-adhering area A_c is very small, and therefore, surface tension is larger than this threshold value. As a result the pore opens easily, but if pore reseals and adhering area increases, the surface tension drops below this threshold value. The situation is worst when vesicle is almost flat, i.e., $\varphi = 0$ and $\sigma = w/2$ (Fig. 3.3). Pore opening for adsorbed vesicle of any arbitrary shape is therefore ensured only when adhesion is larger than $w_{crit}^{pore} = 2\sigma_{crit}$ [38].

Thus, vesicle rupture is not guaranteed when $w > w_{crit}$ but it is assured when $w = w_{crit}^{pore} > 2\sigma_{crit}$. It indicates very high adhesion energy which confirms spontaneous vesicle rupture. High adhesion energy between DOPC vesicle and mica surface in the present experiment leads to the

instantaneous rupture of vesicles and formation of isolated bilayer patches of area equivalent to individual vesicles.

Earlier, quartz crystal microbalance resonant frequency and dissipation (QCM-D) combined with surface plasmon resonance spectroscopy (SPR) revealed that the vesicle rupture occurs only after a critical vesicle coverage [43]. We find that DOPC vesicles of all size rupture on mica and form bilayer patches as soon as they adhere to the surface. Reviakine et al. [5] studied SLB formation on mica also. They found both supported vesicular layers, as well as isolated bilayer patches by varying vesicle size, lipid concentration and presence of Ca^{2+} ions. Recently, Andrecka et al. [15] observed spontaneous rupture of DOPC vesicle similar to the present experiment, as well as wave like bilayer spreading on silica, mica and plasma modified mica surface. They wet the surface by buffer solution (10mM Hepes, pH6.8, 200mM NaCl, 2mM CaCl_2) first and then added the vesicle solution. They concluded that the individual vesicle rupture or wave like cascade rupture depends on the vesicle size and functionalization of the surface. Role of different ion containing buffer solution on SLB formation is complex, thus, the mechanism is not well understood. We, therefore, use ultrapure water for making DOPC vesicle solution. We have observed isolated bilayer patch repeatedly, but no supported vesicular layer has been found by AFM measurement. Leonenko et al. [1] found similar isolated bilayer patch formation as well as double bilayer formation on unmodified and modified mica surface by deposition of DOPC solution with ultrapure water. It turns out that, if the interaction between the adsorbed vesicle and substrate surface is strong enough, the vesicles rupture spontaneously at adsorption as observed in the present case, otherwise rupture of a seed vesicle is required to start a cascade or the nearby vesicles coalesce to grow larger to attain a critical size. The vesicle rupture may also take place if the adhesion property of the substrate surface is altered by deposition of polymer, chemical treatment or nanoparticles incorporation [44] [45] [46]. The distribution of fragment size (figure 3.2 d) also illustrates that the possibility of vesicle fusion within the solution or on the substrate is rare. Anderson et al. [47] also reported that a strong electrostatic attraction between the charged substrate and the uncharged vesicle helps to adhere, deform, rupture and spread as bilayer but the vesicles do not adhere or fuse each other in solution. DLS measurement of the stock solution on different days also shows no considerable change in vesicle size distribution. However, few larger bilayer fragments with the size equivalent to multiple vesicles are also observed as shown in AFM image wherever the adsorbed vesicle density is more than average.

44

To explain the isolated patch formation instead of continuous or semi continuous bilayer formation due to dilute DOPC solution deposition, we have estimated the approximate number of DOPC vesicles in 10 µl of stock solution (0.05mg/ml), deposited on 12 mm × 12 mm mica surface. 10 ul 0.05 mg/ml solution contains 0.5µg DOPC which correspond to 0.636 nanomol. The number of DOPC molecule in 0.636 nanomol is 38.3×10^{13}. If we consider each DOPC molecule to cover 0.7 nm^2 [48], then all the molecules will cover 134 mm^2 area in the form of bilayer out of 144 mm^2 mica surface if all the molecules are assumed to be adsorbed and ruptured. Leonenko el al. [1] stated that it is unlikely that every vesicle-surface interaction results in adhesion. They showed that out of 424 vesicles/μm^2 only 150 vesicles / μm^2 (approx. 35%) are adsorbed during 2 min deposition and a brief rinse. Therefore, formation of isolated bilayer patches is expected for 10 µl, 0.05 mg/ml DOPC solution deposition on 12 mm × 12 mm mica surface.
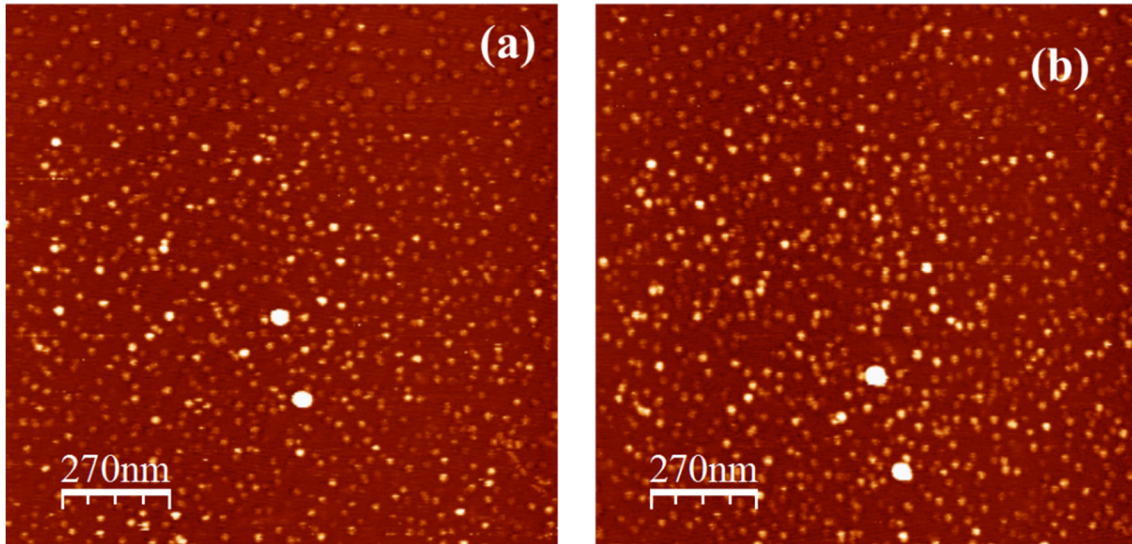
Figure 3.4: 10 microliter 0.05 mg/ml DOPC solution deposited on freshly cleaved mica and incubated for 15 minutes. Time lapsed AFM images taken in liquid mode immersed with the same solution, (a) at time 15-24 min, (b) at time 24-33

To verify the dynamic growth and stability of the bilayer patches during incubation with 10 µl stock solution (0.05mg/ml), we have recorded the AFM images of mica surface with the deposited DOPC solution. At the initial stage of incubation, bilayer fragments are formed as is observed in figure 3.2 (AFM after rinse with water). Appearance of additional patch or any considerable change of the existing bilayer fragments was not observed even after 30 minutes

45

(Figure 3.4). However, a slight lateral shift of the features is observed with time due to the thermal drift of AFM scanner [49]. This dynamic imaging during incubation indicates that no further growth or lateral movement of bilayer fragments take place with the increase of incubation time. It also confirms the strong adhesion of the first bilayer with the mica surface and immobility of the bilayer patches. Leonenko et al. also found immobility of the bilayer patches even after a long time.

In order to verify the merging of individual fragments we performed the same experiment with double quantity (20 micro liters) of DOPC vesicle solution on the same area mica substrate (12 mm ×12 mm) (figure 3.5). It is observed that the average bilayer fragment sizes increase, and most of the fragments are larger than the individual vesicle size. It indicates that when the number of the adsorbed vesicles is twice on the same substrate area, the possibility of merging of the ruptured vesicles increases. Anderson et al. [47] also predicts rare probability of merging in such diluted solution. Andrecka et al [15] never observed signature of vesicle fusion during monitoring bilayer formation from different size DOPC vesicles on different substrate by interferometric scattering microscopy. In some part of the mica surface where the adsorbed number of vesicles are sufficient to cover more area, a semi-continuous bilayer is formed due to the merging of individual bilayer fragments (figure 3.5 a). A similar type of semi-continuous bilayer is also reported for incubation with 0.5 mg /ml concentrated vesicle solution[6]. Richter et al. [9] described the formation of such extended bilayer patches as a result of cascade rupture of adsorbed neighboring vesicles on the surface. In the present case, DOPC on mica (figure 3.2, 3.4 and 3.5), the isolated or extended bilayer patches are not formed by the sequential cascade rupture. Instead, spontaneous rupture of individual vesicles on the mica surface and successive bilayer edge guided merging take place. When the coverage of adsorbed vesicles is low, each vesicle forms isolated patches (figure 2.4), but when the coverage is more, semi-continuous bilayer patches are formed due to the merging of isolated patches. When bilayer fragments are in close proximity, the edges become energetically unfavorable and are expected to promote the interaction with the adjacent lipid material. Such bilayer edges also play an important role to initiate the rupture of surface-bound or near surface vesicles as in the case of wave-induced vesicle rupture [15].   As the surface-bound vesicles are not available due to the instant rupture of the vesicle, the adjacent bilayer patches merge and minimize the energy. For example, if two equal patches of average radius R_1 merge, the resultant average radius would be $\sqrt{2}R_1$, therefore, edge energy will be reduced from $4\pi R_1 \lambda$ to $2\sqrt{2}\pi R_1 \lambda$

due to merging. Thus, the fragments coalesce and grow larger when the numbers of fragments are increased due to the increase in vesicle number. The increase of average bilayer size due to the increase of vesicle number is presented in figure 3.5d. We find only the merging of fragments but not any lateral mobility of bilayer fragments.
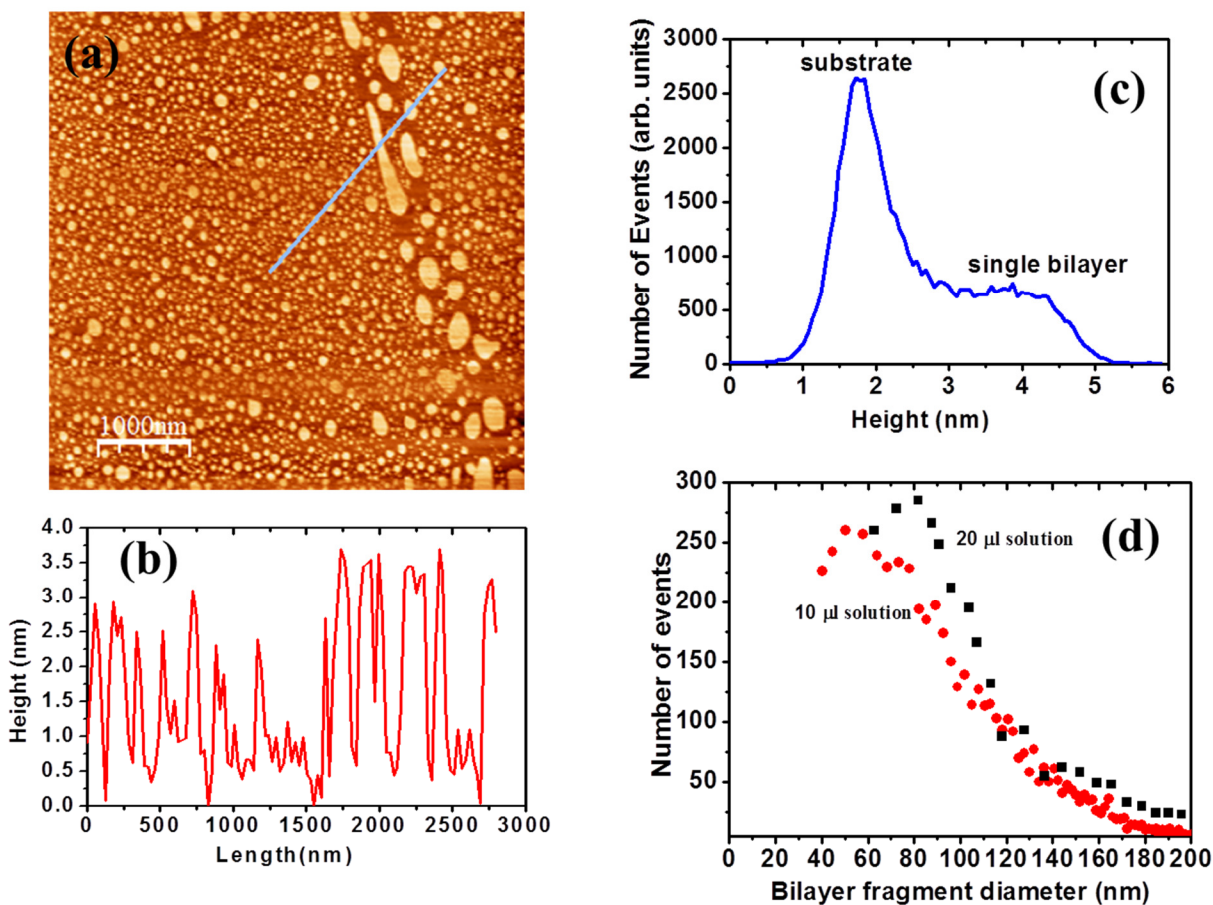
Figure 3.5. (a) AFM image of DOPC bilayer fragments on mica surface after 15 minute incubation with 20 microliter solution and subsequent rinse with water, (b) 1D profile along the marked line, (c) height distribution of surface, (d) lateral size distribution of bilayer fragments (red circles for Fig3.2(a) and black squares for Fig3.5(a)).

3.4.2 Mechanism of bilayer edge guided vesicle rupture and co-existence of double and single bilayer

In order to establish the instant rupture effect without cascading or wave induced bilayer formation [15, 43] [5], we increase the number of DOPC vesicle on the same surface area by increasing the

solution quantity (30 µl and incubation time 15 minutes). We do not find any continuous single bilayer. Instead, we have observed the co-existence of single and double bilayers (figure 3.6). If cascading or wave induced bilayer formation applies to the present case, double bilayer formation should be forbidden until the continuous single bilayer is completely formed. The presence of immobile isolated first bilayer patches leads to the second bilayer formation on it.
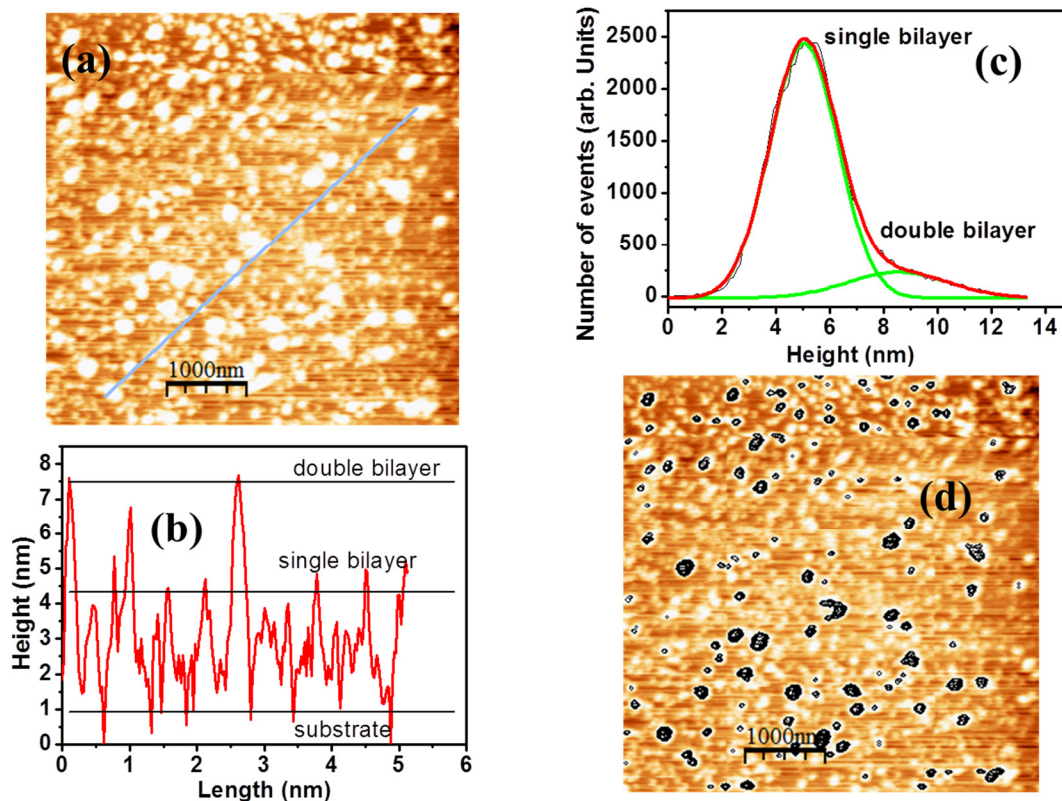
Figure 3.6. Bilayer and double bilayer formation with the increase of incubation time (15 minutes) and solution (3 times). (a) AFM image, (b) height profile along the marked line, (c) Height distribution, (d) contour plot between 4.5 to 8 nm height of AFM image shows the second bilayer of thickness ~ 3.5nm.

The adsorbed vesicle on the first bilayer may not rupture spontaneously because bilayer-bilayer adhesion is weaker than bilayer mica adhesion. However, it is stronger than the two free-standing bilayers because of the entropy loss of the surface-bound bilayer [8] [50]. Nevertheless, spontaneous rupture of adsorbed vesicle on the first bilayer and the formation of the second bilayer are rare if the first bilayer is continuous. But, if the first bilayer patches are small and isolated,

48

bilayer edges play the main role in rupturing the adsorbed vesicle on it. Bilayer edge guided rupture and stacking of double bilayer due to immobility of DOPC bilayer on mica surface can be described as follows:

In figure 3.3 we have shown that the energy of a pore $\Delta E \cong 2\pi r\lambda - \pi r^2\sigma$. Now we consider that a vesicle adsorbed on an already formed bilayer patch and a portion of the vesicle touches the edge of the patch. Assume a vesicle pore of radius r near the bilayer edge and a section of the pore boundary merge with the existing bilayer edge. Now the energy of the pore will be $\Delta E \cong 2\pi r\lambda - \pi r^2\sigma - \chi \times 2\pi r\lambda = 2\pi r\lambda(1-\chi) - \pi r^2\sigma$, where χ,the fraction of the pore boundary merges with the bilayer edge. Maximum energy $\Delta E_{max} = \frac{\pi\lambda^2}{\sigma}(1-\chi)^2$ at $r = \frac{\lambda(1-\chi)}{\sigma}$. Therefore, activation energy ΔE_{max} required for pore formation is reduced with the share of pore boundary with the bilayer edge. In case of single bilayer fragment formation, we have seen instant and spontaneous rupture of vesicle on mica surface due to strong adhesion $w = w_{crit}^{pore} > 2\sigma_{crit}$ and thereby decrease of activation energy. In case of bilayer edge guided vesicle rupture the activation energy is decreased due to the overlap of pore boundary with the bilayer edge. Although the adhesion energy of bilayer patch is not strong enough as mica substrate, the reduction of activation energy and thereby the reduction of required

$\sigma_{crit} = \frac{\pi[\lambda(1-\chi)]^2}{K_B T ln\left(\frac{K_0 A_c}{K_d a^2}\right)}$ favors the vesicle rupture Egawa et al. [25] found the single and double bilayer for successive injection of stock solution. The presence of double bilayer was also reported on silica surface, however, with time, it formed continuous single bilayer because of the mobility of the first bilayer [8]. Double bilayer may also form by hat shaped adsorption of the vesicle as modeled by Taktas et al. [50]. The existence of the double bilayer indicates again the immobility of the first bilayer and edge-induced rupture of the vesicle adsorbed on it.

3.4.3 Sequential deposition and multi bilayer formation

Stimulated by this double bilayer formation, we deposited 10 microliter stock DOPC solution successively three times with 15 minutes interval on a same area mica substrate. Figure 3.7 shows the co-existence of single, double and triple bilayer by three consecutive dropping of 10 microliter DOPC solution at 15 minutes interval and subsequent gentle rinse with water.
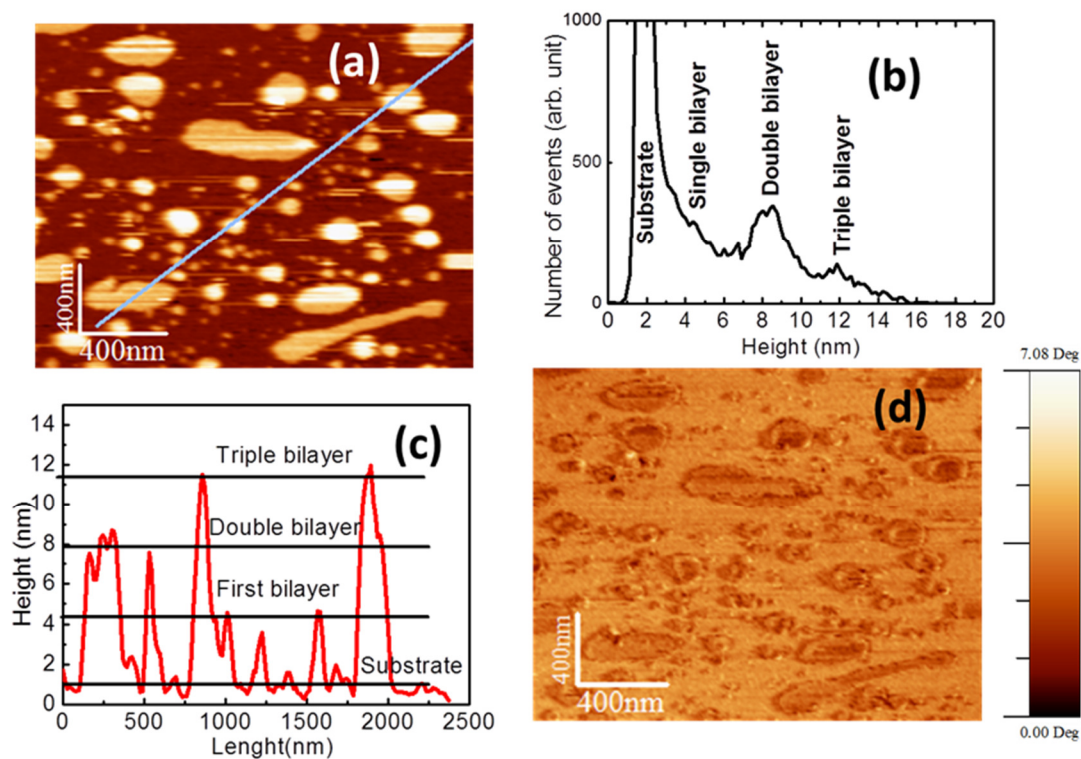
Figure 3.7: Bilayer, double bilayer and triple bilayer formation by sequential deposition of total 30 microliter DOPC solution (10 micro liter in every 15 minutes for three times and rinse after total 45 minutes incubation time) on mica surface. (a) AFM image, (b) height distribution, (c) height profile along the marked line (d) phase imaging of the same area.

Figure 3.7a shows the AFM height image, figure 3.7b shows the height distribution of the entire image and figure 3.7c presents the line profile along the marked line on figure 3.7a. Mainly, there are four groups of distributed heights, corresponding to 1) mica substrate with water layer, 2) first bilayer, 3) second bilayer and 4) third bilayer which are clearly detected. An AFM phase image of the same is also presented in figure 3.7d where the phase is inversely proportional to the height of lipid layers.
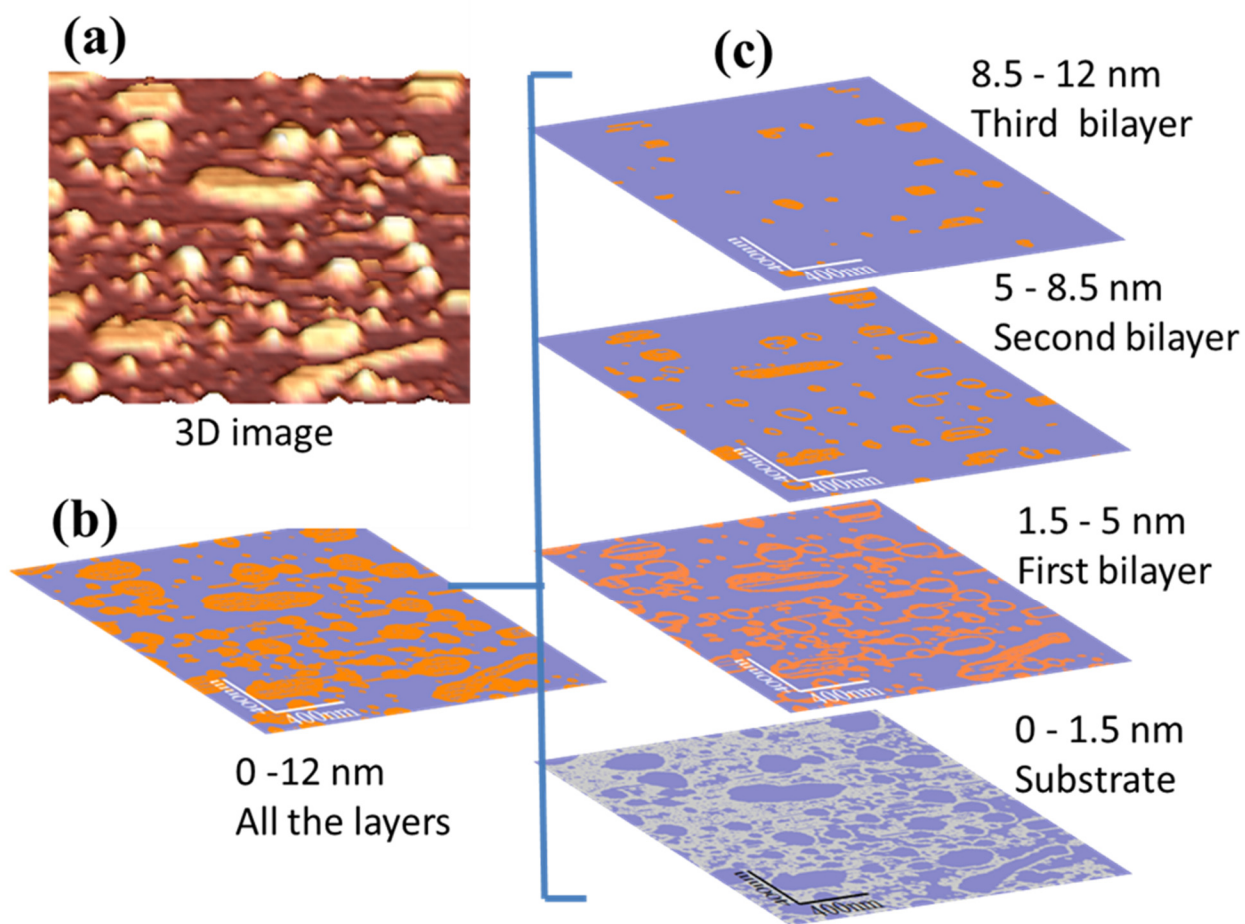
Figure 3.8: (a) 3 D topography image of figure 6a, (b) contour plot of the topography, and (c) contour plot of sliced layers shows single, double and triple bilayer zones separately.

The sequential dropping and sufficient incubation time allow the vesicles to form single, double as well as triple bilayers. Landing of vesicles on the already formed first or second bilayer fragments lead to double/triple layer formation by the edge guided rupture as discussed above. AFM topographic 3 D image and contour plot of co-existing multilayers are presented again in figure 3.8. Figure 3.8a shows 3D AFM image and 3.8b presents the contour plot of the AFM image. To show the different layers, figure 3.8b is sliced correspondence to substrate (0 - 1.5 nm), first bilayer (1.5 - 5 nm), second bilayer (5 - 8.5 nm) and third bilayer (8.5 - 12 nm), respectively, and is presented in figure 3.8c.
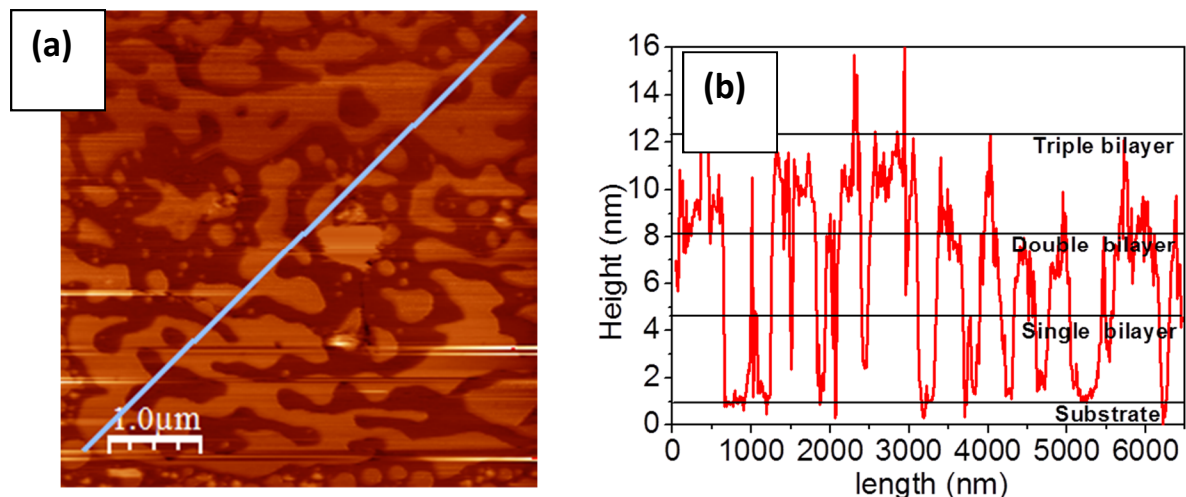
Figure 3.9. AFM image in aqueous medium shows the multi- bilayer formation due to longer incubation time (75 min) and sequential addition of total 50 micro liter DOPC solution (10 micro liter in every 15 minutes) on mica surface, (b) height profile on marked line.

Further, continual increase in vesicle number by the sequential dropping of stock solution and longer incubation time, we confirm the formation of the third bilayer as well as the coexistence of double and single bilayer. Figure 3.9 demonstrates such co-existence of single, double and triples bilayer for 75 minutes incubation with 50 microliter solution on the same area of mica surface. 10 microliter DOPC solution was added for five times at a regular interval of 15 minutes and finally rinsed gently with millipore water. The stacking of multi bilayer is confirmed by the measurement of height profile of AFM images. Figure 3.9b shows the height profile along the marked line on the AFM image where three groups of height range (1.5-5.0 nm), (5.0 – 8.5 nm) and (8.5-12.0 nm) are observed corresponding to the single, double and triple bilayer respectively. Usually, multiple bilayer formation by vesicle rupture process is rare. Sironi et al. [21] set up a large number of bilayer stacking by drop casting and drying of aqueous liposome solution. Heath et al. [20] developed a layer after layer methodology to form multiple bilayers by vesicle rupture using Poly-L-Lysine (PLL) as an electrostatic polymer linker. Jensen et al. [51] also fabricated multilamellar membrane by spin coating. In general, most of the reported multiple bilayers are either formed by drying the aqueous solution or by using linker between the bilayers [20] [21] [51]. In the present case, the third bilayer formation by sequential addition of vesicle solution is possible when the

52

first bilayer is strongly bound with the substrate and the cohesive force exists between the successive bilayers formed by the edge induced rupture mechanism.
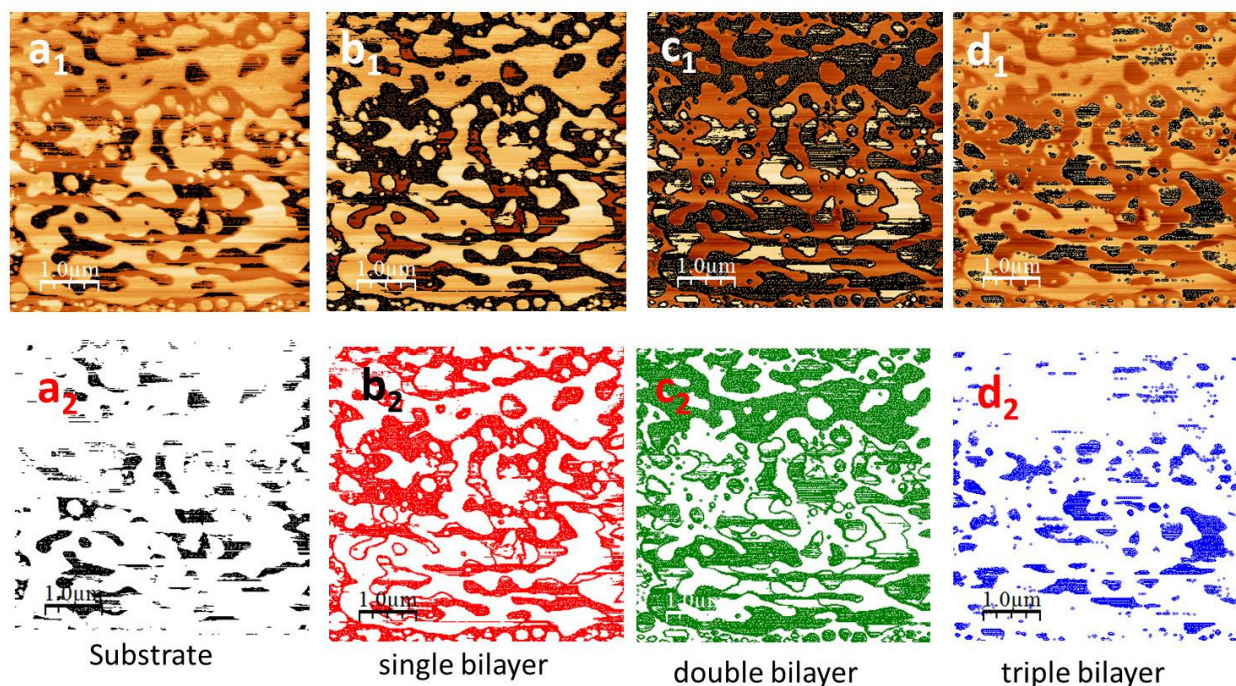
Figure 3.10. **Top row:** Contour plot (black) of AFM image 9a shows (a_1) bare substrate zones (height between 0 to 1.5 nm), (b_1) single bilayer patches (height between 1.5 to 5.0 nm), (c_1) double bilayer patches (height between 5.0 to 8.5 nm), and (d_1) triple bilayer patches (height between 8.5 to 12.0 nm).

Bottom row: The same is represented by different colors (a_2) bare substrate zones (black), (b_2) single bilayer patches (red), (c_2) double bilayer patches (green) and (d_2) triple bilayer patches (blue).

Figure 3.10 shows the contour plot of AFM image recorded after sequential dropping of 50 microliter solution and total 75 minutes of incubation. It clearly shows the co-existence of single, double and triple bilayers. It distinguishes the bare substrate zones of height 0 to 1.5 nm (3.10a), single bilayer patches of height between 1.5 and 5.0 nm (3.10b), double bilayer patches of height between 5.0 and 8.5 nm (3.10c), and triple bilayer patches of height between 8.5 and 12.0 nm

(3.10d). Strong adhesion between mica surface and vesicle leads to the first bilayer formation whereas multi-bilayer arrangement is observed due to bilayer edge guided rupture and physisorption of bilayer on bilayer. Third bilayer formation is possible only for soft landing of vesicle on second bilayer and rupture by the edge of the second bilayer. The stability of the third bilayer is very low. We observed that the third bilayer is stable on gentle rinse, but it is washed out even by moderate rinsing by water. We do not observe fourth or more bilayer by sequential addition technique because bilayer-bilayer adhesion is supposed to decrease with the increase of stacked bilayer numbers.

3.4.4 *In situ* vesicle deposition and time lapsed AFM

Instead of imaging the surface after incubation and rinse, we have monitored the isolated single bilayer formation as well as the second and third bilayer formation due to *in situ* injection of DOPC solution and time lapse AFM measurements. Figure 3.11 shows time lapse AFM images of mica surface incubated with 10 microliter 0.05 mg/ml DOPC solution as well as successive injection of additional vesicle of same concentration during imaging. Figure 3.11 (a) shows the AFM image in DOPC solution after 15 minute incubation. Additional 10 microliter vesicle solution was injected into the liquid cell at t = 42 min and time lapse AFM images were recorded. Figure 3.11 (b) shows the image taken at 42-61 min, after *in situ* injection of additional vesicle solution. Figure 3.11(c) and (d) show the images at t= 61-70 and 70-79 min, respectively. The time lapse AFM measurements are consistent with the earlier final state (after incubation and rinse) data where isolated bilayer patches as well as second and third bilayer patches are observed.
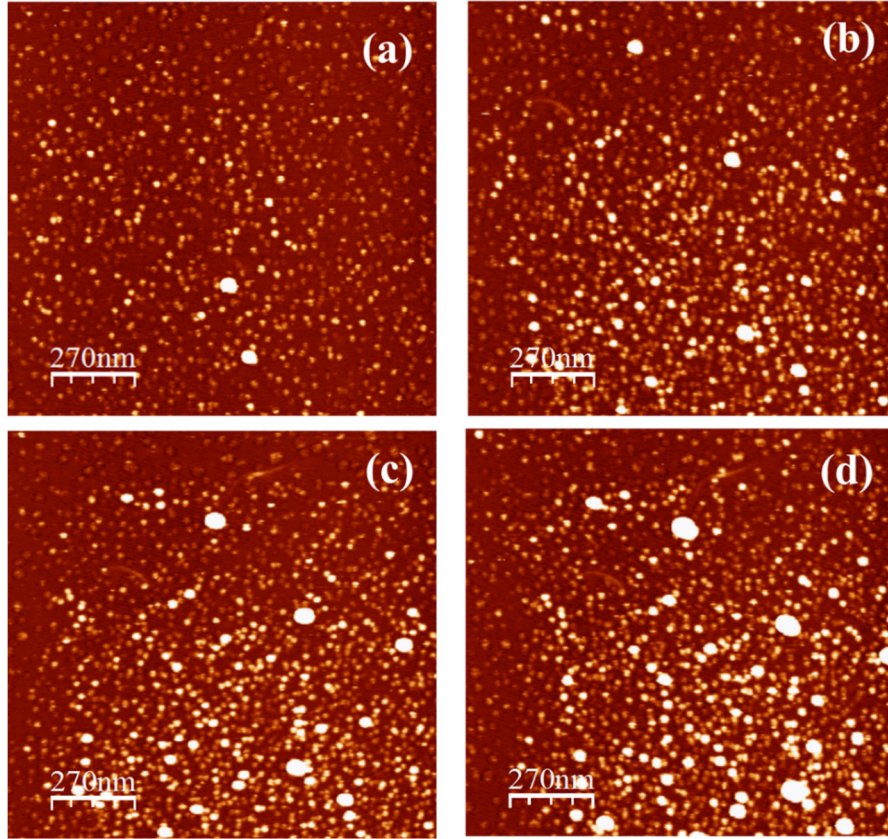
Figure 3.11: In situ sequential deposition and time lapse AFM scan. 10 microliter of 0.05 mg/ml, DOPC solution deposited on mica at t=0 and incubated for 15 minutes, (a)AFM image with DOPC solution without rinse (t=33-42 min). At t= 42 min, additional 10 microliter solution injected into the liquid cell without stopping the scan, (b) AFM image at t=52-61 min. (c) AFM image t= 61-70 min . (d) AFM image t= 70-79 min.

Figure 3.12 shows the contour plot of sliced first, second and third bilayers for *in situ* DOPC solution deposition and time lapse AFM measurements (figure 3.11). Figure 3.12 a_1,b_1,c_1,d_1, shows the dynamics of the first bilayer only. Similarly, figure 3.12 a_2,b_2,c_2,d_2 and figure 3.12 a_3,b_3,c_3,d_3 shows development and dynamics of the second and third bilayer, respectively. It is observed that the coverage by isolated bilayer increases with time after *in situ* injection of DOPC solution as well as the second and third bilayers appear and increase in number. However, the numbers of second and third bilayer patches are few compared to the first bilayer. We rarely observe adsorbed vesicle on the mica surface; either by deposition and rinse with water or time lapse measurement with successive deposition of DOPC solution. Brison et al. [5] reported SLB formation on mica, but in some cases, they reported the patches as adsorbed vesicle. In the present case adsorbed

vesicles (~ 60 nm diameter) can be easily distinguished from the ruptured bilayer(s). Leonenko et al. [1] also mentioned that the observation of adsorbed vesicles [5] may be due to the difference in sample preparation [1]. In case of non-rinse time lapse AFM images (figure 3.11, 3.12) the heights of severely flattened intact vesicle on mica and on first bilayer are equivalent to second and third bilayer, respectively. We believe that severely flatten adsorbed vesicles will be unstable and will result in the formation of second or third bilayer by rupture at the edge. Leonenko et al. [1] also concluded that the two bilayer height patches as the double bilayer.
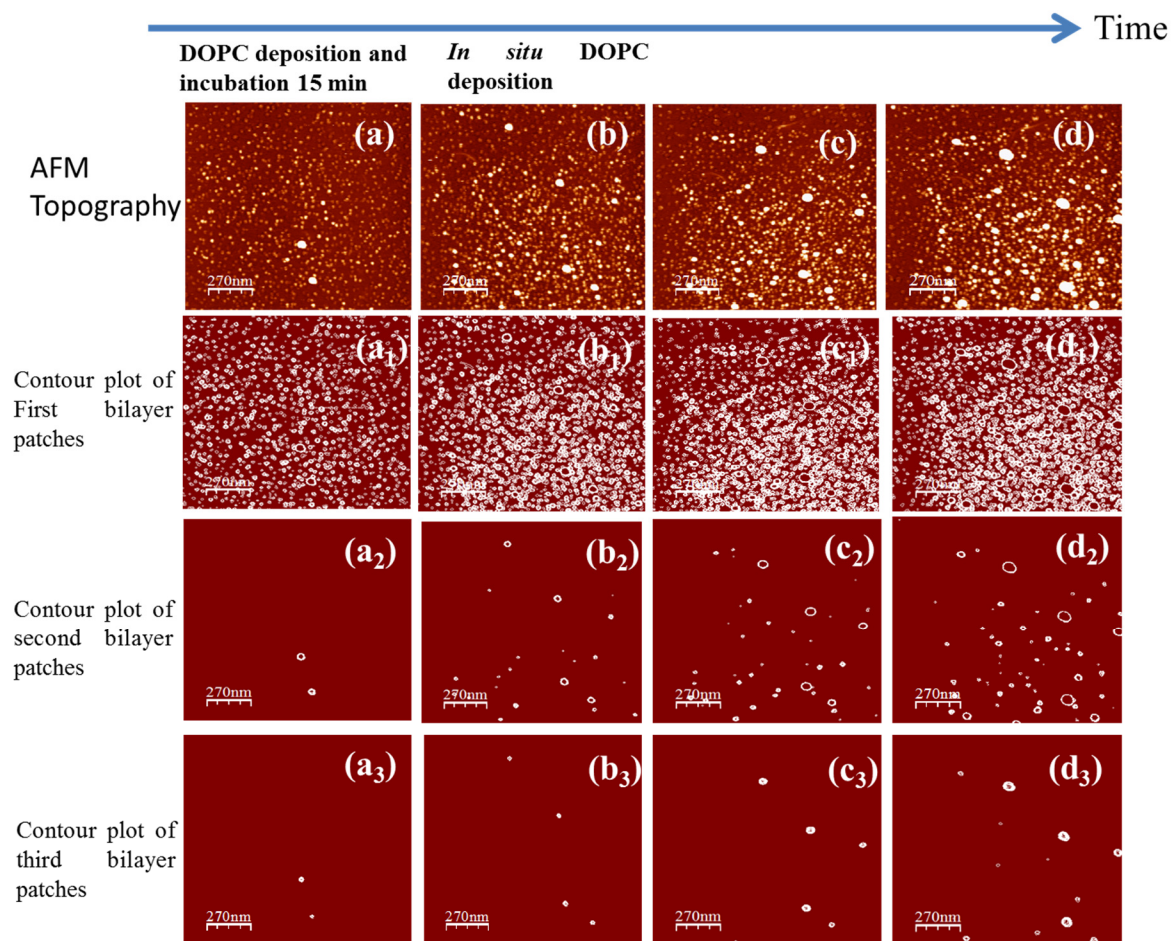
Figure 3.12: In situ sequential deposition and time lapse AFM scan. Top row: shows the, b, c, d of fig. 3.11. Corresponds to (a,b,c,d), (a_1,b_1,c_1,d_1) are the contour plot of sliced first bilayer (height between 1.5 to 5.0 nm) patches only; (a_2,b_2,c_2,d_2) are the second bilayer (height between 5.0 to 8.5 nm) patches only; and (a_3,b_3,c_3,d_3) third bilayer (height between 8.5 to 12.0 nm) patches only.

Formation of single, double and triple bilayer on mica due to DOPC vesicle adsorption is schematically summarized in figure 3.13. It shows selection of strong adhesive mica substrate and diluted DOPC stock solution (0.05mg/ml) where total number of vesicles in 10 µl is insufficient to cover the entire substrate area (12 mm × 12mm) forms random isolated patches (13a). Figure 3.13 b shows addition of DOPC solution of same concentration increases the bilayer coverage area as well as forms a second bilayer due to adsorption and rupture of vesicle at the edges of previously formed bilayer patches. Due to immobility of the first bilayers the ruptured vesicle piles partially or fully on first bilayer and forms
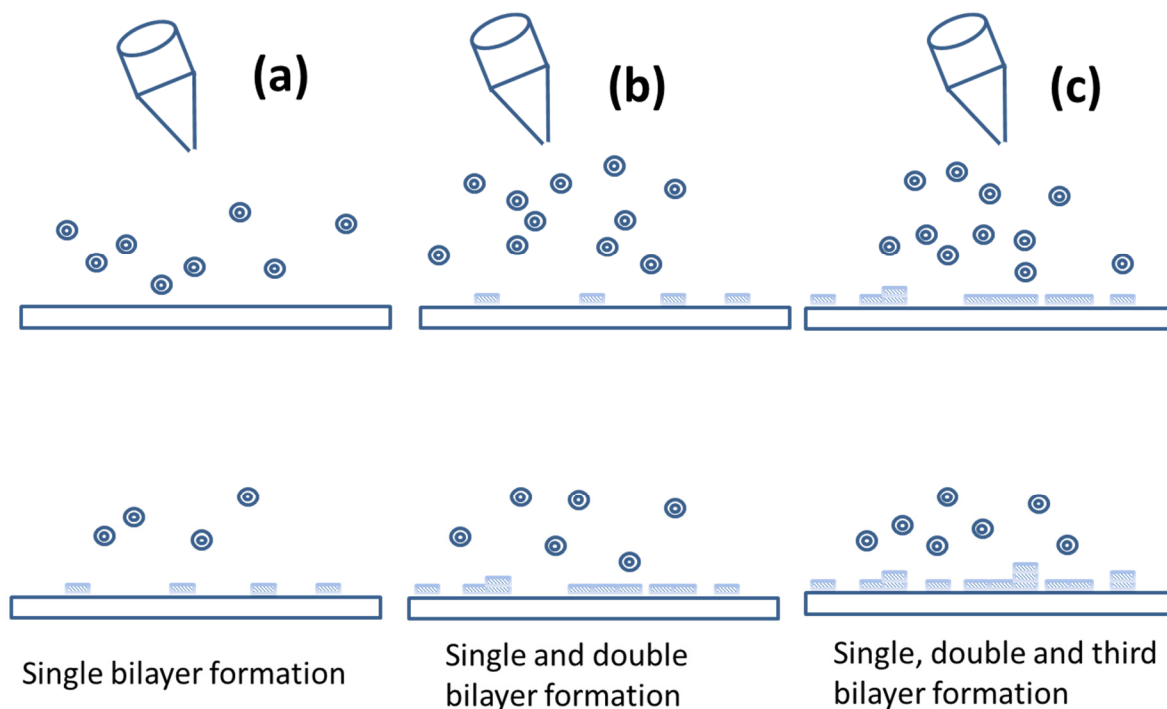
Figure 3.13. Schematic representation of vesicle adsorption, rupture and (a) single (b) double (c) triple bilayer formation

the second bilayer. The third bilayers (figure 3.13 c) are observed by sequential addition of droplets from the stock solution during incubation. The added vesicles are gently adsorbed on the already formed single or double bilayer patches and are ruptured when they find the bilayer edge. Although the adhesion between second and third bilayer is assumed to be weak, immobility of first and second bilayer allow part of the ruptured vesicle to stay on the second bilayer. Thus vesicles

in the first deposited diluted solution are depleted and form isolated bilayer patches. Successive addition of stock solution increases again the number of vesicles on the same surface. Thus, in addition to increasing first bilayer coverage area, the presence of bilayer edges of previously formed bilayer patches aid to form second and third bilayers due to sequential deposition of diluted DOPC solution on mica surface. No requirement of special substrate treatment or linker addition, second or third bilayers formation by sequential dilute solution dropping is consistent and simple as well as more close to the natural multilayer system.

The instant rupture of adsorbed vesicle, observed isolated bilayer patch formation, as well as coexistence of second and third bilayer is due to strong adhesion between mica surface and DOPC lipid molecules. The adhesion between mica and vesicle can be understood through the interaction force between mica surface and lipid vesicles in aqueous media. The total interaction force acting between the support and lipid bilayer in water media can be divided into two major parts. The first one is the attractive force between zwitterionic DOPC molecule and negatively charged freshly cleaved mica surface, where the other is the repulsive hydration force, originated due to the tendency of bulk water to fill the space between bilayer and support [52] [47]. The charge density on the substrate surface strongly influences the vesicle adhesion and rupture process [47]. It is shown that presence of external ions modify the interaction by screening the charge as well as directly interact with the support and lipid molecules [53] [54]. The influence of divalent ions like Ca^{2+} shows surprising effect on vesicle adsorption and rupture [9]. Mica has layered structure, where negatively charged aluminosilicate layers are interconnected by positively charged K^+ ions as described before. The freshly cleaved mica surface shows super hydrophilic behavior. At the time of cleavage, top K^+ layer is disrupted and expose the basal negatively charged aluminosilicate layer. If the cleaved mica surface is kept in air the surface charge is compensated by the bulk lattice charge [55]. In the present case, the strong adhesion of mica surface is not fully understood; however, strong negative surface charge of freshly cleaved mica is the major source of strong adhesion. Cha et al. [56] also reported that adhesion increases with increase of surface charge density. They showed charge neutral (zwitterionic) vesicles readily rupture and form supported phospholipid bilayers when the density of surface charge is high. We have seen that the water contact angle of freshly cleaved mica is lowest; it increases with time as the surface charge is slowly compensated by the bulk charge. We observe isolated bilayer patches as well as coexistence of second and third bilayer for dilute DOPC solution deposition without addition of

ionic solution, however, uniform patch distribution is observed in local (Jharkhand, India) mica whereas both large and small bilayer patches are observed on MTI mica. This indicates mobility of bilayer patches on MTI mica is little more which increases merging probability and creates larger bilayer patches. Second and third bilayer patches are also found to form on MTI mica, however, are less in number due to less available bilayer edges (data not shown). This observation indicates the adhesion property of Jharkhand mica is slightly more than the MTI mica. Markedly difference in bilayer formation was also reported for different silica surface [9].

3.5. Conclusion

We examined the growth of single as well as multiple bilayers of DOPC vesicle on highly hydrophilic mica surface by simple vesicle fusion method without any complex preparation of the substrate or incorporation of external reagent. AFM measurements of water rinsed bilayer surface shows no movement, cascading or wave-like vesicle rupture, rather the vesicles are ruptured spontaneously at the contact of strong adhesive mica surface. The interaction between the edges of adjacent isolated bilayer fragments plays the role of merging. Multi bilayers are formed by further adsorption of vesicle on the already formed bilayer and rupture by the edge of the supported bilayer patches.

The direct observation of co-existence of single, double and triple lipid bilayer by quantitative AFM measurement shows excellent prospect not only for easy preparation of single and multiple lipid bilayer but also for the study of the interaction of proteins or drugs with single and multiple DOPC bilayers in a single system.

Further study of such system by X-ray, cryo-TEM and other complimentary techniques as well as selection of other substrate-lipid combinations with strong adhesion property may reveal more information and way out to increase the layer beyond the third bilayer. Formation of coexisted bilayer and stacked multiple bilayers in natural aqueous solution will opens up possibilities for new biophysical studies on interaction between membranes as well as membrane associated proteins with co-existed single and multiple bilayers.

References:

[1]   Z.V. Leonekko, A. Carnini and D.T. Cramb, Biochimica et Biophysica Acta 1509 (2000) 131-147.

[2]   K.B. Blodgett, J. Am. Chem. Soc. 57 (1935) 1007.

[3]   R. Richter, A. Mukhopadhyay and A. Brisson, Biophys. J. 85 (2003) 3035.

[4]   C. Kataoka-Hamai, M. Higuchi, H. Iwai and Y. Miyahara, Langmuir 26 (2010) 14600.

[5]   I. Reviakine and A. Brisson, Langmuir 16 (2000) 1806.

[6]   S.J. Attwood, Y. Choi and Z. Leonenko, Int. J. Mol. Sci. 14 (2013) 3514.

[7]   K.L. Weirich, J.N. Israelachvili and D.K. Fygenson, Biophys. J. 98 (2010) 85.

[8]   J. Jass, T. Tjärnhage and G. Puu, Biophys J. 79 (2000) 3153.

[9]   R. Richter, R. Berat and A.R. Brisson, Langmuir 22 (2006) 3497.

[10]   A. Åkesson, T. Lind, N. Ehrlich, D.Stamou, H.P. Wacklin and M. Cárdenas, Soft Matter 8 (2012) 5658−5665.

.

[11]   T.K. Lind, H. Wacklin, J. Schiller, M. Moulin, M. Haertlein, T.G. Pomorski and M. Cárdenas, PLoS ONE 10 (2015) e0144671.

[12]   R.P. Richter and A.R. Brisson, Biophys. J. 88 (2005) 3422−3433.

[13]   H.P. Wacklin, Langmuir 27 (2011) 7698.

[14]   H.P. Wacklin and R. K.Thomas, Langmuir 23 (2007) 7644.

[15]   J. Andrecka, K.M. Spillane, J. Ortega-Arroyo and P. Kukura, ACS Nano 7 (2013) 10662.

[16]   U. Bernchou, J. Brewer, H.S. Midtiby, J.H. Ipsen, L.A. Bagatolli and A.C. Simonsen, J. Am. Chem. Soc. 131 (2009) 14130.

[17]   X. Han, A.S. Achalkumar, M.R. Cheetham, S.D.A. Connell, B.G. Johnson, R.J. Bushby and S.D. Evans, Chem Phys Chem 11 (2010) 569

[18]   M. Kang, M. Tuteja, A. Centrone, D. Topgaard and C. Leal, Adv. Funct. Mater. (2018) 1704356.

[19]   Y. Zhu, A. Negmi and J. Moran-Mirabal, Membranes 5 (2015) 385-398.

[20]   G.R. Heath, M. Li, I.L. Polignano, J.L. Richens, G. Catucci, P. O'Shea, S.J. Sadeghi, G. Gilardi, J.N. Butt and L.J.C. Jeuken, Biomacromolecules 17 (2016) 324.

[21] B. Sironi, T. Snow, C. Redeker, A. Slastanova, O. Bikondoa, T. Arnold, J. Kleine and W.H. Briscoe, Soft Matter 12 (2016) 3877.

[22] M. Vogel, C. Mu¨nster, W. Fenzl and T. Salditt, Phys. Rev.Lett. 84 (2000) 390.

[23] L. Perino-Gallice, G. Fragneto, U. Mennicke, T. Salditt and F. Rieutord, Eur. Phys. J. E: Soft Matter Biol. Phys. 8 (2002) 275.

[24] S.A. Tristram-Nagle. in (Dopico, A.M., ed.) Methods in Membrane Lipids, Humana Press 2007, pp. 63–75.

[25] H. Egawa and K. Furusawa, Langmuir 15 (1999) 1660-1666.

[26] Y. Okamoto, K. Tsuzuki, S. Iwasa, R. Ishikawa, A. Sandhu and R. Tero, Journal of Physics: Conference Series 352 (2012) 012017.

[27] M.J. Hope, M.B. Bally, G. Webb and P.R. Cullis, Biochim. Biophys. Acta. 812 (1985) 55.

[28] D. Bhowmik and P. Karmakar, Surf Interface Anal. 51 (2019) 667-673.

[29] D. Bhowmik and P. Karmakar, Nuclear Inst. and Methods in Physics Research B 422 (2018) 41-46.

[30] K. Müller and C.C. Chang, Surf. Sci. 14 (1969) 39.

[31] A. Gimeno, P. Ares, I. Horcas, A. Gil, J.M. Gomez-Rodriguez, J. Colchero and J. Gomez-Herrero, Bioinformatics 31 (2015) 2918-2920.

[32] S.p. Mornet, O. Lambert, E. Duguet and A. Brisson, Nano Letters 5 (2005) 281-285.

[33] S.J. Attwood, Y. Choi and Z. Leonenko, Int .J. Mol. Sci 14 (2013) 3514-3539.

[34] Z. LV, S. Banerjee, K. Zagorski and Y.L. Lynbchenko, Methods Mol Biol 1814 (2018) 129-143.

[35] R. Tero, K. Fukumoto, T. Motegi, M. Yoshida, M. Niwano and A. Hirano-Iwata, Scientific Reports 7 (2017) 17905.

[36] H. Schonherr, J.M. Johnson, P. Lenz and S.G. Boxer, Langmuir 20 (2004) 11600.

[37] J.N. Israelachvili, Intermolecular and Surface Forces, Third ed., Academic Press, Waltham, MA, 2011.

[38] A. Takáts-Nyeste and I. Derényi, Phys. Rev. E 90 (2014) 052710.

[39] E. Karatekin, O. Sandre and F. Brochard-Wyart, Polym. Int. 52 (2003) 486.

[40] B.L.-S. Mui, P.R. Cullis, E.A. Evans and T.D. Madden, Bio-phys. J. 64 (1993) 443.

[41] U. Seifert and R. Lipowsky, 42 (1990) 4768.

[42] W. Helfrich and R.-M. Servuss, Il Nuovo Cimento D 3 (1984) 137-151.

[43]   C.A. Keller, K. Glasmästar, V.P. Zhdanov and B. Kasemo, Phys. Rev. Lett 84 (2000) 5443.

[44]   M. Tanaka, M. Tutus, S. Kaufmann, F.F. Rossetti, E. Schneck and I.M. Weiss, Journal of Structural Biology 168 (2009) (2009) 137–142.

[45]   A. Melcrova, S. Pokorna and L. Cwiklik, Sci.Rep. 6 (2016) 38035.

[46]   A. Verma and F. Stellacci, Small (2009) 1-10.

[47]   T.H. Anderson, Y.J. Min, K.L. Weirich, H.B. Zeng, D. Fygenson and J.N. Israelachvili, Langmuir 25 (2009) 6997.

[48]   N. Kucerka, S. Tristram-Nagle and J.F.Nagle, J Membr Biol. 208 (2005) 193-202.

[49]   Y. Wang, H. Wang and S. Bi, AIP Advances 4 (2014) 057130.

[50]   A.a. Tak´ats-Nyeste and I. Der´enyi, Langmuir 30 (2014) 15261.

[51]   M.H. Jensen, E.J. Morris and A.C. Simonsen, Langmuir 23 (2007) 8135-8141.

[52]   A. Pertsin and M. Grunze, J. Chem. Phys. 140 (2014) 184707.

[53]   J. Raedler, H. Strey and E. Sackmann, Langmuir 11 (1995) 4539-4548.

[54]   C. Hennesthal and C. Steinem, J. Am. Chem. Soc. 122 (2000) 8085-8086.

[55]   T.E. Balmer, H.K. Christenson, N.D. Spencer and M. Heuberger, Langmuir 24 (2008) 566-1569.

[56]   T. Cha, A. Guo and X.-Y. Zhu, Biophysical Journal 90 (2006) 1270-1274.

Chapter 4

Investigation of nanomechanical properties of cholesterol rich domains in mica supported lipid-cholesterol membrane:

4.1. Introduction:

In chapter 3 we have examined the growth of single as well as multiple bilayers of DOPC vesicle on highly hydrophilic mica surface by simple vesicle fusion method without any complex preparation of the substrate or incorporation of external reagent and discussed the possible mechanism. Next, we are interested in studying various bio-molecular interactions with the solid supported lipid bilayer. In this chapter we have investigated how cholesterol initiates the formation of cholesterol rich nano-domains in pure DOPC solid lipid bilayer at room temperature. The cell membrane undergoes various changes to modify its composition and mechanical properties to control the functioning of cellular mechanisms in which cholesterol is highly involved. The height modulation and the mechanical properties of lipid bilayer have been explored for insertion of 1 to 40 mole percent of cholesterol by Peak Force Quantitative Nano Mechanical Atomic Force Microscopy (PF-QNM AFM). Cholesterol rich and cholesterol poor domains are distinctly observed at 5% cholesterol insertion in the pure DOPC SLB. The cholesterol rich nano domain with increased height is observed upto 25% cholesterol insertion within the membrane. Further increase of cholesterol leads to shrinkage of bilayer height and increase of DMT modulus. It suggests the occurrence of interdigitation of the ordered acyl chains of the two leaflets within the membrane at high cholesterol concentration.

Before we discuss our experimental results, we summarize earlier studies in section 4.2. The experimental part is described in section 4.3. Detailed results and discussion are given in section 4.4. Finally, we summarized this chapter in section 4.5.

4.2. Earlier studies:

Diversity in the chemical composition and phase behavior of the cell membrane enables it to play a significant role in controlling various cell related activities like cell signaling [1], budding [2], signal transduction [3], and enzymatic activities [4][5]. Among all chemical composition, cholesterol is a ubiquitous component of all eukaryotic cells. It regulates variety of cellular event including endocytosis and exocytosis. Cholesterol makes the membrane less permeable to ions[6] proteins[7] and other biomolecules keeping the basic fluid nature of the membrane, as well as provides mechanical stability by imparting higher ordering of the lipid molecules in the membrane. Various experimental techniques are exploited to gain insights into the various cellular functions using artificial model membrane, such as lipid bilayer. A form of high-resolution secondary ion mass spectrometry (Nano SIMS) has revealed lipid distribution within a phase-separated membrane[8]. Fluorescence microscopy and fluorescence correlation spectroscopy is utilized to visualize distinct lipid phases and lateral heterogeneities within artificial membranes [9]. A cholesterol induced modulated phase, denoted as P_β, is found in the study of phase behaviour of dipalmitoyl phosphatidylcholine (DPPC)-cholesterol mixtures by small angle x-ray diffraction studies of oriented multilayers[10][11]. Infra-red and Raman studies indicate that carbonyl group of phosphatidylcholine is perturbed by the inclusion of cholesterol[12]. C Levine and Wilkins[13] found through comprehensive x-ray study that cholesterol helps to orient hydrophobic tails of the phospholipids to the normal of the bilayer plane[13]. As a result, phosphate to phosphate distance is increased and the bilayer gets thickened. AFM is also very popular technique as it offers a label-free measurement to monitor the changes in a coupled system therefore provides multiple signatures to characterize the SLB formation along with subsequent membrane morphological responses, as previously established in several work [14] [15] Sullan et al. [16] demonstrated the influence of different amount of cholesterol on the morphology and nanomehanical properties of artificial lipid bilayer using correlated AFM based imaging and force mapping. They found cholesterol mediated liquid ordered domain in the phase segregated lipid bilayer. Various ternary systems composed of saturated lipids, an unsaturated lipids and cholesterol are known to exhibit phase separation between cholesterol rich liquid ordered phase(lo) and cholesterol poor liquid disordered phase(ld) [17] at intermediate cholesterol concentration. This phase separation helps integral membrane proteins to respond by changing conformation of the membrane [18]. Such a

phase separation has not been seen in a binary lipid-cholesterol mixture. However, various literature depicts the evidence of cholesterol containing domain formation in the lipid –cholesterol binary system[18] [19]. Sarangi et al produced direct experimental evidence of dynamic heterogeneity at the nanodomain formed in binary phospholipid-cholesterol bilayers using super-resolution stimulated emission depletion(STED) microscopy coupled with fluorescence correlation spectroscopy (FCS). Matti Javanainen et al simulated a binary system of DPPC-cholesterol bilayer and observed the spontaneous formation of cholesterol rich nanodomains in disordered and cholesterol poor membrane instead of phase separation [19].

The influence of cholesterol on unsaturated phospholipids has received considerable research attention nowadays [20] [21]. DOPC is an unsaturated lipid whose transition temperature is low(-18°C), usually remains in liquid disordered phase in solid supported bilayer structure at room temperature. [22] Unlike saturated lipid, incorporation of greater amount of cholesterol in an unsaturated lipid like DOPC having two mono-unsaturation at the acyl chains cannot produce enough rigidity to the membrane. [23] The natural membrane itself utilize cholesterol of various proportions for proper functioning. In mitochondria, Golgi body and ER contain very low cholesterol concentration (<10%), whereas in plasma membrane (about 30%), and the nerve cell (> 40%) possess much higher amount of cholesterol. Strikingly unsaturated PC lipid level also high in mitochondria (~40%) and DOPC lipid resides in these organelles also[24].But most of the studies regarding the interaction of cholesterol and unsaturated lipid are computation based[25] and there are few direct experimental observations in solid supported lipid bilayer found in literature where cholesterol concentration is systematically varied to DOPC like unsaturated phospholipid bilayer system [26] [27]. So inquisitively in order to view the effect of cholesterol on unsaturated lipid bilayer we choose pure DOPC and different amount of cholesterol in our study and investigated mechanical properties of the lipid cholesterol binary system. [28, 29] We systematically proved by AFM measurement that cholesterol containing nano-domain also exists in purely unsaturated lipid like DOPC bilayer which resemble with the formation of lipid ordered domains.

4.3. Experimental:

Lipid mixtures were prepared in chloroform solvent by combining the appropriate molar ratios of DOPC and cholesterol(0%,1%,5%,10%,15%,20%,25%,35%,40%) and small unilamellar vesicles (SUVs) were prepared by following the extrusion method described by Hope et al. (1985) [30] as discussed in the experimental section in chapter 2 . Final concentration of the SUV solution is maintained at 0.05mg/ml. The size distribution of extruded vesicles was measured by the DLS technique. The procedure is discussed elaborately in chapter 2. Solid lipid bilayer is prepared by vesicle fusion method. Utmost care was taken to prevent the sample from de-wetting.

All AFM measurements were performed in a standard liquid cell operated in Peak Force QNM (Peak Force-Quantitative Nano-Mechanical) mode with ScanAsyst-fluid probe. In this measurement, the probe (tip) engages the sample until a set value of the applied force is reached and then disengages. In this mode, each tapping utilizes engage and disengage sequence of a force curve, which in turn extracts the information regarding the mechanical properties of the sample in every single location as shown in figure 4.1[14, 31, 32]. In this experiment, the tip radius was 10 nm and the spring constant was 0.35–1.4 N/m. The maximum tip sample separation was 1 um and the peak force was kept fixed at 1 nN. The scan rate, integral gain and proportional gain were adjusted by Scan-Asyst Auto Mode where other scan parameters were controlled manually. The system was calibrated following the standard procedure [31] before the measurements. The AFM images were line flattened with WSxM software to eliminate slopes, bows, and/or bands in the images. Using the same software, the statistical distribution of heights and DMT modulus and deformations were presented. The reduced Young's Modulus is obtained by using the Derjaguin, Muller, Toropov (DMT) model [32, 33].
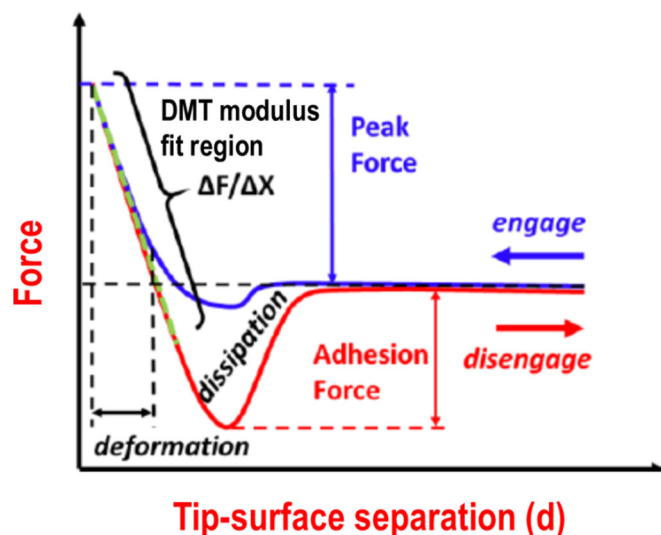
Figure 4.1. Schematic plot of force vs tip-surface separation represents different regions of nano-mechanical quantities.

4.4. Results and Discussion:

4.4.1 Topographic inhomogeneity of DOPC lipid bilayer in presence of cholesterol:

Topographical images and one-dimensional line profiles of freshly cleaved mica, SLB of pure DOPC and DOPC with 5% cholesterol are shown in figure 4.2. Figure 4.2(a) shows the smooth AFM topography of freshly cleaved mica taken under millipore water. The line profile along the marked line shows an average surface height of 0.5 nm. Figure 4.2(b) shows the topography of a pure DOPC lipid bilayer on the mica surface, where isolated bilayer patches are observed. The line profile shows the average bilayer height around 3.2 nm which is consistent with the earlier reports on SLB of DOPC [37]. Figure 4.2(c) presents the image of the DOPC bilayer with the insertion of 5% cholesterol, where we notice a new height group at 4 nm in addition to the pure DOPC SLB (3.2 nm) and bare mica (0.5 nm). The observed zonal rise in the height of the bilayer at 5 mol% of cholesterol suggests that the cholesterol is non-uniformly distributed within the DOPC bilayer [38].
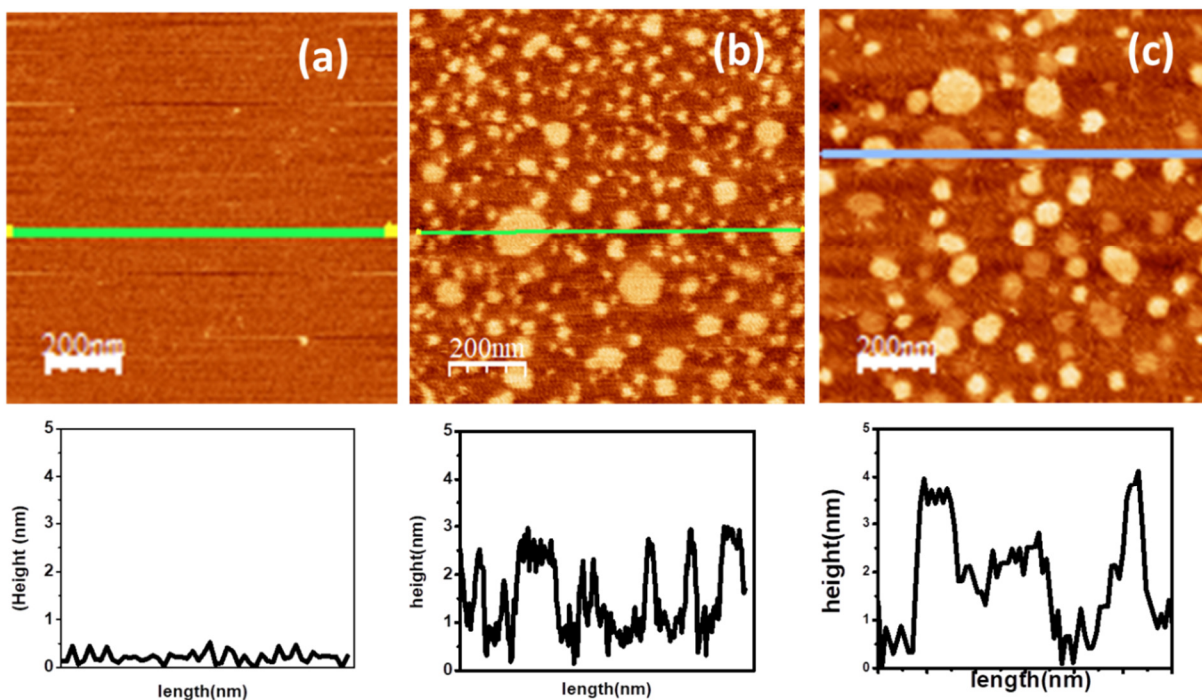
Figure 4.2: AFM topography and height profile along the marked line for (a) pure mica, (b) pure DOPC lipid bilayer (c) DOPC lipid bilayer with 5% cholesterol.

To understand the effect of cholesterol on the structure of the DOPC lipid bilayer, we prepared the bilayers with varying mole fractions of cholesterol from 0% to 40%. The topography and the line profiles are shown in figure 4.3. Figure 4.3(a) shows the bilayer image for 0% cholesterol which is similar to figure 4.2(b), however, cholesterol-containing bilayers with higher thickness are clearly distinguishable for the addition of 5% cholesterol (figure 4.3(b)).

The difference in height variation of the bilayer is more prominent at 10% cholesterol (figure 4.3(c)). There are two specific height distributions observed in figure 4.3(c) where cholesterol-rich domains with increased height (around 4 nm) are observed. Kawakami et al. [39] demonstrated the coexistence of liquid-disordered and liquid-ordered phases for unsaturated and saturated phospholipids, respectively, at relatively low molar fractions of cholesterol [39]. Here, we find the coexistence of cholesterol rich and poor bilayers for DOPC like unsaturated phospholipid. The coverage by the cholesterol rich bilayer is increased further on increasing cholesterol concentration of 15% and 20% (figure 4.3(d) and 4.3(e)). For 25% cholesterol (figure 4.3(f)), cholesterol-rich zones of thickness 4 - 4.5 nm are dominating.
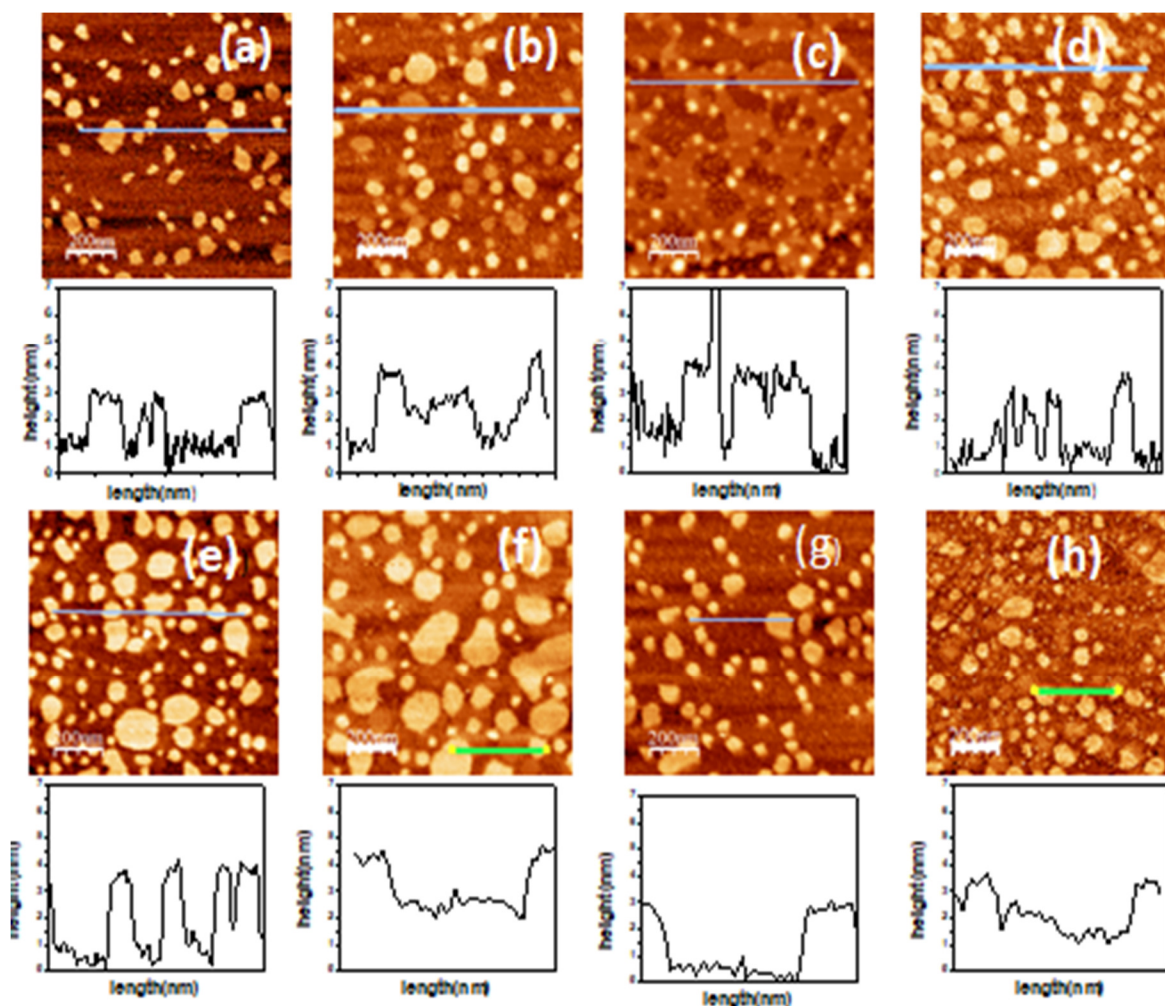
Figure 4.3 : The height variation of DOPC bilayer for different mole % of cholesterol (a) 0% cholesterol, height range 2.5 nm - 3.2 nm; (b) 5% cholesterol, two height ranges: 2.9 nm-3.1nm, 3.5 nm - 4 nm ; (c) 10 % cholesterol, two height ranges: 2.5 nm - 3 nm, 4 nm - 4.7 nm; (d) 15% cholesterol, two height ranges: 2.9 nm - 3.1 nm, 4 nm - 4.5 nm; (e) 20% cholesterol, height range: 3.5 nm - 4.5 nm; (f) 25% cholesterol, height ranges :2.5 nm - 4.6 nm; (g) 35% cholesterol, height range: 2.5 nm - 3.2 nm; (h) 40% cholesterol, height range :2.3 nm - 3 nm.

For cholesterol concentration > 25 mol %, the bilayer shows a lowering in height due to the reverse condensation of DOPC lipid molecules in the lateral direction. The figures 4.3(g) and 4.3(h) show the DOPC bilayer images for the addition of 35% and 40% cholesterol where the bilayer thickness shrinks to 3.5 nm. The simulation study by Olsen et al. [40] shows that more cholesterol insertion within the DOPC lipid bilayer leads to interdigitation of phospholipid tail which reduces the height

of the lipid bilayer [41]. In our study, we also speculate that interdigitation of phospholipid chains might lead to the shrinkage of cholesterol rich bilayer for cholesterol concentration > 25%. The drop of DOPC bilayer height at higher cholesterol (25-35%) following an initial increase, observed by simulation [40] [41], is in agreement with our experimental results.

We discuss the statistics in order to gain more insights into the cholesterol induced nano-domains. The figure 4.4 shows the histogram of height distribution of DOPC lipid bilayers for insertion of 0% -40% cholesterol.
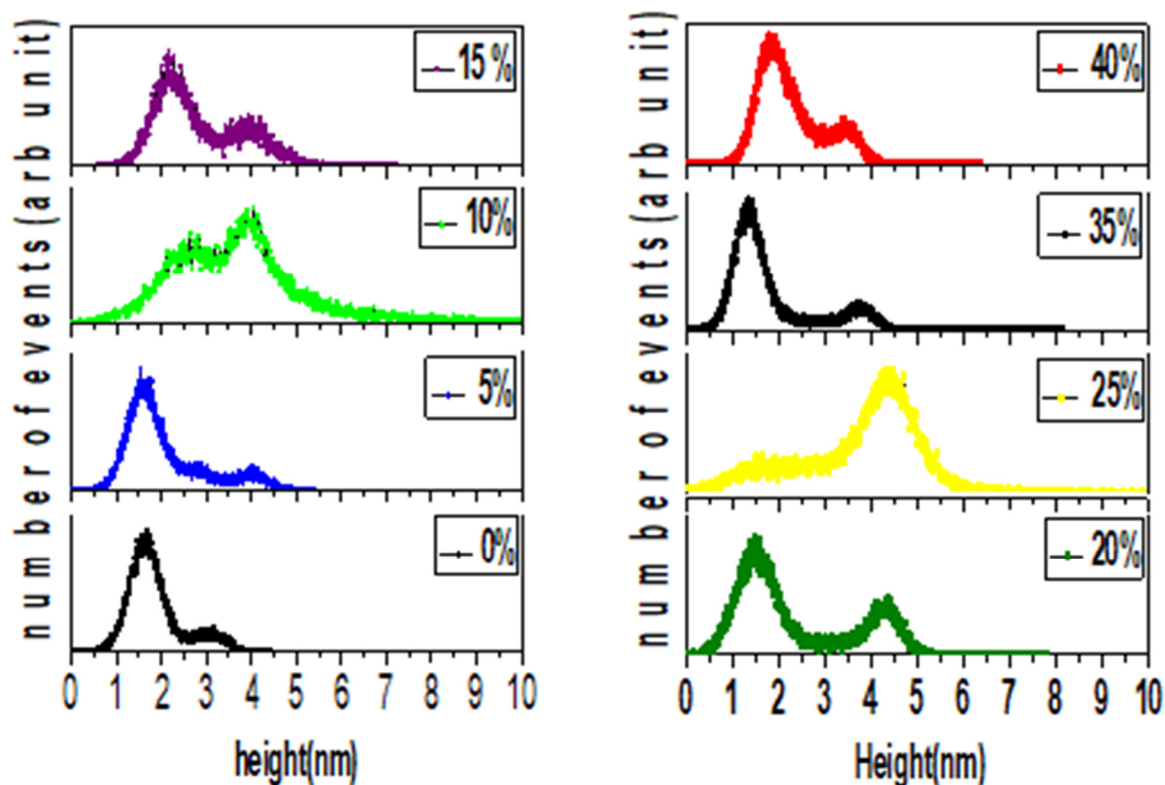
Figure 4.4: Height distribution of DOPC lipid bilayer in presence of different cholesterol concentration. (a) cholesterol concentration 0% to 15 % (b) 20% -40%. Histogram of height distribution are obtained from AFM height images shown in figure 4.4.

For the 0 mole% cholesterol, two peaks one at 1.5 nm and the other at 3 nm are found. The first one is for mica and the other peak is for the bilayer. We found a broader peak for mica (figure 4.4)

in comparison to pure mica (in figure 4.2).It may be due to the fact that the deposition of vesicles alters the surface character of pure mica. The histogram shows both the peaks (mica and bilayer) for 5% cholesterol also, but the second peak splits into two. The intercalation of more cholesterol (10% -25%) into the bilayer, peaks are observed near 3.5 nm and 4.5 nm. Hung et al. [42] determined the electron density map to measure the phosphate to phosphate distance(PtP) across the bilayers using X-ray diffraction method. They found that PtP for DOPC bilayer increases non-linearly with increasing mole fraction of cholesterol. They suggested that the PtP distance can be stretched from 3.6 nm to 4.2 nm in presence of cholesterol [42]. Therefore, the increase in DOPC bilayer thickness in presence of cholesterol can be 0.8 nm. They also found a peak shift in the electron density profile of the DOPC bilayer with the variation of cholesterol. In our case, the observed difference in height (0.7 -1.4 nm) between the cholesterol rich and poor bilayers is steady with the X ray diffraction measurement [42]. In the case of purely saturated lipid like DPPC, Zeinab Al-Rekabi et al. [22] noticed a distinct cholesterol rich liquid ordered phase in presence of moderate cholesterol concentrations. In the case of unsaturated lipid, the cholesterol also shows a strong influence on the DOPC lipid bilayer. When apolar moieties of cholesterol and DOPC molecule interact by London dispersion forces and by the Lifshitz–van der Waals forces [43], the polar groups on the DOPC molecule can form hydrogen bonds with the OH of cholesterol and water molecule. This interaction may lead to the formation of cholesterol rich bilayers in the DOPC-cholesterol binary system.

The figure 4.5 shows the average height variation of cholesterol enrich domain with the varying mole% of cholesterol. The error is estimated from the broadening of the Gaussian height distribution of the AFM image.
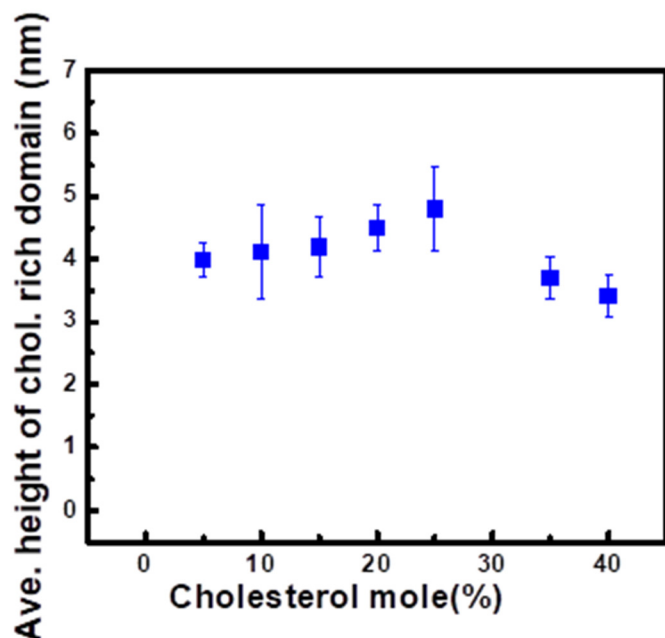
Figure 4.5: Average height variation of cholesterol rich bilayer as a function of cholesterol (mol%).

The height of the cholesterol rich bilayer increases slowly with increasing cholesterol concentration and is maximum at 20-25% as shown in figure 4.5 [44]. At this mole fraction of cholesterol, most of the DOPC molecules are expected to be aligned parallel to the bilayer normal, which in turn increases the segmental order parameter of the chains [45] . Usually, an unsaturated double bond in the alkyl chain lowers water penetration into the bilayer but the incorporation of cholesterol decreases hydrophobicity and increases water penetration along the polar head groups to the location of rigid steroid ring of cholesterol [43]. It may be another reason for the height rise of the bilayer at lower cholesterol content. A nominal decrease in height is observed for further addition of cholesterol (35%-40%). The height decrease at higher cholesterol concentration (figure 4.5) may be due to the folding up the acyl chain of phospholipids or interdigitation of acyl chains [40]. Kawakami et al. [39] tracked by QCM-D frequency shift and established that the molecular density of SLBs with high cholesterol is greater than SLBs with lower cholesterol fractions resulting the lowering of height of DOPC SLB. Alwarawrah et al posited through atomistic MD simulation that at higher cholesterol concentration, the DOPC head group expands towards the water –bilayer interface to occupy more lateral area. As a result, the DOPC bilayer height decreases (umbrella effect). According to their observation, the average DOPC bilayer height decreases after

25-35 mole % insertion of cholesterol following an initial increase [31]. Therefore, the decrease in height of cholesterol rich bilayer above 25% cholesterol is consistent with the earlier reports.

In the presence of cholesterol, the segmental order parameter of saturated DPPC bilayer in the liquid ordered phase becomes approximately twice that in the pure system without cholesterol [46]. Rekabi et al. [22] found the height of pure DPPC bilayer is 5 nm in purely aqueous environment through multi-frequency atomic force microscopy (AFM), namely amplitude modulation–frequency modulation (AM–FM) study. With the increase of cholesterol mole fraction into the bilayer, the average height of the bilayer changes from 5.1 ± 0.90 nm for pure DPPC to 1.1 ± 0.01 nm for DPPC: Chol (60%). In our study, the height difference between pure DOPC bilayer and cholesterol rich DOPC bilayer is found to be 1 ± 0.5 nm for all observed cholesterol content.

4.4.2 Nanomechanical properties of DOPC-Cholesterol membrane:

So far, we reported the variation of height and the coexistence of cholesterol rich and cholesterol poor bilayer patches. It is expected that the height variation may lead to various nanomechanical changes in the SLBs. In addition to the height profile of DOPC SLB, we have recorded the various nanomechanical properties, such as DMT modulus [36], deformation simultaneously on the same area by PF-QNM AFM. Quantitative Nanomechanical Mapping (QNM) analyses the force curves from Peak Force Tapping mode in real-time to give AFM images of various physical quantities. Figure 4.7 shows the DMT modulus and deformation images of the DOPC phospholipid SLB premixed with different amounts of cholesterol (0%- 40 mole%).
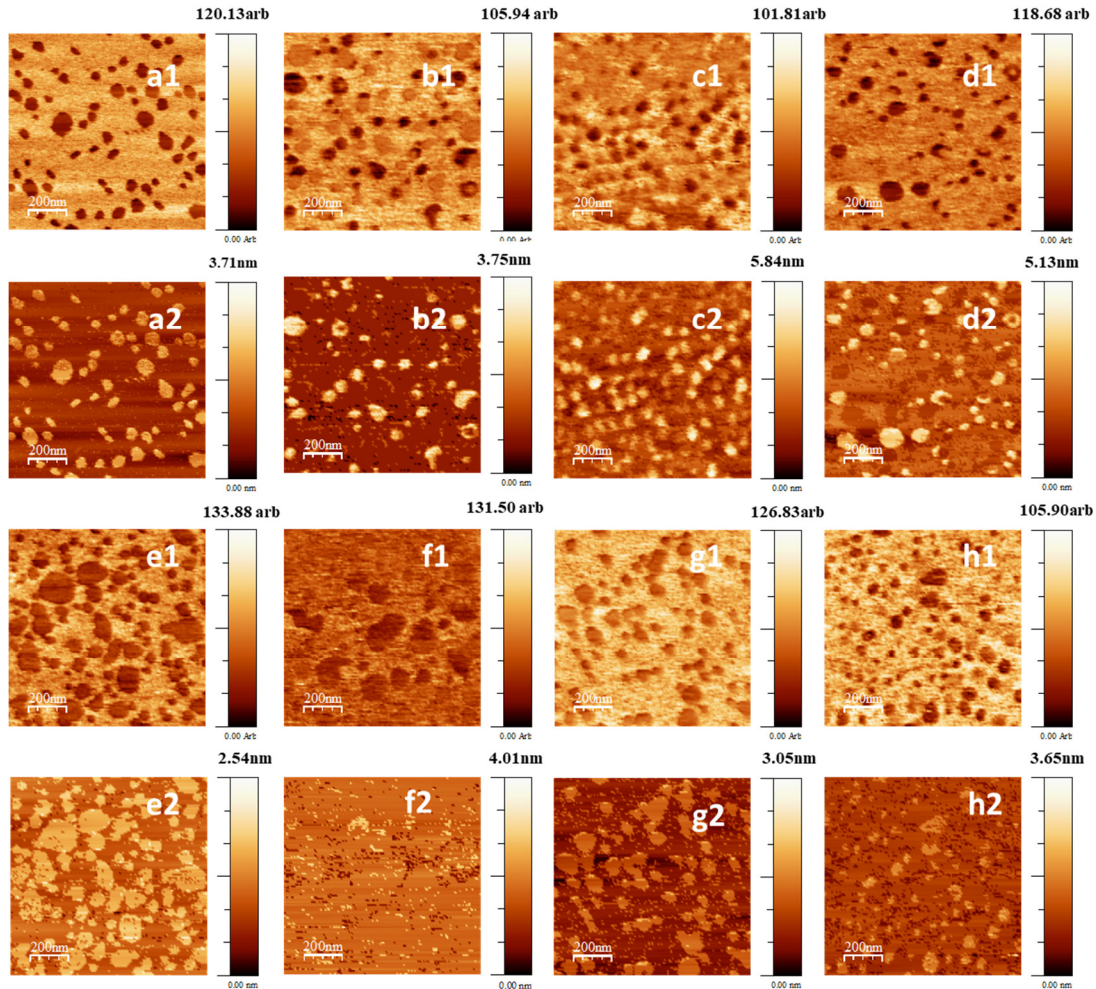
Figure 4.6: DMT modulus and deformation images of DOPC SLB in presence of 0-40% cholesterol; DMT modulus image for (a1) 0 mole %, (b1) 5 mole %, (c1)10 mole %, (d1)15 mole %, ((e1) 20 mole %, (f1) 25 mole %, (g1) 35 mole %, (h1) 40 mole % of cholesterol. Deformation images for (a2) 0 mole %, (b2) 5 mole %, (c2)10 mole %, (d2)15 mole %, ((e2) 20 mole %, (f2) 25 mole %, (g2) 35 mole %, (h2) 40 mole % cholesterol.

It is observed that the DMT of the bilayer is always less while the deformation is always greater than the mica surface (Figure 4.6 (a1)- (h1)). In presence of cholesterol, two distinct values of DMT, one for cholesterol poor (20-40MPa) and the other for cholesterol rich (40-60MPa) bilayer are clearly visible (data taken from the fitted peaks of the histogram, figure 4.7). Similarly, different values of deformation are noticed for the two different characters of bilayers.

For comparison, histogram plots, obtained from the PF-QNM image, of DMT modulus and deformation data for increasing concentration are presented in figure 4.7.
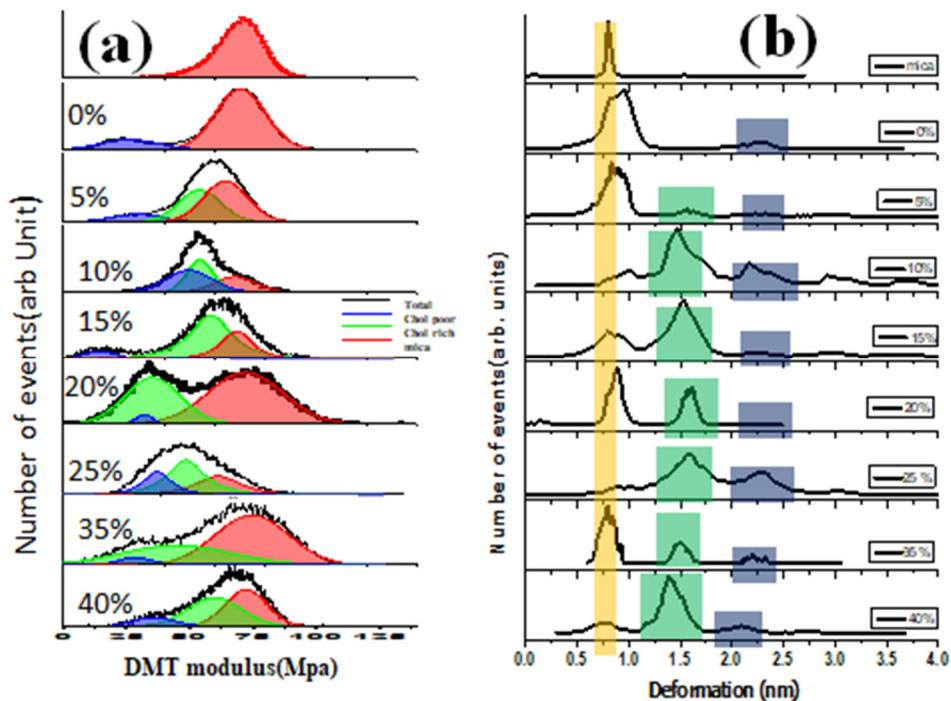
Figure 4.7: Histogram of DMT modulus and deformations of the DOPC bilayer for different mole% of cholesterol. (a) DMT modulus of cholesterol rich bilayer (green), cholesterol poor bilayer (blue) and mica (red). (b) Deformations of mica (yellow), cholesterol rich bilayer (green) cholesterol poor bilayer (blue).

Figure 4.7(a) shows a single peak at 70 MPa for DMT modulus of bare mica surface imaged in millipore water, while two new peaks at lower DMT modulus values appear due to the presence of cholesterol rich and cholesterol poor bilayers of DOPC on mica with the increase of cholesterol. Cholesterol rich bilayers show a higher DMT modulus than cholesterol poor bilayers.

Figure 4.7(b) shows the deformation distribution graphs for various cholesterol contents in the DOPC bilayer structure including bare mica. Graphs show distinct peaks for pure mica, cholesterol rich and poor bilayers. We found specifically 3 peaks of deformations, one for mica (0.5-1 nm), the second is for DOPC cholesterol rich bilayers (1.5-2 nm) and the third is for DOPC cholesterol poor bilayers (2-2.5 nm). Thus, the rigidity of the cholesterol rich bilayers is higher

75

than the cholesterol poor regions. In the case of 10% and 15 % cholesterol, additional deformation peaks are observed. These additional peaks may be due to different protrusions observed at 10-15% cholesterol. These isolated tubular protrusions are noticed on the flat DOPC bilayer surface at 10% cholesterol insertion (Figure 4.3(c)). Three-dimensional protrusion is a common mechanism to regulate stress in confined lipid bilayer systems. Cholesterol regulates the stress passively through membrane remodeling, and in the case of confined two-dimensional SLBs, such conditions give rise to membrane protrusions with distinct three-dimensional geometries [39]. The protrusions show a height range of 5-10 nm with a very low DMT modulus (<10 MPa) (Figure 4.8)
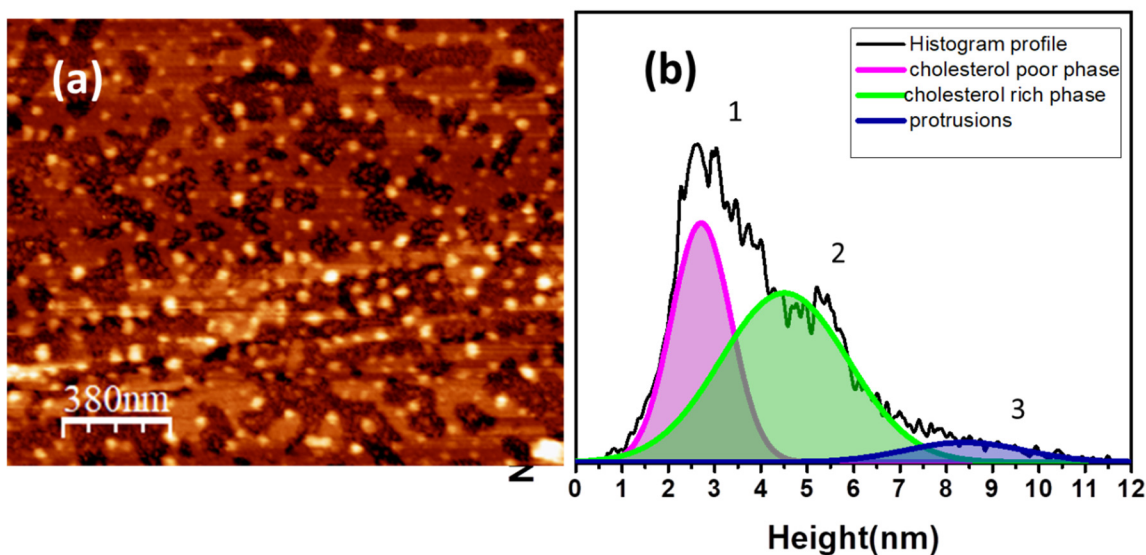
Figure 4.8: (a) AFM image of DOPC bilayer with 10 mole% cholesterol, (b) Histogram plot of the height, fitted peak1 corresponds to cholesterol poor phase, peak 2 corresponds to cholesterol rich phase and peak 3 corresponds to the protrusion regions. The small peak around 0.5 nm appears due bare mica surface.

Therefore, the presence of cholesterol in the bilayer is also determined by the rise of DMT modulus value as cholesterol shows the ability to stiffen the unsaturated DOPC lipid membrane [16].

In order to navigate the effect of cholesterol on the nanomechanical properties of the bilayer, we plot the DMT modulus and deformations against cholesterol concentration (figures 4.9 and 4.10). It is well known that hydrophobic and hydrophilic interactions play an important role in modulating the nanomechanical property of the bilayer [47]. Further cholesterol is known to

76

alter the hydrophilic and as well as hydrophobic interactions between lipid molecules in the bilayer [48].Thus the nano-mechanical property of the cholesterol rich bilayer is expected to be different from bilayer without cholesterol.
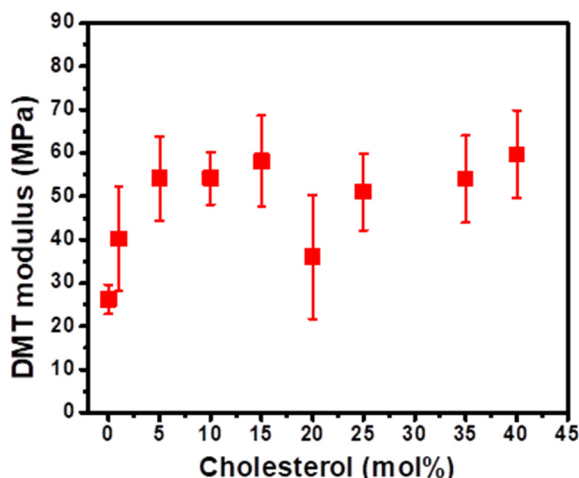
Figure 4.9: DMT modulus of cholesterol rich bilayer (except 0mol% cholesterol which contains pure bilayer only) as a function of cholesterol (mol%).

In Figure 4.9, we observe an increasing trend of DMT modulus of the bilayer for the addition of 0% to 10% cholesterol, but it remains almost constant for further incorporation of cholesterol except at 20-25% where a considerable decrease is noticed. The decrease may be due to more relaxed lipid packing at 20-25% cholesterol concentration and immiscibility with DOPC. Quaroni et al. [14] investigated the mechanical properties of bilayers of 1, 2-dipalmitoyl-sn-glycero-3-phosphocholine (DPPC) in the gel phase by using peak force tapping with quantitative nanomechanical mapping. They found the value of Young's modulus of supported bilayer stacks decreases with the increase of the height of the stack. In order to correlate the variation of DMT modulus of cholesterol rich bilayers, we also have investigated the deformation profiles. Figure 4.10 shows the variation of deformation of the cholesterol rich bilayers with cholesterol concentration.
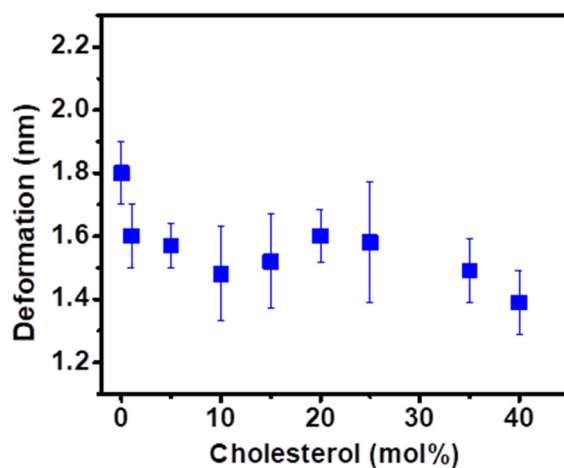
.
Figure 4.10: Variation in deformation of cholesterol rich bilayer (except 0 mol% cholesterol which contains pure bilayer only) as a function of cholesterol (mol %).

The trend shows an interesting feature of cholesterol rich domains. With the increase of cholesterol intercalation, the deformation of the bilayer decreases. This indicates the stiffening of the membrane. However, at intermediate cholesterol concentrations, the deformity of the membrane shows a reverse effect. The experiment shows that in the range of 15%-25% mole fraction of cholesterol the membrane becomes more flexible or fluid. Thus, at moderately high cholesterol concentrations, fluidity of DOPC bilayer increased. Szostak and colleagues [49] noted the tendency of cholesterol to flip-flop across the bilayer leaflets which leads to stress relaxation and deformation of cholesterol-rich membranes to a greater extent than pure phospholipid membranes in response to stress by redistributing cholesterol density between two leaflets of the DOPC bilayer. The deformation is further reduced for higher cholesterol concentration (>25%). At this concentration, the phospholipids may interdigitate their acyl chains so that the two leaflets of DOPC lipid bilayer overlap[40] which in turn increases DMT modulus (figure 4.9) and thus reduces the overall deformation (figure 4.10) of the DOPC lipid bilayer.

4.5. Conclusion:

We explored the influence of different cholesterol levels (1–40 mol %) on the morphology and nanomechanical stability of dioleoylphosphatidylcholine/cholesterol (DOPC/Chol) solid supported membrane by means of atomic force microscopy (PF-AFM QNM) imaging. To date, most of the reports deal with the influence of cholesterol in multi-component systems. A few approaches are reported to discuss the nature of the impingement of cholesterol into the purely unsaturated lipid bilayer. To the author's knowledge, this investigation successfully implemented PF-QNM AFM to decipher condensation behavior of the purely unsaturated DOPC lipid bilayer in presence of cholesterol. We are also able to quantify the nanomechanical properties of the phospholipid - cholesterol membrane. Cholesterol-containing bilayers with greater rigidity are found in comparison to the surrounding region. The tubular protrusion, a generic phenomenon of the natural cell membrane, is also noticed successfully at low cholesterol concentrations.

References:

[1]   G.W. Feigenson, Annu Rev Biophys Biomol Struct. 2007; 36: 63–77. 36 (2007) 63-77.

[2]   G.v. Meer, D.R. Voelker and G.W. Feigenson, Nat Rev Mol Cell Biol. 9(2) (2008) 112–124.

[3]   J.T. Groves and J. Kuriyan, Nat Struct Mol Biol. 2010 17(6) (2010) 659–665.

[4]   J. Seeliger, N. Erwin, C. Rosin, M. Kahse, K. Weisea and R. Winter, Phys. Chem. Chem. Phys 17 (2015) 7507-7513.

[5]   F.J.-M.d. Meyer, J.M. Rodgers, T.F. Willems and B. Smit, Biophys J 99(11) (2010) 3629-38

[6]   O.G. Mouritsen and M.J. Zuckermann, Lipids 39(11) (2004) 1101-13.

[7]   F. Cornelius, Biochemistry 40(30) (2001) 8842-51.

[8]   C.R. Anderton, K. Lou, P.K. Weber, I.D. Hutcheon and M.L. Kraft, Biochim Biophys Acta 1808(1) (2011) 307-15.

[9]   S. Chiantia, J. Ries and P. Schwille, Biochimica et Biophysica Acta 1788 (2009) 225–233.

[10]   S. Karmakar, V.A. Raghunathan and S. Mayor, Condensed Matter 17 (2005) S1177.

[11]   S. Chakraborty, M. Doktorova, T.R. Molugu, F.A. Heberle, H.L. Scott, B. Dzikovski, M. Nagao, L.-R. Stingaciu, R.F. Standaert, F.N. Barrera, J. Katsaras, G. Khelashvili, M.F. Brown and R. Ashkar, Proc Natl Acad Sci U S A. 117(36) (2020) 21896-21905.

[12]   C. Matthäus, B. Bird, M. Miljković, T. Chernenko, M. Romeo and M. Diem, Methods Cell Biol. 2008; 89: . 89 (2008) 275–308.

[13]   S.D. Connell and D.A. Smith, Molecular Membrane Biology 23 (2006) 17-28.

[14]   L. Quaroni, K. Bandopadhyay, M. Mach, P. Wydro and S. Zapotoczny, arXiv:2102.02188 (2021).

[15]   S.D. Connell, G.R. Heath and J.A. Goodchild, Mol Biol 1886 (2019) 29-44.

[16]   R.M.A. Sullan, J.K. Li, C. Hao, G.C. Walker and S. Zou, Biophys J 99(2) (2010).

[17]   J.M. Crane and L.K. Tamm, Biophysical Journal Volume 86 (2004) 2965–2979.

[18]   S.-T. Yang, A.J.B. Kreutzberger, J. Lee, V. Kiessling and L.K. Tamm, Chem Phys Lipids. 199 (2016) 136–143.

[19] M. Javanainen, H. Martinez-Seara and I. Vattulainen, Scientific Reports 7 (2017) 1143(1-10)

[20] N.K. Sarangi, K.G. Ayappa and J.K. Basu, Sci Rep 7 (2017) 11173

[21] J. Pan, S. Tristram-Nagle and J.F. Nagle, PHYSICAL REVIEW E80 (2009) 021931.

[22] Z. Al-Rekabi and S. Contera, Proc Natl Acad Sci U S A 115(11) (2018) 2658-2663.

[23] D. Lyu, L. Zhang and Y. Zhang, RSC Adv 10 (2020) 11088-11094.

[24] H. Martinez-Seara, T. Róg, M. Pasenkiewicz-Gierula, I. Vattulainen, M. Karttunen and a.R. Reigada, Biophys J. 95(7) (2008) 3295–3305.

[25] LorenaRedondo-Morata, PatriciaLosada-Pérez and M. InésGiannotti, Current Topics in Membranes 86 (2020) 1-55.

[26] I. Ermilova and A.P. Lyubartsev, Soft Matter 15 (2019) 78-93.

[27] P.R. Adhyapak, S.V. Panchal, A. Venkata and R. Murthy, BBA - Biomembranes 1860 (2018) 953–959.

[28] E. Domingos, Guilherme and S. Antonio, Journal of Molecular Liquids 315 (2020) 113698.

[29] A. Parker, K. Miles, K.H. Cheng and J. Huang, Biophys J. 86(3) (2004) 1532–1544.

[30] C.G. Siontorou, G.-P. Nikoleli, D.P. Nikolelis and S.K. Karapetis, Membranes (Basel) 7(3) (2017) 38.

[31] H. An, M.R. Nussio, M.G. Huson, N.H. Voelcker and J.G. Shapter, Biophys J. 99(3) (2010) 834–844.

[32] R.S. Gracia, N. Bezlyepkina, R.L. Knorr, R. Lipowsky and R. Dimova, Soft Matter 6(7) (2010) 1472-1482.

[33] M.J. Hope, M.B. Bally, G. Webb and P.R. Cullis, Biochim. Biophys. Acta. 812 (1985) 55.

[34] Y. Hua. Bruker. USA 2014.

[35] S. Bhattacharjee, D. Lavanyakumar, V. Naik, S. Mondal, S.R. Bhattacharyya and P. Karmakar, Thin Solid Films 645 (2018) 265–268.

[36] B.V. Derjaguin, V.M. Muller and Y.P. Toporov, J. Colloid Interface Sci. 53 (1975) 314–326.

[37] R. Richter, R. Berat and A.R. Brisson, Langmuir 22 (2006) 3497.

[38]   C.L. Armstrong, D. Marquardt, H. Dies, N. Kučerka, Z. Yamani, T.A. Harroun, J. Katsaras, A.-C. Shi and M.C. Rheinstädter, PLOS ONE 8(6) (2013) e66162.

[39]   L.M. Kawakami, B.K. Yoon, J.A. Jackman, W. Knoll, P.S. Weiss and N.-J. Cho, Langmuir 33 (2017) 14756–14765.

[40]   B.N. Olsen, A.A. Bielska, T. Lee, M.D. Daily, D.F. Covey, Paul H. Schlesinger, N.A. Baker and D.S. Ory, Biophysical Journal 105 (2013) 1838-1847.

[41]   M. Alwarawrah, J. Dai and J. Huang, J Phys Chem B. 2010 114(22) (2010) 7516–7523.

[42]   W.-C. Hung, M.-T. Lee, F.-Y. Chen and H.W. Huang, Biophysical Journal 92 (2007) 3960–3967.

[43]   M. Jurak and E. Chibowskia, RSC Adv 5 (2015) 66628-66635.

[44]   E. Ikonen, Nat. Rev. Mol. Cell Biol. 9 (2008) 125.

[45]   T.T. Mills, G.E.S. Toombes, S. Tristram-Nagle, D.-M. Smilgies, G.W. Feigenson and J.F. Nagle, Biophys J. 95(2) (2008) 669–681.

[46]   M.B.Sankaram and T.E.Thompson, Proceedings of the National Academy of Sciences of the United States of America 88(19) (1991) 8686-8690.

[47]   N. Maftouni, M. Amininasab, M.R. Ejtehadi, F. Kowsari and R. Dastvan, J. Chem. Phys. 138 138 (2013) 065101.

[48]   F.d. Meyer and B. Smit, Proc Natl Acad Sci U S A 106(10) (2009) 3654–3658.

[49]   R.J. Bruckner, S.S. Mansy, A. Ricardo, L. Mahadevan and J. Szostak, Biophysical Journal 97(12) (2009) 3113-22.

Chapter 5

Effect of anionic silver nanoparticle (AgNP) on the formation of solid supported phospholipid bilayer

5.1. Introduction:

Nanotechnology has become a growing field of interest in biology. Over the past two decades, engineered nanoparticles (ENM) have been progressively used for biological applications such as antimicrobial agents, diagnosis therapeutics imaging, targeted drug and gene delivery. [1-4]. Silver nanoparticle (AgNP) is one of such nanoparticles which show microbial activity owing to the size as well as its large surface-to-volume ratio [5]. Silver nanoparticles have the ability to pierce bacterial cell walls, alter the structure of cell membranes and even cause cell death[6]. AgNP continuously release silver ions which adhere to the cell wall and cytoplasmic membrane. Cell membrane becomes porous after the intake of silver ions which eventually disrupt the bacterial cell wall [6]. Spotting various biological applications of silver nanoparticle, a detailed comprehension is necessary regarding the interaction of AgNP with the cell membrane. The natural membrane is composed of various lipids, proteins, carbohydrates and other biomolecules, so it is difficult to study the specific interaction of nanoparticle with the cell membrane in native state. Solid supported lipid bilayer which mimics the cell membrane is a good substitute to study such biological system. A number of studies have been carried out elucidating the complex interaction of nanoparticle with solid supported bilayer system [7-9]. Among them, Atomic Force Microscopy (AFM) is a good technique to investigate morphological as well as nanomechanical changes of the membrane due to its interaction with the nanoparticles. Exploiting AFM as an experimental tool, Roiter et al. [10] showed that nanoscale pores are formed on the lipid bilayer by nanoparticles of diameter less than 22nm. Ridolfi et al. [11] observed the gold nanoparticles reside preferentially along the lipid phase boundaries in cholesterol mediated lipid bilayer. Despite of intense research in this field, the interaction between AgNP and pure zwitterionic DOPC bilayer

as well as cholesterol mediated DOPC bilayer by measuring the nanomechanical parameters are not well studied. On the other hand, the surface chemistry of nanoparticle is one of the important parameters which affect its overall interaction with the bilayer membrane. Coating of nanoparticle with specific ions is an excellent technique to enhance its activities. The coating of nanoparticle with specific ions increase the stability of AgNPs and reduces their cluster formation [12]. The average orientation of the lipid head group is altered in the presence of coated negatively charged nanoparticles [13]. The anionic nanoparticles are also found to induce gelation in fluid lipid bilayer at room temperature [14].

In this article, considering the previous observations, we choose cholesterol mediated DOPC solid supported bilayer (0% and 5%) and citrate coated anionic silver nanoparticles. We restricted the particle size ~10 nm to observe the pronounced effect of nanoparticle on DOPC lipid bilayer as it is generally reported that smaller citrated-coated silver NP causes more cellular toxicity and disruption to membranes [15, 16].

5.2. Experimental:

Small unilamellar vesicles (SUVs) were prepared by following the extrusion method described by Hope et al. [17] as discussed in the previous chapters. Citrate coated silver nanoparticle of size 10 nm (AgNP) (.02mg/ml) was also purchased from Avanti Polar Lipids (Alabaster, AL) and used without further processing.

In this experiment, the mica substrates were prepared in three different ways: (i) to observe interaction of AgNP nanoparticle with pure mica surface, we added one drop (11µl) of 0.02 mg/ml citrate coated AgNP on the freshly cleaved mica and dried, the dried surface was immersed in millipore water and AFM images were recorded. (ii) For preparation of DOPC-AgNP hybrid system on mica surface, we added one drop of AgNP solution (.02mg/ml) on the mica surface. The sample was left untouched for 5 minutes. After that, we added 50µl DOPC SUV (0.5mg/ml) aqueous solution on the altered mica surface. The sample was incubated for 45 minutes. Then the sample was gently rinsed and imaged by AFM in the fluid (water) mode. (iii) Finally, to study the effect of simultaneous deposition of 5 mole % cholesterol mediated DOPC vesicles and AgNP nanoparticle, previously prepared vesicle solution of 50 µl and AgNP of 11 µl were deposited

simultaneously. Each sample was incubated for 15-20 minutes. The surface was gently rinsed and placed for AFM measurements. Utmost care was taken to prevent de-wetting of the samples.

The AFM was operated in Peak Force QNM (Peak Force-Quantitative Nano-Mechanical) liquid mode with Scan Asyst-fluid probe as described in section 4.3. The information regarding the mechanical properties of the sample is extracted at every single point as shown in figure 4.1 (chapter 4) [18, 19]. The AFM images were flattened and the statistical distribution of heights, DMT modulus, adhesion, energy dissipation and deformations are presented. The reduced Young's Modulus is obtained by using the Derjaguin, Muller, Toropov (DMT) model [20].

5.3. Results and discussion:

Figure 5.1 shows a DOPC bilayer on a freshly cleaved mica surface. It shows the bilayer height around 3.3 nm which covers a vast portion of the mica surface. The vesicles are ruptured spontaneously at the contact of mica surface. The interplay between the edges of isolated bilayer fragments lead to merging and form larger bilayer patches.[21].
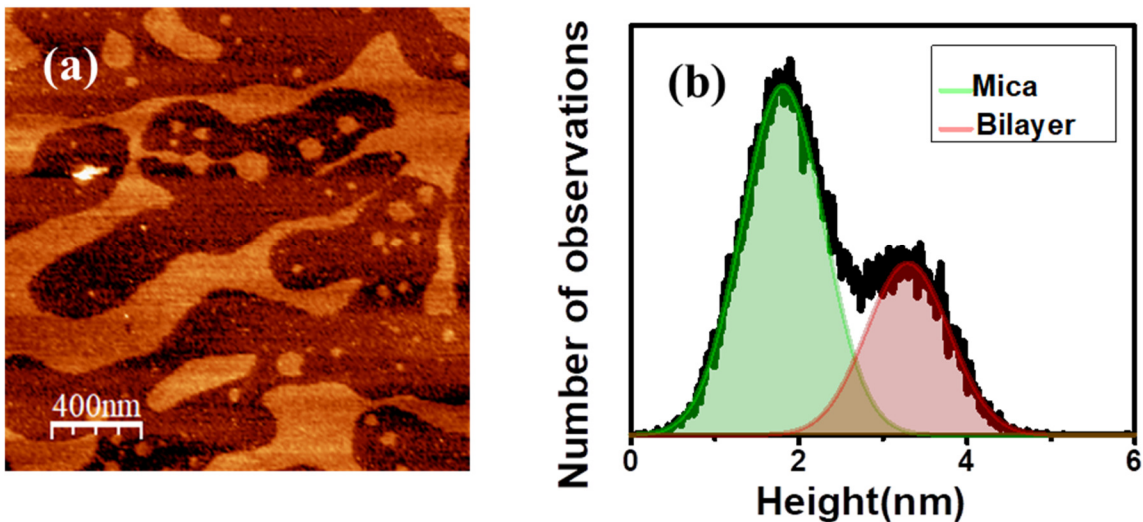
Figure 5.1: DOPC bilayer on freshly cleaved mica surface 1(a) height image of pure DOPC lipid bilayer 1(b) histogram distribution of height.

5.3.1. Dispersed anionic silver nanoparticle (AgNP) on freshly cleaved mica surface:

To observe the surface morphology of the AgNP on atomically flat mica surface, the nanoparticles were dispersed as described in the experimental section and captured by AFM. Figure 5.2 shows the surface morphology of the mica surface after the dispersion.
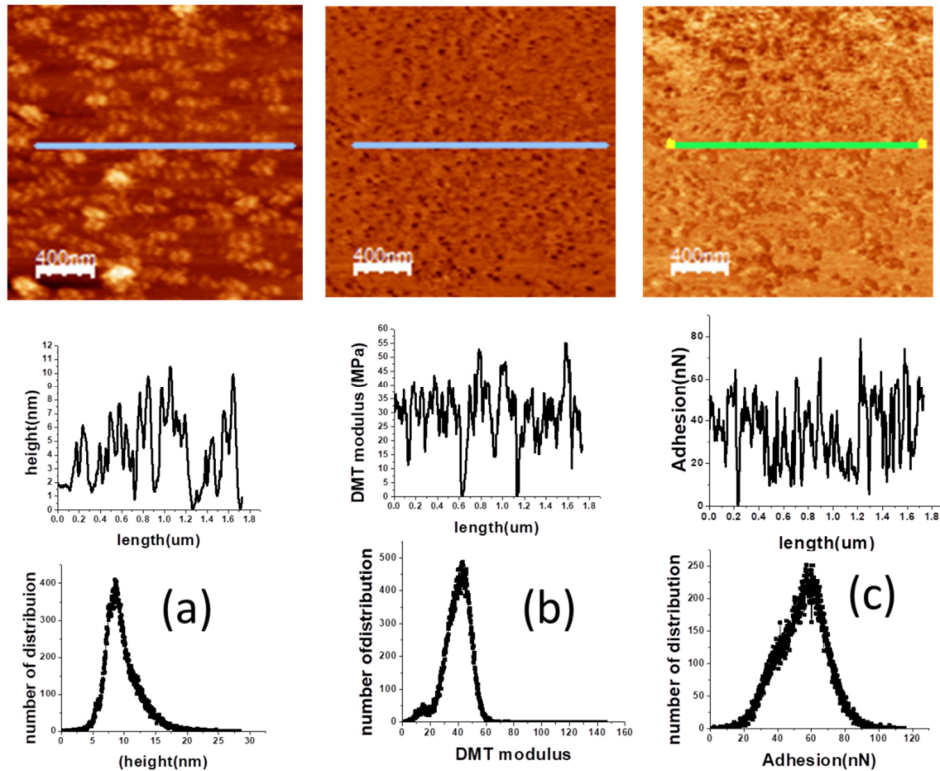
Figure 5.2: The topography of height, DMT modulus and adhesion along with 1-D profile and histogram (a)The topography of height along with line profile and histogram of distribution.(b)the topography of DMT modulus with line profile and histogram of distribution (c) the topography of adhesion with line profile and histogram of distribution.

Figure 5.2(a) shows the topography of the deposited anionic silver nanoparticle. One dimensional (1D) height profile along the marked line and the histogram distribution of 2D image is shown below the AFM image. The AgNP are not crowded on the mica surface. It may be due to the fact

that citrate coated silver nanoparticle in aqueous solution bears a high negative zeta potential value [22]. As zeta potential is related with the electric potential of the interface of the diffuse ion layer surrounding Ag nanoparticle and the bulk solution, so the possibility of crowding of the nanoparticles is less. The electrostatic interaction between the silver nanoparticle and the mica stabilizes the nanoparticles on the mica surface. The 1-D profile as well as the histogram shows the size of the Ag nanoparticles within the range of 1-25 nm with a peak at 10 nm which is consistent with the value found in TEM (provided by the manufacturer). Figure 5.2(b) shows 2D image of DMT modulus along with 1-D profile and histogram of the distribution. The DMT modulus histogram shows two peaks, one at 20 MPa and other at 40 MPa. The presence of silver nanoparticle contributes to the higher value of DMT modulus. The lower peak in the histogram of DMT modulus may be the contribution of sodium citrate buffer coupled with the mica surface Figure 5.2(c) shows the adhesion map of the anionic silver nanoparticles. The map reveals that the presence of the AgNP reduces the adhesion compared to the rest of the mica surface. The histogram distribution of adhesion also shows two peaks. The peak at 40 nN corresponds to the adhesion of anionic AgNP whereas the higher value of 60 nN may be due to the sodium citrate coupled mica surface.

5.3.2. Preparation of DOPC-AgNP hybrid bilayer:

Figure 5.3 shows AFM data of DOPC-AgNP hybrid bilayer on the mica surface prepared by addition of AgNP solution followed by the deposition of DOPC vesicle and 45 minutes incubation (described in the experimental section).
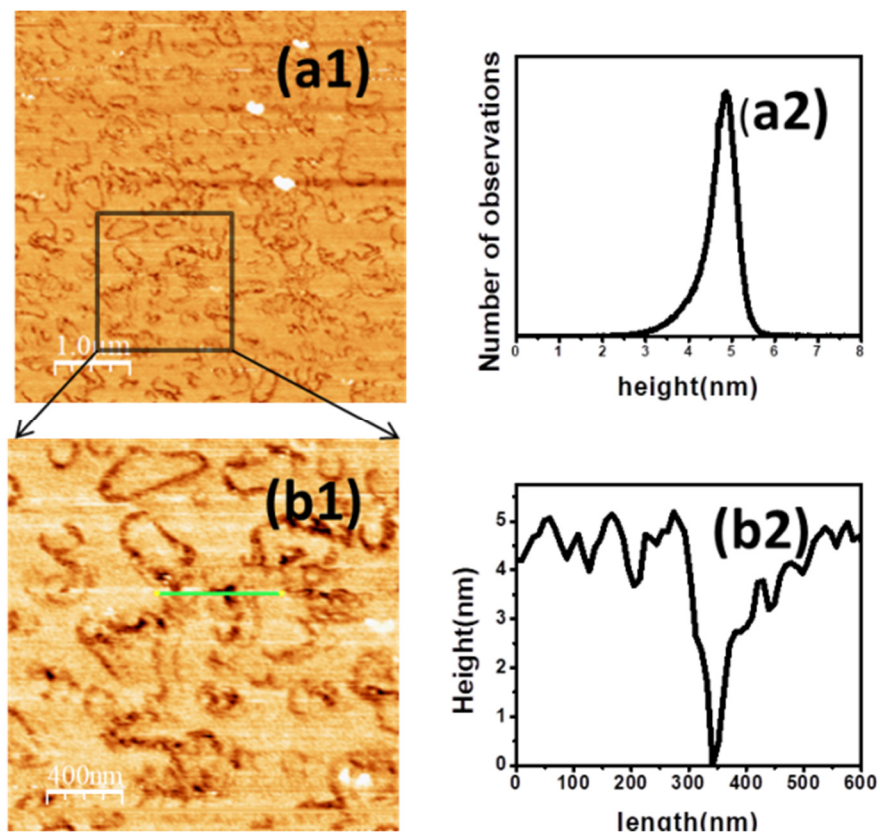
Figure 5.3: Pore formation in DOPC bilayer in presence of AgNP fabricated mica surface (a1) image of bilayer (a2) histogram of height image (a1) (b1) Enlarged image of a porous region in DOPC bilayer (b2) 1-D image along the indicated surface

Figure 5.3(a1) shows the semi continuous lipid bilayer with multiple irregular scratches on it. A small number of AgNP are also exposed at the scratched regions. Figure 5.3(a2) shows the histogram of the height distribution with a peak at 5 nm. An enlarged image and 1D line profile near a porous zone is shown in figure 5.3(b1) and figure 5.3(b2). The observed scissions on the DOPC bilayer are due to the presence of pre-implanted AgNP on mica surface. The nanoparticles penetrate into the phospholipid bilayer structure and disrupt the regular structure of the membrane [23]. Few of the AgNPs involved in the bilayer disruption are visible at the scratch regions. Earlier AFM study revealed similar pore formation on DMPC bilayer due to the presence of substrate-supported silica nanoparticles with diameters ranging from 1.2 to 22 nm[10]. The pore formation and bilayer scission are further confirmed by simultaneous DMT modulus, adhesion and energy dissipation measurements.

Figure 5.4 represents the 2-D map of DMT modulus, adhesion and the energy dissipation along with the height image.
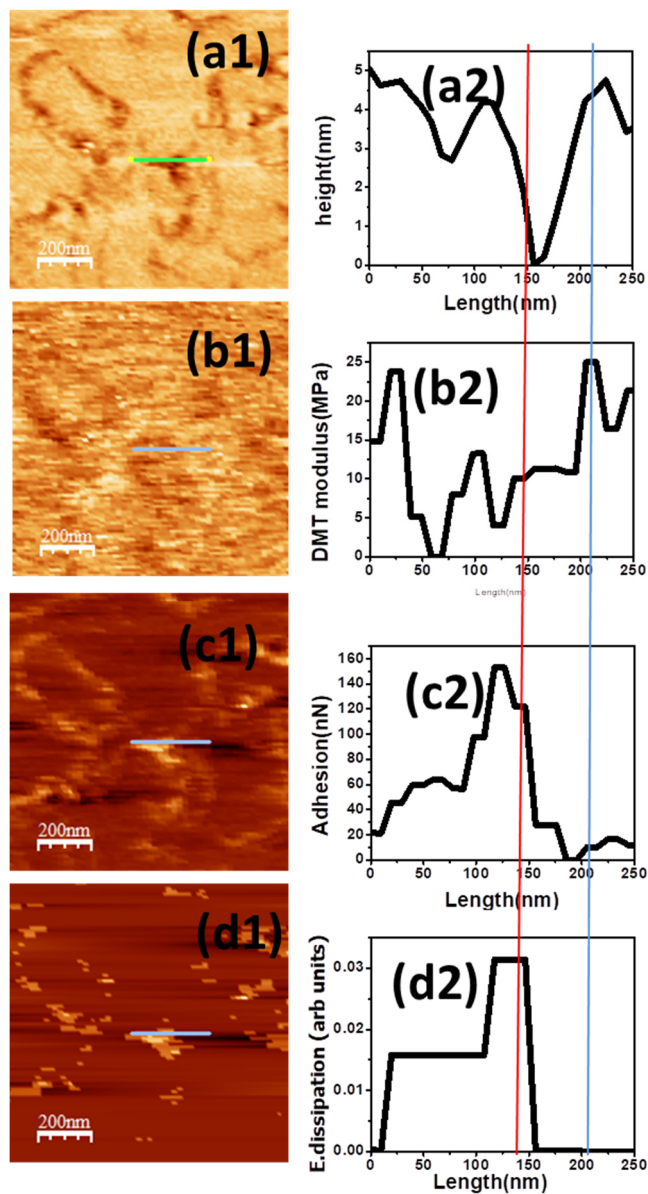
Figure 5.4: The 2-D image of DOPC lipid- AgNP hybrid bilayer (a1) the 2-D image of height (a2) line profile along the indicated surface (b1) the 2-D image of DMT modulus (b2) the line profile along the marked surface(c1) the 2-D image of adhesion (c2) line profile along the indicated surface (d1) the 2-D image of energy dissipation (d2) the line profile of the specified surface

Figure 5.4(a1), (b1), (c1) and (d1) represents the 2-D image of height, DMT modulus, adhesion and energy dissipation, respectively. The corresponding profiles along the marked lines are also shown in figure 5.4(a2), (b2), (c2) and (d2), respectively. The falls in height profile (Figure 5.4(a2)) indicates the disruption on the bilayer. The DMT modulus line profile along the same region (figure 5.4(b2)) shows a fall at the disrupted position. Similarly, adhesion and energy dissipation at the disrupted surface is high (figure 5.4(c2&d2)) compared to the rest of the surface. Thus, we conclude from the height and nanomechanical measurements that the AgNP has the ability to create pore in the DOPC lipid bilayer.

So far, we have successfully examined the morphological and the mechanical change of the nano structured hybrid DOPC bilayer. Now to study the effect of simultaneous addition of AgNPs and DOPC vesicles, we added both AgNP and DOPC lipid vesicle solution at the same time on the atomically flat mica surface.
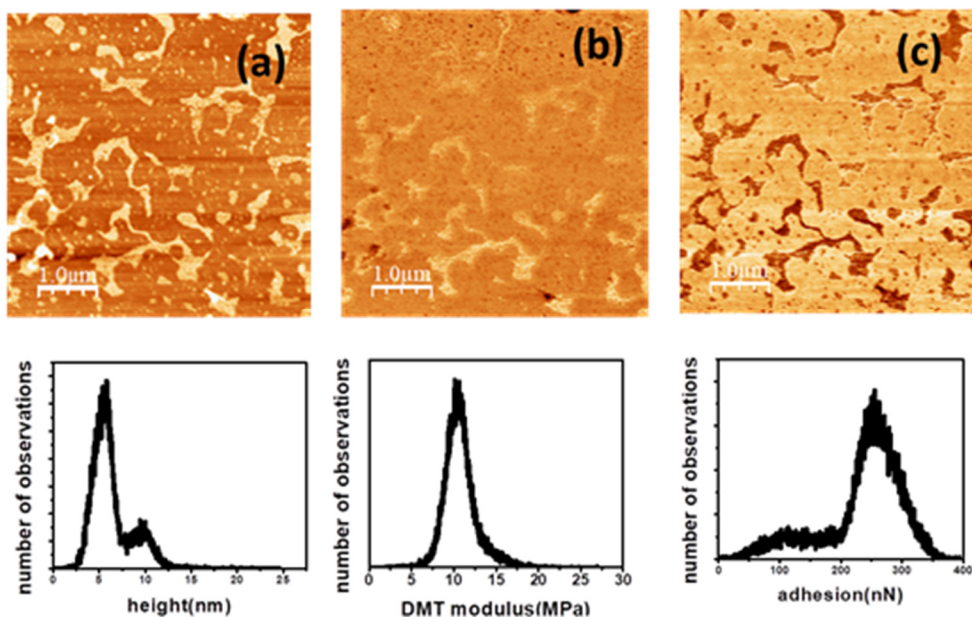
Figure 5.5: the topography of the disrupted DOPC bilayer (a) The topography of height along with the histogram of distribution (b) Topography of DMT modulus of the surface along with the histogram of distribution (c) Topography of adhesion along with the histogram of distribution.

Figure 5.5(a), 5.5(b) and 5.5(c) represent the 2-D image of height, DMT modulus and adhesion of disrupted bilayer along with histogram distribution of 2-D image in presence of anionic Ag NP respectively. The height distribution displays two height ranges, (i) 2-7 nm which corresponds to pure lipid bilayer and (ii) 7-13 nm which represents the nanoparticle trapped bilayer region. The height distribution suggests that the larger nanoparticles cause the membrane to partially wrap around or engulf the particle [24]. When we added the Citrate coated AgNP and DOPC vesicle solution simultaneously, owing to electrostatic interaction, the silver nanoparticle was trapped in the discontinuous bilayer. Here lipid tail protrusion may play an important role for insertion of silver nanoparticle in the supported bilayer [25]. In our study, DMT modulus image as well as the histogram distribution shows higher rigidity of nanoparticle trapped bilayer in comparison to other parts of the of the sample (figure 5.5b) [26]. Velikonza et al. [13] observed that the lipid head groups which are in close vicinity to the negatively charged nanoparticle extend more to the direction perpendicular to the membrane surface which leads to localized ordering of the lipid molecules in the close proximity of the nano particle. In our case, this local ordering may lead to the stiffening of DOPC bilayer in presence of AgNP. The nanoparticle trapped bilayer also shows less adhesion in comparison to the other surface of the sample. The energy dissipation of the same topography is presented in figure 5.6.
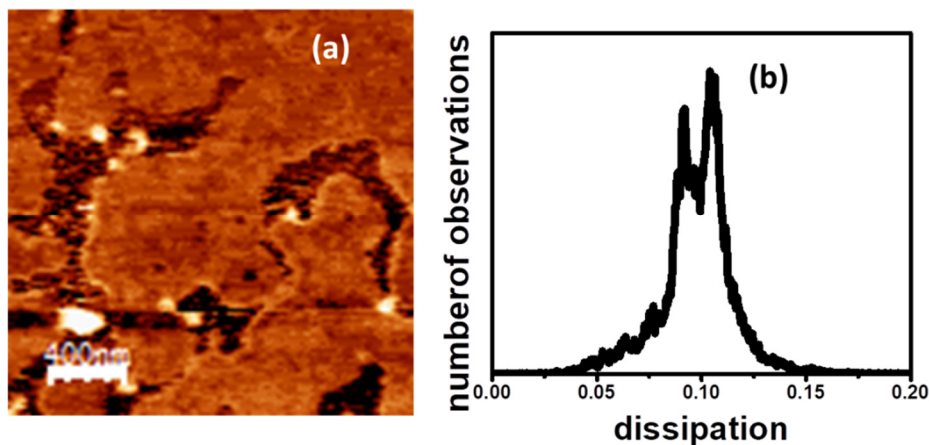
Figure 5.6: (a) The image of energy dissipation of the DOPC lipid bilayer during simultaneous addition of AgNP and DOPC vesicle on freshly cleaved mica surface (b) histogram of the distribution

Figure 5.6(a) shows the energy dissipation image of figure 5.5(a). Three different coloured regions is shown in figure 5.6(a) and histogram in figure 5.6(b) denotes three different energy dissipations.

91

The darkest regions and the lowest energy dissipation peak contribute to the nanoparticle trapped bilayer which is similar to high DMT modulus image. It again signifies that the nanoparticle trapped bilayer region is very rigid. Non trapped silver nanoparticles are visible at the boundary of the nanoparticle trapped bilayer. The observation is similar to earlier reports that the nanoparticles like to reside at the interface of the bilayer [9].

5.3.3. Effect of AgNP on cholesterol incorporated DOPC lipid bilayer:

So far, we have investigated the interaction of silver nanoparticle with the purely mica supported DOPC phospholipid bilayer (0% cholesterol). The disruption of the lipid bilayer is observed due to the pre-implanted and simultaneous incorporation of AgNPs. Now we study the disruption effect of DOPC phospholipid bilayer by AgNPs in presence of cholesterol, a stabilizing agent of phospholipid bilayer. We added AgNP solution (0.02mg/ml) and 5 mole % cholesterol mediated DOPC solution (0.5mg/ml) together on the freshly cleaved mica surface. The sample was incubated for 45 minutes, and gently rinsed before the AFM imaging. The topography and the height distribution are presented in figure 5.7.
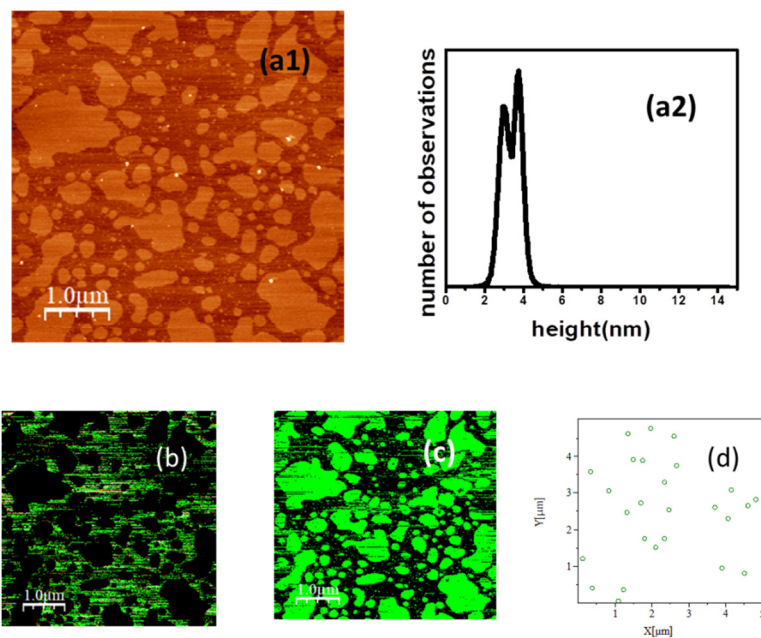
Figure 5.7: nanoparticle incorporated 5 mole% cholesterol mediated DOPC lipid bilayer (a1) the image of height (a2) histogram of height distribution (b) the height layer from 0nm to3nm (c) height layer from 3nm to 5 nm (d) distribution of nanoparticles on the same surface

Figure 5.7(a1) shows 2-D image of the cholesterol incorporated DOPC bilayer with impinged AgNP. It is observed that the cholesterol mediated bilayer formation is not much hindered by the incorporation of nanoparticle. However, cholesterol rich and cholesterol poor domains are observed which is confirmed by the two peaks in the height distribution (figure 5.7(a2). Few adhered AgNPs are noticed on the surface of the bilayer which do not contribute any significant role in the height distribution. Three layered height groups are noticed in figure 5.7(b-d) with height ranges 0-3 nm, 3-5 nm and 5 -12 nm. Figure 5.7(b) and 5.7(c) represents the cholesterol rich and cholesterol poor bilayer while 5.7(d) represents the positions of the adhered nanoparticle in the same surface. The DMT modulus and the adhesion profile along a localized region of the bilayer are presented in figure 5.8.
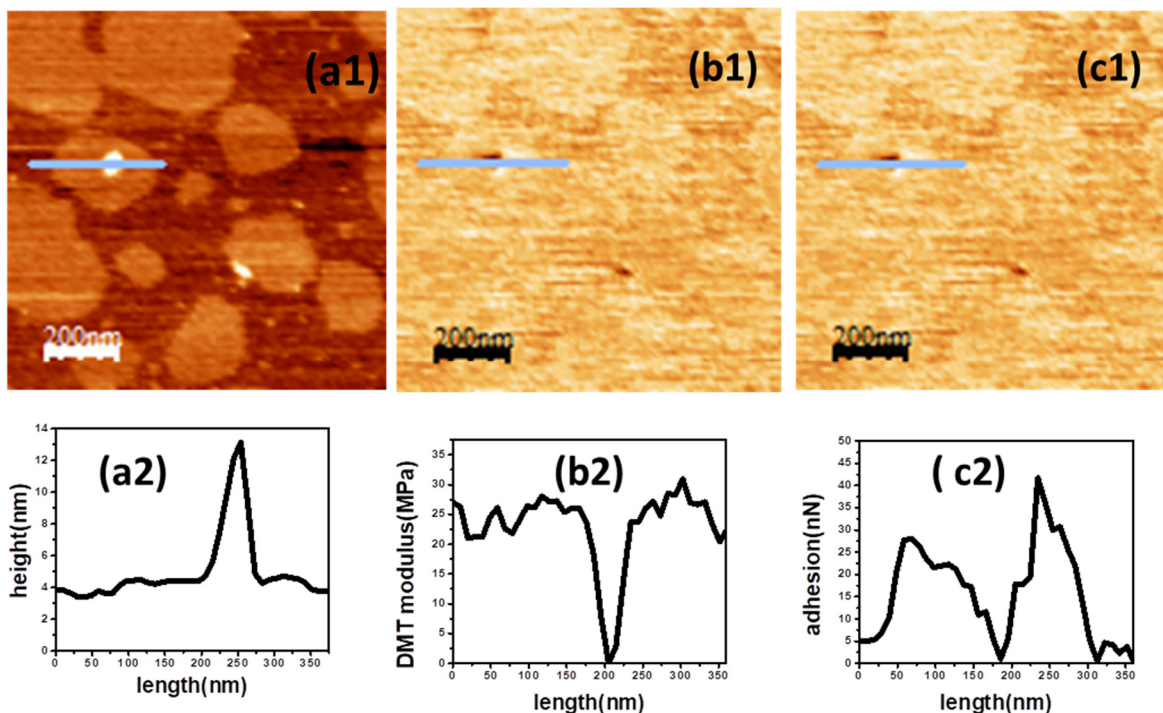
Figure 5.8: AgNP on the 5% cholesterol mediated DOPC lipid bilayer surface(a1) topography of height of nanoparticle attached DOPC bilayer (a2) line profile along the bilayer nanoparticle surface.(. (b1) topography of DMT modulus(b2) the line profile of DMT modulus (c1) topography of adhesion of nanoparticle on DOPC-cholesterol bilayer(c2) line profile of adhesion along the surface.

Figure 5.8(a1) shows the topography of a single adhered AgNP on the cholesterol rich DOPC bilayer of height 4nm. The line profile (figure 5.8(a2)) reveals the possible height of the nanoparticle is ~10 nm. There is a dent in DMT modulus as well as in adhesion topography at the adhere site of the nanoparticle (Figure 5.8(b1) and Figure 5.8(c1). The line profile of DMT modulus and Adhesion in the figures 5.8(b2) and 5.8(c2) displays a drop at the attachment site. It suggests that the cholesterol mediated DOPC lipid bilayer tends to be porous at the attachment site of the nanoparticle. However, total disruption of the bilayer does not occur for cholesterol mediated DOPC lipid bilayer as revealed in the AFM study. Thus, it may be inferred from the observation that the effect of AgNP is less pronounced in cholesterol mediated DOPC lipid bilayer than pure DOPC lipid bilayer.

5.4. Summary:

The results presented in this paper demonstrate that AgNP has the ability to induce defects in the pure and cholesterol mediated DOPC lipid bilayer. The nanoparticle trapped bilayer regions show height elevation and increased rigidity. The unbound nanoparticles are also visible at the boundary of the trapped region. On the other hand, The AgNP cannot produce many defects on the cholesterol mediated DOPC lipid bilayer in comparison to pure DOPC lipid bilayer. The effectiveness of AgNP in nanoscale disruption of supported lipid bilayers correlates the particle's ability to induce cell membrane permeability and to internalize into the lipid bilayer. This inducing effect is reflected in the change of the DMT modulus, adhesion and energy dissipation at the adhering site of nanoparticle with the lipid bilayer. The bilayer disruption is extremely important because natural and synthetic nanoparticles utilize nanopores to reach to the inner part of the cell through these nano opening. By observing the interaction of nanoparticles in in-vitro system using artificial lipid bilayer, one can predict the possible mechanism related to nanoparticle intake in real cell membrane. The observed degree of lipid bilayer disruption correlates well with *in vitro* studies of enzyme leakage, nanoparticle uptake and cytotoxicity [27] The reported study enhances the fundamental knowledge on AgNP - DOPC SLB interactions which establish a key aspect to consider the designing of NPs-related biological applications.

References:

[1] E. Sánchez-López, D. Gomes, G. Esteruelas, L. Bonilla, A.L. Lopez-Machado, R. Galindo, A. Cano, M. Espina, M. Ettcheto, A. Camins, A.M. Silva, A. Durazzo, A. Santini, M.L. Garcia and E.B. Souto, Nanomaterials (Basel) 10(2) (2020) 292.

[2] T. Kim and T. Hyeon, Nanotechnology 25(1) (2014) 012001.

[3] J.K. Patra, G. Das, L.F. Fraceto, E.V.R. Campos, M.d.P. Rodriguez-Torres, L.S. Acosta-Torres, L.A. Diaz-Torres, R. Grillo and M.K. Swamy, Journal of Nanobiotechnology 16 (2018).

[4] M.K. Riley and W. Vermerris, Nanomaterials (Basel) 7(5) (2017) 94.

[5] M. Oves, M. Aslam, M.A. Rauf, S. Qayyum, H.A. Qari, M.S. Khan, M.Z. Alam, S. Tabrez, A. Pugazhendhi and I.M.I. Ismail, Materials Science and Engineering: C 89 (2018) 429–443.

[6] I.X. Yin, J. Zhang, I.S. Zhao, M.L. Mei, Q. Li and C.H. Chu, Int J Nanomedicine 15 (2020) 2555-2562.

[7] B.Y. Moghadam, W.-C. Hou, C. Corredor, P. Westerhoff and J.D. Posner, Langmuir 28(47) (2012) 16318–16326.

[8] R.V. Goreham, V.C. Thompson, Y. Samura, C.T. Gibson, J.G. Shapter and I. Köper, Langmuir 31(21) (2015) 5868-74.

[9] R.C.V. Lehn, M. Ricci, P.H.J. Silva, P. Andreozzi, J. Reguera, K. Voïtchovsky, F. Stellacci and A. Alexander-Katz, Nature Communications 5 (2014) 4482.

[10] Y. Roiter, M. Ornatska, A.R. Rammohan, J. Balakrishnan, D.R. Heine and S. Minko, Nano Lett. 8(3) (2008) 941.

[11] A. Ridolfi, L. Caselli, C. Montis, G. Mangiapia, D. Berti, M. Brucale and F. Valle, J Microsc 280(3) (2020) 194-203.

[12] H.M. Fahmy, A.M. Mosleh, A.A. Elghany, E. Shams-Eldin, E.S.A. Serea, S.A. Alia and A.E. Shalan, RSC Adv 9 (2019) 20118-20136.

[13] A. Velikonja, P.B. Santhosh, E. Gongadze, M. Kulkarni, K. Eleršič, Š. Perutkova, V. Kralj-Iglič, N.P. Ulrih and A. Iglič, Int J Mol Sci. 14(8) (2013) 15312–15329.

[14] G. Rossi and L. Monticelli, Biochimica et Biophysica Acta (BBA) - Biomembranes 1858 (2016) 2380-2389.

[15] M. Akter, T. Sikder, M. Rahman, A.K.M. AtiqueUllah, K. Fatima, B. Hossain, S. Banik, T. Hosokawa, T. Saito and M. Kurasaki, Journal of Advanced Research 9 (2018) 1-16.

[16] C. Peetla and V. Labhasetwar, Mol. Pharmaceutics 5 (2008) 418–429.

[17] M.J. Hope, M.B. Bally, G. Webb and P.R. Cullis, Biochim. Biophys. Acta. 812 (1985) 55.

[18] S. Bhattacharjee, D. Lavanyakumar, V. Naik, S. Mondal, S.R. Bhattacharyya and P. Karmakar, Thin Solid Films 645 (2018) 265–268.

[19] Y. Hua. Bruker. USA 2014.

[20] B.V. Derjaguin, V.M. Muller and Y.P. Toporov, J. Colloid Interface Sci. 53 (1975) 314–326.

[21] A. Basu, P. Karmakar and S. Karmakar, The Journal of Membrane Biology 253(03) (2020) 205-219.

[22] K. Afshinnia and M. Baalousha, Sci Total Environ 581-582 (2017) 268-276.

[23] M.R. Rasch, E. Rossinyol, J.L. Hueso, B.W. Goodfellow, J. Arbiol and B.A. Korgel, Nano Lett 10(9) (2010) 3733-9.

[24] Y. Li, X. Zhang and D. Cao, J. Phys. Chem. B 117 (2013) 6733–6740.

[25] R.C.V. Lehn, M. Ricci, P.H.J. Silva, P. Andreozzi, J. Reguera, K. Voïtchovsky, F. Stellacci and A. Alexander-Katz, Nature Communications 5(4482) (2014).

[26] B. Wang, L. Zhang, S.C. Bae and S. Granick, Proc Natl Acad Sci U S A 105(47) (2008) 18171-5.

[27] P.R. Leroueil, S.A. Berry, K. Duthie, G. Han, V.M. Rotello, D.Q. McNerny, J.R.B. Jr, B.G. Orr and M.M.B. Holl, Nano Lett. 8(2) (2008) 420-4.

Chapter 6

Preparation of giant unilamellar vesicles from large unilamellar vesicles(LUV) and characterization by zeta potential and dynamic light scattering:

6.1. Introduction:

In the previous chapters we have discussed the formation and growth of Solid supported lipid bilayer and its interaction with cholesterol and anionic silver nanoparticle which are very important molecular interaction in the biological perspective. Although planar bilayer can be a model system to study biological membranes, giant unilamellar vesicles will be more appropriate to study functions and properties of bio membranes. Size of GUV resembles with the cell. One of the major drawbacks of SLB as a model system of biological membranes is the extensive hydrodynamic coupling between the bilayer and the substrate in which bilayer is formed. Such a coupling results in a much slower diffusion of bilayers than that of free bilayers. Further, undesirable interaction between substrate and bilayer may lead to problem in reconstituting integral membrane proteins into the bilayer. One approach to circumvent this problem is to prepare unilamellar vesicles as a model system of bio-membrane, although this system is not very good stable compared to SLB. Therefore, besides SLB, we intend to prepare GUV from LUV. In the present chapter, we discuss the formation of Giant Unilamellar Vesicles from Large Unilamellar vesicles which acts as an excellent model membrane. We also describe our preliminary results on GUV reconstituted with an antimicrobial peptide, NK-2.

The present chapter is organized as follows. The section 6.2 describes the earlier studies followed by the experimental results in section 6.3 and discussion in the section 6.4.A conclusion is detailed in section 6.5.

6.2. Earlier studies:

Biological membranes are complex, regulated by various membrane components. Therefore, it is often useful to study model membranes in order to understand the physical mechanisms of many biological phenomena occurring on the cell surface. Unilamellar vesicles are often used as bio-mimetic systems. Vesicles are basically microscopic sac that encloses a volume with molecularly thin bilayer membrane. These are formed by self-assembly of amphiphilic molecules, such as phospholipids, diblock co polymer etc [1] [2]. Phosphatidylcholines (PCs) are the most abundant phospholipids in all eukaryotic cells, whereas, phosphatidyl glycerols (PGs) and phosphatidylethanolamines (PEs) were found in bacterial cell [3].The phospholipids, when suitably mixed with water or similar solvent form bilayers, commonly known as multilamellar vesicles (MLV). However, MLV do not serve as a good model system of biological membranes, as cellular membrane is a single bilayer of lipid molecules. Therefore, one needs to prepare model membrane containing single bilayer, known as unilamellar vesicles. MLV can form unilamellar vesicles whose size ranging from tens of nanometers (Small unilamellar vesicles, large unilamellar vesicles) to tens of micrometers (giant unilamellar vesicles) depending on the preparation methods used. Giant unilamellar vesicles (GUV), owing to their large size, can directly be observed under an optical microscopy and therefore, they serve as an excellent model system to study many biological phenomena [4] [5] [6].

Lipid-peptide interaction is one of the most important systems where GUVs are used in order to get some insight into the structure and functions of membrane proteins [7]. Study of antimicrobial activity of an antimicrobial peptide on the model membrane has drawn lots of attention due to their potential for bio-medical applications, such as antibiotics [8]. Giant vesicles are also used as micro reactors for enzymatic RNA synthesis [9]and used to compartmentalize nanoparticles of controlled size distributions [10]. Aqueous phase separation, bio mineralization and many other phenomena which mimic biological compartmentalization can be studied using GUV [11] [12]. Vesicles are also extensively used as carriers of bioactive agent, including drug, vaccines, cosmetics [13] [14].

6.3. Experimental:

Phospholipids, such as, Dioleoyl phosphatidylcholine (DOPC), Dioleoyl phosphatidylgylcerol

98

(DOPG) and Dioleoyl phosphatidylethanolamine (DOPE) were purchased from Sigma Aldrich and were used for vesicle preparation without further purification. LUV was prepared using extrusion technique as discussed in earlier chapters[15].

Zeta potential and size distribution were obtained at a temperature ($\sim 30^0 C$) with Zetasizer Nano ZS (Malvern Instruments, UK).The details are provided in chapter 2. The rate of decay of intensity-intensity autocorrelation function is measured which is used to calculate size distributions of LUV using Stoke-Einstein Relation.

Zeta potential was measured from electrophoretic mobility (μ) by Laser Doppler Velocimetry [24, 25]. ζ is now obtained from the model described by Smolushovski-Huckel equation, $\zeta = \frac{2\mu\eta}{3\epsilon\epsilon_0 f(\kappa a)}$, where ϵ and ϵ_0 are the relative permittivity of the medium and permittivity of the free space, respectively. η be the coefficient of viscosity of the aqueous solution. The Henry function is the function of vesicle radius a and the inverse Debye length κ. The μ provides information about the effective charges, Q_{eff}, of the vesicles. The Q_{eff} per vesicle have also been estimated from the measured electrophoretic mobility, according to the equation, $Q_{eff} = 6\pi\eta a_{eff}\mu$, where, a_{eff} is the effective radius of the vesicle including stern layer.

Average ς and the size distribution were obtained from 3-4 successive measurements. Each measurement includes 100-200 runs.

GUV were formed in 100 mM Sucrose prepared in 1 mM HEPES (pH 7.4) buffer using electrofomation, as described by Pott et al. [16]. We have modified the method. Instead of dried lipid film, we have used LUV suspension to deposit onto the ITO glass. In brief, 2 mm LUV suspension, prepared using an extrusion method, was deposited on both the ITO glasses as small little droplets. These droplets were allowed to dry overnight in a closed chamber containing saturated solution of NaCl. This is to avoid complete drying of the droplets. The hydration of these droplets facilitates electroformation process. Electroformation chamber for vesicle preparation consists of two ITO coated glasses separated by a teflon spacer of thickness ~ 2 mm. An alternating voltage of 1-2 Volts (peak to peak amplitude) and 10 Hz frequency was applied to the chamber for a couple of hours. For best result we have gradually increased the alternating voltage starting from 0.7 volts to 1.5 volts in the interval of 15 minutes. Similarly, at the end of 1-–2 hour, voltage was gradually decreased before we switched off the alternating field. This method helps to detach

vesicles from the substrate. The average diameter of the GUV obtained was 20-100 µm. After the formation of GUV, vesicles solution was transferred to a glass vial for storage. For better contrast in phase contrast microscopy, GUV solution was diluted in 100 nm Glucose prepared in 1 mm HEPES (pH 7.4), for observation. Both glucose and sucrose solution were kept same osmolality in order to balance the osmotic pressure between the interior and the exterior of the GUV. Production of GUV in the present protocol is very much reproducible.

6.4. Results and Discussions:

We have chosen phospholipids, such as, DOPC, DOPG and DOPE, due to their low chain melting transition temperature (T_m = -18^{0}C) so that vesicles can be prepared at room temperature (25 ^{0}C)$^.$ At room temperature, vesicles prepared from above phospholipids are in fluid lamellar (L_α) phase. Before preparing GUV, size distribution and zeta potential were measured. Size distributions of the LUV have been confirmed by dynamic light scattering. Typical size distribution of DOPC LUV is shown in Fig. 1(a). Average size in terms of effective hydrodynamic diameter was found to be ~ 100 nm. The size distribution reveals that LUVs are mainly mono-dispersed.
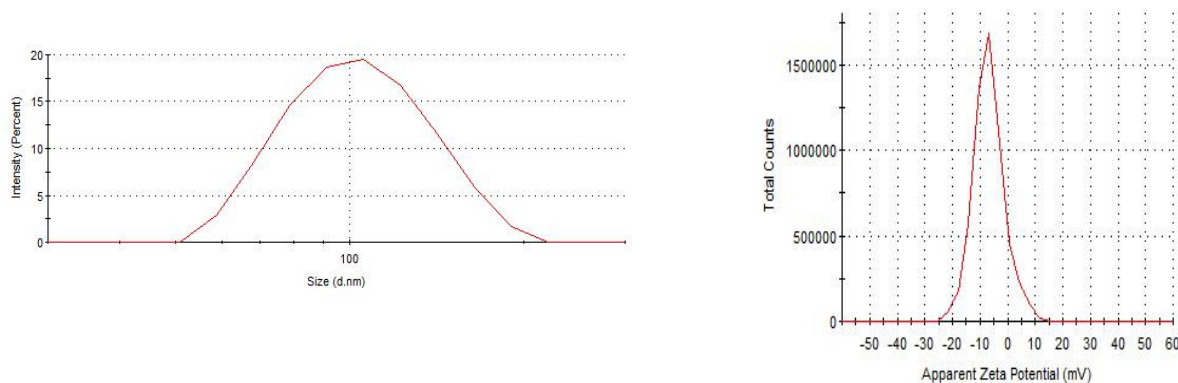

Figure 6.1: (a) and (b) show size and zeta potential distributions obtained from LUV made up of DOPC. These are captured images from the software provided by Malvern Instrument.

Table 1: Summary of size distribution and zeta potential results:

PDI: the polydispersity index. μ: electrophoretic mobility, Q_{eff}: effective elementary charges per vesicles in the unit of electronic charge . Errors are calculated from 3 consecutive measurements. As κ is a function of ionic composition, zeta potential was estimated from the Smoluchowski approximation with f(κa) = 1.5.

phospholipids	Size (d nm)	PDI	μ (cm²/Vs) 10⁻⁴	Zeta Potential (mV)	Q_{eff} (e)
DOPC	98 ± 2	0.06	-0.5 ± 0.1	- 6 ± 2	65
DOPC-DOPE (4:1)	99 ± 3	0.07	-1.3 ± 0.1	-16 ± 3	66
DOPC-DOPG (4:1)	98 ± 3	0.06	-4.0 ± 0.2	-52 ± 3	205
DOPE-DOPG (4:1)	100 ± 4	0.10	-4.4 ± 0.2	-56 ± 4	225
DOPG	99 ± 3	0.08	-4.8 ± 0.3	-61 ± 3	245

Zeta potential can be used to study the physico-chemical properties of the membranes and it can provide a good approximation of surface potential at low and moderate electrolyte concentrations (< 100 mM). Although zeta potential usually appears with respect to charged surface, a negative zeta potential of DOPC obtained from the experiments is intriguing. The orientation of hydration layers of the membranes, head group, water polarization as well as presence of impurity may be the possible origin of non-zero zeta potential in DOPC. Zeta potential for DOPG is found to be ~ - 61 mV as expected. Zeta potential of LUV obtained from mixture of PC-PG and PE-PG was found to decrease, as shown in table -1. This is expected as the amount of charge decreased with the mixture. Larger zeta potential obtained from PC-PE mixture as compared to pure DOPC could be a consequence of increasing the rigidity in the presence of DOPE. As the zeta potential is sensitive to pH of the aqueous solution, we have kept the pH fixed at 7.4 for all measurements. DOPE alone cannot form vesicles. This is due to fact that the DOPE head group forms hydrogen bonds with the water molecules making the bilayer very stiff. We have used a mixture of DOPC-

DOPE (4:1) to form LUV. Size and zeta potential distributions were found to be very similar to that of DOPC.

Although LUV can serve as model systems of biological membranes to study the interaction with ions or different bio-molecules, there are few major disadvantages. LUV often display broad size distribution. Therefore, properties such as permeability, spectra, etc. may not be identical for different LUV. Curvature of the membrane also plays important role in governing lipid packing, phase separation and many other phenomena occurring in the membrane surface. Small size LUV possesses a high curvature, compared to the much flatter cellular membrane. As LUV cannot be observed under an optical microscope, much information, such as shape deformation or fluctuation, phase separation etc. cannot be visualized directly. We can overcome above disadvantages, by preparing GUV. Here, we shall discuss the preparation of GUV from DOPC only.

After characterizing LUV from DOPC, we have successfully obtained giant unilamellar vesicles from large unilamellar vesicles as shown in Figure 6.2. Similar results were found for DOPG and DOPC-DOPE mixture also. The present work is an innovative approach to preparing GUV from LUV using electroformation. There are several advantages of this protocol over conventional electroformation [16]. Once we prepare LUV, in organic solvent such as choloform will no longer be required. Therefore, the process of preparing a lipid solution and solvent evaporation after coating onto a ITO glass can be avoided. Major advantage of our method is the use of LUV for experiments prior to the preparation of GUV. For example, we have measured size distribution and zeta potential of LUV prepared from charged as well as neutral phospholipid vesicles. In fact, we can study the interaction of various divalent and monovalent ions, drugs, antimicrobial peptide with LUV prior to the preparation of GUV. Therefore, if we prepare GUV from LUV, it would be a good protocol to reconstitute various biomolecules in GUV. This is also useful to envisage the influence of curvature and size on the bilayer properties of the vesicles.
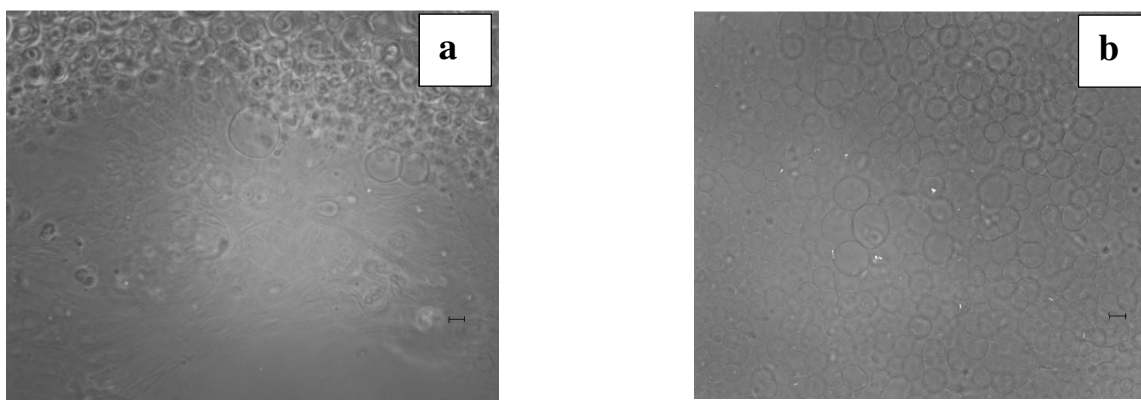
Figure 6.2: Phase contrast micrograph of GUV made from DOPC during their formation from LUV. Fig (a) and (b) shows the formation of GUV 10 minutes and one hour later from the application of alternating field, respectively. Images were taken from two different regions of the sample. Scale bar 5 μm.

Here we report an example, how an antimicrobial peptide, NK-2, can be reconstituted in GUV (Figure 6.3). Figure 6.3 a shows GUV prepared from LUV without the presence of NK-2. Halo region of the phase contrast image is due to the presence of sucrose in the interior and glucose in the exterior of GUV. In the absence of halo region in figure 6.3 b exhibits no contrast between the interior and exterior fluids of the membranes. Therefore, it is conceivable that there are some pores induced by NK-2 which are present on the GUV. Interior and exterior fluids can exchange through the pores. This process leads to decrease in contrast in the halo region of the image of GUV. Therefore, the image of GUV in the presence of NK-2 is very similar to the image when GUV are prepared with the aqueous solution and diluted with the same solution.
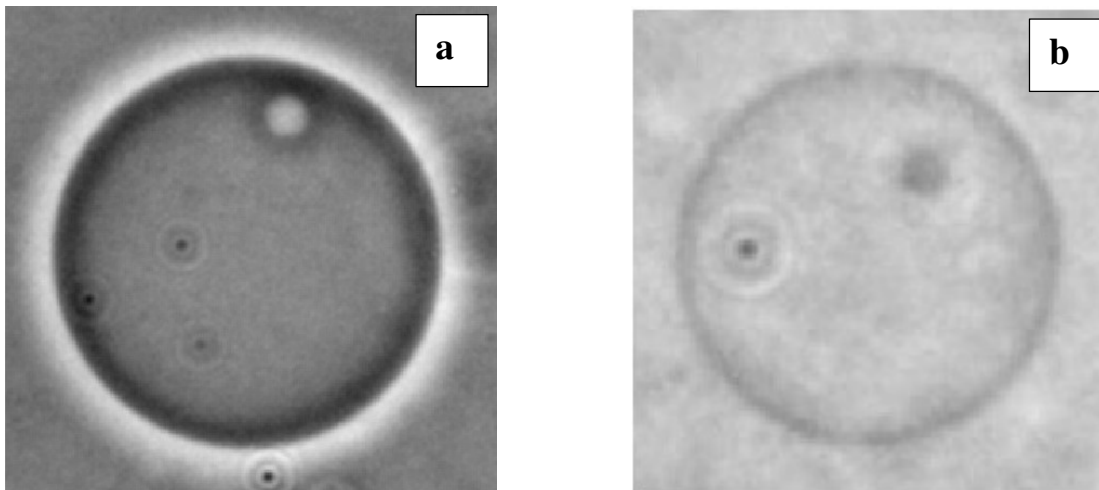
Figure 6.3: (a) A phase contrast micrograph of GUV made from LUV composed of DOPC and DOPG mixture at 4:1ratio. (b) shows GUV made from LUV of same composition as figure (a) in presence of NK-2. Size of these GUVs are ~ 20 μm.

The present preparation protocol will enable us to measure mechanical properties after reconstituting different bio-molecules such as proteins, peptides, cholesterol, etcf. Mechanical properties of the lipid bilayer play vital role in determining various processes, such as fusion, budding etc. GUVs are excellent model systems to determine binding and stretching modulus of lipid bilayer using either micropipette aspiration techniques or Fourier analysis of fluctuation spectra. GUVs are also useful to introduce molecules, such as DNA using microinjection techniques.

6.5. Conclusion:

Preparation and characterization of lipid membranes are the key step for understanding the properties and functions of cellular membrane. In the present study, we have discussed the formation and characterization of phospholipid bilayer, an excellent model system of biological membranes, in the form of LUV, GUV. We have successfully obtained GUV from LUV using electroformation. We have also measured size distribution and zeta potential of LUV using dynamic light scattering. The several advantages of the present approach to prepare GUV over the conventional electroformation were also discussed. Giant unilamellar vesicles (GUVs) provide the

possibility to directly visualize certain interactions in a small but optically resolvable volume encapsulated by the vesicle membrane. We have presented an example, where an antimicrobial peptide NK-2 was reconstituted in GUV prepared from LUV. The present study provides us an important insight into the physico-chemical properties of membranes in terms of their size and geometry. Therefore, GUV serves an excellent and simpler model system whose size, geometry, and composition can be tailored with great precision.

References:

[1]   D.E. DISCHER and A. EISENBERG, SCIENCE 297 (2002) 967-973.

[2]   J.R. Howse, R.A.L. Jones, G. Battaglia, R.E. Ducker, G.J. Leggett and A.J. Ryan, Nat Mater 8(6) (2009) 507-11.

[3]   B. Alberts, D. Bray, J. Lewis, M. Raff, K. Roberts and J.D.W.p.N.Y.a.L. 1994, Garland Publishing, (1994) 1361.

[4]   S.F. Fenz and K. Sengupta, Integr. Biol 4 (2012) 982-995.

[5]   R. Dimova, S. Aranda, N. Bezlyepkina, V. Nikolov, K.A. Riske and R. Lipowsky, J Phys Condens Matter 18(28) (2006) S1151-76.

[6]   P. Walde, K. Cosentino, H. Engel and P. Stano, ChemBioChem 11 (2010) 848-865.

[7]   S. Galdiero, A. Falanga, M. Cantisani, M. Vitiello, G. Morelli and M. Galdiero, Int. J. Mol. Sci. 14 (2013) 18758-18789.

[8]   K.A. Brogden, Nature Reviews Microbiology volume 3, pages (2005) 3 (2005) 238–250.

[9]   A. Fischer, A. Franco and T. Oberholzer, Chembiochem 3(5) (2002) 409-17.

[10]   J. Song, L. Cheng, A. Liu, J. Yin, M. Kuang and H. Duan, J. Am. Chem. Soc 133,28 (2011) 10760–10763.

[11]   P. Yang and R.Dimova, In Tech 523 (2011).

[12]   Y. Li, R. Lipowsky and R. Dimova, J. Am. Chem. Soc. 130, 37 (2008) 12252–12253.

[13]   M.N. Holme, I.A. Fedotenko, D. Abegg, J. Althaus, L. Babel, F. Favarger, R. Reiter, R. Tanasescu, P.-L. Zaffalon, A. Ziegler, B. Müller, T. Saxer and A. Zumbuehl, Nature Nanotechnology 7 (2012) 536–543.

[14]   V.P. Torchilin, Nature Reviews Drug Discovery 4 (2005) 145–160.

[15]   M.J. Hope, M.B. Bally, W. Webb and P.R. Cullis, Biochem. Biophys. Acta 55 (1985) 812.

[16]   T. Pott, H. Bouvrais and P. Méléard, Chem Phys Lipids 154(2) (2008) 115-9.

List of Publications:

- Supported Planar Single and Multiple Bilayer Formaion by DOPC Vesicle Rupture on Mica substrate: A Mechanism revealed by Atomic Force Microscopy Study: **Amrita Basu**, Prasanta Karmakar, Sanat Karmakar: Journal of Membrane Biology (2020), 253, 205-219.

- Preparation of Giant Unilamellar Vesicles and Solid Supported bilayer from Large Unilamellar Vesicle: Model Biological Membranes: **Amrita Basu**, Pabitra Maity, Prasanta Karmakar, Sanat Karmakar, Journal of Surface Science and Technology: (2016) 32 (3-4) 83-90.

- Nanomechanical properties of cholesterol rich domains in mica supported unsaturated lipid membrane: An atomic force microscopy study: **Amrita Basu,** Prasanta Karmakar,Sanat Karmakar, Submitted to European Biophysics Journal (Under review).

- Effect of silver nanoparticle on the formation of solid supported phospholipid bilayer: An AFM Study: **Amrita Basu**, Prasanta Karmakar and Sanat Karmakar, submitted to Bulletin of Materials Science.

Supported Planar Single and Multiple Bilayer Formation by DOPC Vesicle Rupture on Mica Substrate: A Mechanism as Revealed by Atomic Force Microscopy Study

Amrita Basu[1] · Prasanta Karmakar[2] · Sanat Karmakar[1]

Abstract

A planar lipid bilayer on a solid support serves as model system that explains fundamental aspects of membrane biology and enables us to characterize wide-range surface-sensitive techniques, including molecular engineering. The present study aims at understanding the process of single and multiple bilayer formation after the exposure of small unilamellar vesicles (SUVs) of dioleoyl phosphatidylcholine (DOPC) to mica substrate. Isolated single bilayer formation and co-existence of double and triple lipid bilayers in the aqueous medium have been quantitatively measured by atomic force microscopy and discussed the physicochemical mechanism. It has been observed that due to the strong adhesion of DOPC SUV to mica surface, vesicles of diluted solution rupture spontaneously and form isolated bilayer patches when they come in contact with the mica surface. No further lateral growth or movement of the bilayer patches has been observed upon increase of incubation time. However, the increase of vesicle number on the same surface area by successive deposition of DOPC solution of same concentration and increasing incubation time shows merging of the nearby patches as well as development of stacked second and third bilayers due to edge-guided rupture of adsorbed vesicles on first or second bilayer patches. Mechanisms of single and multi-bilayer formation and a theoretical interpretation of the process have been elucidated.

Introduction

Biological membranes are complex and are regulated by various proteins, cholesterol, and other active biomolecules. Therefore, it is often useful to study model membrane in order to gain insight into the structure and functions of membranes which may be difficult to study in vivo. Unilamellar vesicles are excellent model systems to study. Besides unilamellar vesicles, solid supported lipid bilayers (SLBs) are useful for studying many biological processes, especially cell adhesion, fusion, signaling, adsorption of molecules, to name a few (Leonenko et al. 2000). A variety of techniques, viz Langmuir–Blodgett deposition (Blodgett 1935), vesicle fusion (Richter et al. 2003), lipid—detergent method (Kataoka-Hamai et al. 2010), and many more have been applied to prepare SLB. Among them, the vesicle fusion method is quite reliable and easy. However, the mechanism of SLB formation by simple vesicle fusion is not yet adequately understood.

Moreover, various differing reports are present in hitherto published literature regarding the mechanism of SLB formation. Reviakine and Brisson (2000) used the vesicle fusion method on mica to study the early stage of SLB formation and compared their results with available theoretical works. They observed that the SLB formation depends highly on vesicle size, lipid concentration, and the presence of Ca^{2+} ions in the medium though Attwood et al. (2013) noted that the SLB could be formed even in the absence of Ca^{2+} ion. Weirich et al. (2010) revealed that the vesicles need rearrangement before rupture. Besides, Jass et al. (2000) demonstrated that when liposomes are attached to a hydrophilic surface, they get flattened until two membrane bilayers stack on top of each other. Moreover, the authors reported that

✉ Prasanta Karmakar
prasantak@vecc.gov.in

1   Soft Matter and Biophysics Laboratory, Department of Physics, Jadavpur University, 188, Raja S. C. Mallick Road, Kolkata 700032, India

2   RIB Group, Variable Energy Cyclotron Centre, 1/AF, Bidhannagar, Kolkata 700064, India

the upper layer of the stacked layers slides over the lower layer and forms a bilayer patch. In order to gain insights into the fundamental as well as the applied aspects of membrane, various experimental techniques, such as atomic force microscopy (AFM, Åkesson et al. 2012; Richter et al. 2003, 2006), dissipation-enhanced quartz crystal microbalance (QCM-D, Åkesson et al. 2012; Lind et al. 2015), ellipsometry (Richter and Brisson 2005), neutron reflection (Åkesson et al. 2012; Wacklin 2011; Wacklin and Thomas 2007), interferometric scattering microscopy (Andrecka et al. 2013), and fluorescence microscopy (Åkesson et al. 2012; Bernchou et al. 2009), have been used.

In addition to the single bilayer, formation of multilayer model membrane is of great importance for studying its interaction with drugs, nanoparticles or membrane-embedded protein. For example, embedded proteins of larger dimension cannot be accommodated in a single solid lipid model bilayer due to their structural deformation (Han et al. 2010). The lipid multilayer model system can be an effective solution in the aforementioned scenario of structural deformation. Multilayer lipid membranes are also found in the natural environment, e.g., in mitochondrial cristae, in neuron, in thylakoid, etc. Different procedures have been followed to form artificial lipid multilayers (Heath et al. 2016; Kang et al. 2018; Perino-Gallice et al. 2002; Sironi et al. 2016; Vogel et al. 2000; Zhu et al. 2015). Vogel et al. (2000) reported the formation of lipid multilayer by depositing lipid solution dissolved in an organic solvent on silica and glass substrate by "spin coating" method. A "rock and roll" method for the construction of multilayer was followed where lipid solvent solution was deposited on different substrates (Tristram-Nagle 2007). Heath et al. (2016) reported the formation of multiple bilayers by adding poly-L-lysine (PLL), an electrostatic linker, repeatedly in a controlled condition to the junction of two lipid bilayers. Single and double bilayers were also observed by injecting dioleoylphosphatidylethanolamine (DOPE) liposome suspension diluted with MgCl$_2$ aqueous solution on mica surface (Egawa and Furusawa 1999). Okamoto et al. (2012) prepared single and double bilayers by depositing DOPC in buffer solution on graphene oxide surface by vesicle fusion method. Sironi et al. (2016) used a different procedure where aqueous liposome solution was drop cast on mica substrate and dried to form a large number of stacked anhydrated bilayers. In all these works, lipids were dissolved in an organic solvent and/or additional linker was added between the bilayers or the aqueous medium was dried to form the artificial multibilayer structure. The native characteristics as well as fluid nature of such stacked bilayers may be lost due to incorporation of ligands and linkers. Therefore, spontaneously growing multiple bilayers in the aqueous medium without using additional interlayer or ligands is more desirable for the realistic model system.

In this article, the mechanism of DOPC vesicle rupture and consequent single and multiple SLB formation on the freshly cleaved mica surface have been investigated. For quantitative measurement of SLB fragments in liquid medium, along lateral and vertical directions, atomic force microscope has been used. The result of such measurement has showed instant rupture of DOPC vesicles at the contact of highly hydrophilic mica surface and, also, formation of immobile SLB patches. When the number of vesicle in the solution is inadequate to cover the entire substrate, instead of continuous bilayer film, isolated small bilayer patches are formed, resulting in a large number of available bilayer edges. Further addition of DOPC vesicles on the same substrate causes new bilayer patch formation and enlargement by coalescing nearby patches. It is observed that the sequentially deposited vesicles are also adsorbed on the already formed bilayer patches forming stacked bilayers. This phenomenon is attributed to the rupture of adsorbed vesicles by the edges of the supporting bilayer patches. To the best of our knowledge, this is the first report of co-existence of single, double, and triple bilayers in an aqueous medium by simple sequential addition of diluted DOPC vesicle solution on the highly hydrophilic mica surface.

Experimental

Preparation of Small Unilamellar Vesicles (SUVs)

Dioleoylphosphatidylcholine (DOPC) was purchased from Sigma-Aldrich and used for vesicle formation without further purification. SUVs were prepared by following the extrusion method described by Hope et al. (1985). An appropriate amount of lipid dissolved in chloroform (stock solution with concentration 1 mg/ml) was taken in a glass vial. The organic solvent was then removed by gently passing nitrogen gas. The sample was placed in vacuum desiccators overnight to remove the traces of organic solvent. The required amount of Millipore water was added to make the final concentration of 0.05 mg/ml. The solution was vortexed for 30 min at room temperature. This procedure results in formation of multilamellar vesicles (MLVs). The SUV was then produced from the MLV suspension by several times extrusion through a polycarbonate membrane having pore diameter 50 nm using a Liposofast extruder from AVESTIN (Canada).

Dynamic Light Scattering (DLS)

The size distribution of extruded vesicles was measured by the DLS technique. The extruded vesicles were taken in a cuvette, and the size distribution was obtained at 30 °C with a Zetasizer Nano ZS (Malvern Instruments, UK). It uses 4

mW He–Ne laser of wavelength 632.8 nm. The scattered light detected at a scattering angle of 173° was directed to a signal processing correlator. The rate of decay of intensity autocorrelation function was measured, and size distribution was calculated by Stokes–Einstein relation.

Preparation of Mica Substrate

Naturally available high-grade muscovite mica have been used from Jharkhand, India. For consistency, a single ~ 200 mm × 150 mm mica sheet was cut into pieces of 12 mm × 12 mm. The chemical property of the mica was investigated by X-ray photoelectron spectroscopy (Bhowmik and Karmakar 2019). Contact angle measurement of freshly cleaved mica shows super hydrophilic nature with contact angle less than 5° (Bhowmik and Karmakar 2018). The mica substrates were cleaved with scotch tape and without any further processing. DOPC vesicle solution was deposited immediately. Muscovite mica is a naturally available layered structured material where negatively charged aluminosilicate layers are interconnected by positively charged K^+ ions. Due to weak ionic bonding via K^+ ions, aluminosilicate layers are easily separable. During cleaving by scotch tape, K^+ ions are shared by the two newly generated surfaces (Müller and Chang 1969). As a result, the cleaved surface becomes negatively charged due to depletion of K^+ ions. With time the negative surface charge is compensated by the bulk positive charges. Immediate deposition of vesicle solution just after cleaving results in strong adhesion between mica and vesicle through attractive interaction between negatively charged mica surface and zwitterionic DOPC vesicles. Muscovite mica substrate have been used also from MTI Corporation.

Atomic Force Microscopy

For AFM measurements, Bruker made Multimode Scanning Probe Microscope with Nanoscope V controller have been used. A liquid-resistant 10 μm scanner and a standard fluid cell with cantilever holder and O-ring (Bruker, MTFML-V2) with liquid flow arrangement were used. The AFM in tapping as well as ScanAsyst modes was operated. Super sharp silicon nitride (Bruker SNL10) probe with tip radius 2 nm and spring constant 0.12 N/m for tapping mode was used. A resonance frequency of the probe in pure water was manually selected at ~ 5.8 kHz and manually adjusted the amplitude set point for the best imaging. For Peak Force ScanAsyst mode, high-resolution probes (Bruker, SCAN ASYST-FLUID) with spring constant 0.35–1.4 N/m were used, where scan parameters were controlled in auto mode. In all cases, the images were acquired at scanning rate 1–2 Hz. The AFM images were flattened by "Flatten plus" of WSxM software to eliminate slopes, bows, and/or bands in the images (Gimeno et al. 2015). Using the same software,

the line profiles and statistical distribution of heights and lateral sizes were presented. In Figs. 7, 9, and 10, contour plots of the AFM images were presented by the same software. By selecting the range of heights corresponding to the first, second, and third bilayers, the height images were sliced to show single, double, and triple bilayers separately.

Preparation of Solid Supported Bilayer and AFM Measurements

DOPC vesicle deposition and AFM measurements were done in the following way:

Mica substrates were attached to the metal disks using double-sided tape. The attached mica was cleaved two/three times to get a uniform and fresh surface with an adhesive tape. The DOPC vesicle solution was deposited immediately on the freshly cleaved mica surface by a micropipette. In the first set of experiment, 10, 20, and 30 μl of 0.05 mg/ml SUV solution were deposited on three freshly cleaved mica surfaces and incubated for 15 min. In the second set of experiment (case of sequential deposition), the 10 μl of the same DOPC solution was added successively on mica substrate every 15 min and incubated for a total time of 45 to 75 min (as indicated) in a closed container to avoid evaporation. In both the cases, after the incubation period, samples were rinsed gently with Millipore water and immediately covered with pure water as well as placed on the AFM scanner for measurements in liquid mode. In third set of experiment, 10 μl of 0.05 mg/ml DOPC solution was deposited on freshly cleaved mica and incubated for 15 min like the first experiment of the first set, but here the time-lapse AFM images were recorded without rinsing the deposited solution. Mica surface covered with DOPC solution was imaged continuously for 15 min. Then additional 10 μl 0.05 mg/ml DOPC solution was injected in situ in the liquid cell by a syringe without stopping the scan. Time-lapse AFM images were recorded for another 70 min. Every full scan took around 9 min.

Results and Discussion

Formation of Single SLB Fragments on Mica from DOPC SUV

Size distribution of SUV obtained from extrusion method is shown in Fig. 1. The polydispersity index (0.07) clearly indicates that the vesicles are fairly monodispersed. These SUVs of concentration 0.05 mg/ml were used for SLB formation. Figure 2a shows the AFM image of bilayer fragments formed by rupture of uniform DOPC vesicles for 15 min incubation and subsequent rinse by Millipore water. It is clearly evident from the one-dimensional line profile
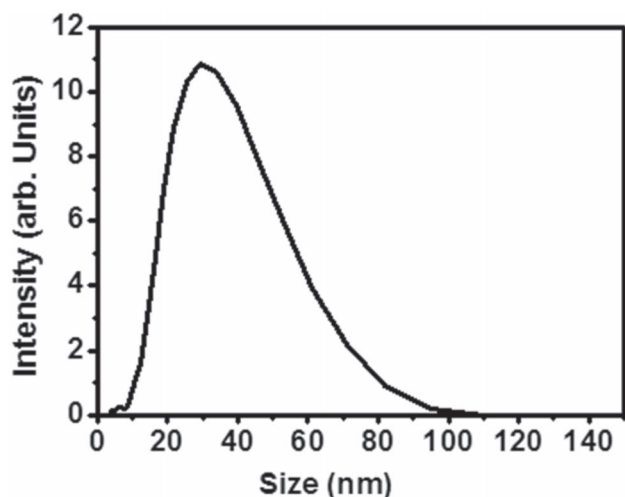
Fig. 1 Size distribution of DOPC vesicles as measured by dynamic light scattering (DLS) (Color figure online)

adsorbed ultrathin water layer, and the other one is for single bilayer fragments with a broad peak maximum at 4.2 nm. Mornet et al. also reported an ultrathin water layer of thickness 0.5–1.5 nm between the substrate and lipid bilayer by cryo-transmission electron microscopy (Mornet et al. 2005). Typical bilayer thickness is around 4–5 nm (Attwood et al. 2013; Lv et al. 2018), but lower average height of bilayer is observed because some times higher tapping force could result in lowering the height of the bilayer (Tero et al. 2017). The measured average height of the bilayer fragments is in agreement with the earlier reports (Lind et al. 2015; Schonherr et al. 2004). The distribution of the diameter of the bilayer patches is also shown in Fig. 2d, which shows the peak at around 50–60 nm. It is also evident that the patches of maximum size are found to be at 180 nm. Interestingly, the bilayer patch size distribution is consistent with the vesicle size distribution measured by DLS (Fig. 1). It shows the size distribution maxima at around 30 nm and sizes up to 90 nm (Fig. 1). Therefore, it is conceivable that the individual vesicle of radius R_0 forms the isolated bilayer fragment of radius nearly equal to $2R_0$.

When the SUV in the solution reaches randomly on the mica surface, it may rupture depending on the probability of the pore formation on the vesicle membrane and the

(Fig. 2b) that the average height of the bilayer patches is ~ 3.0 nm. Height distribution of the entire surface is shown in Fig. 2c. It shows two peaks. The first one is from 0.5 to 2 nm, peaked at 1.2 nm for the bare mica surface with
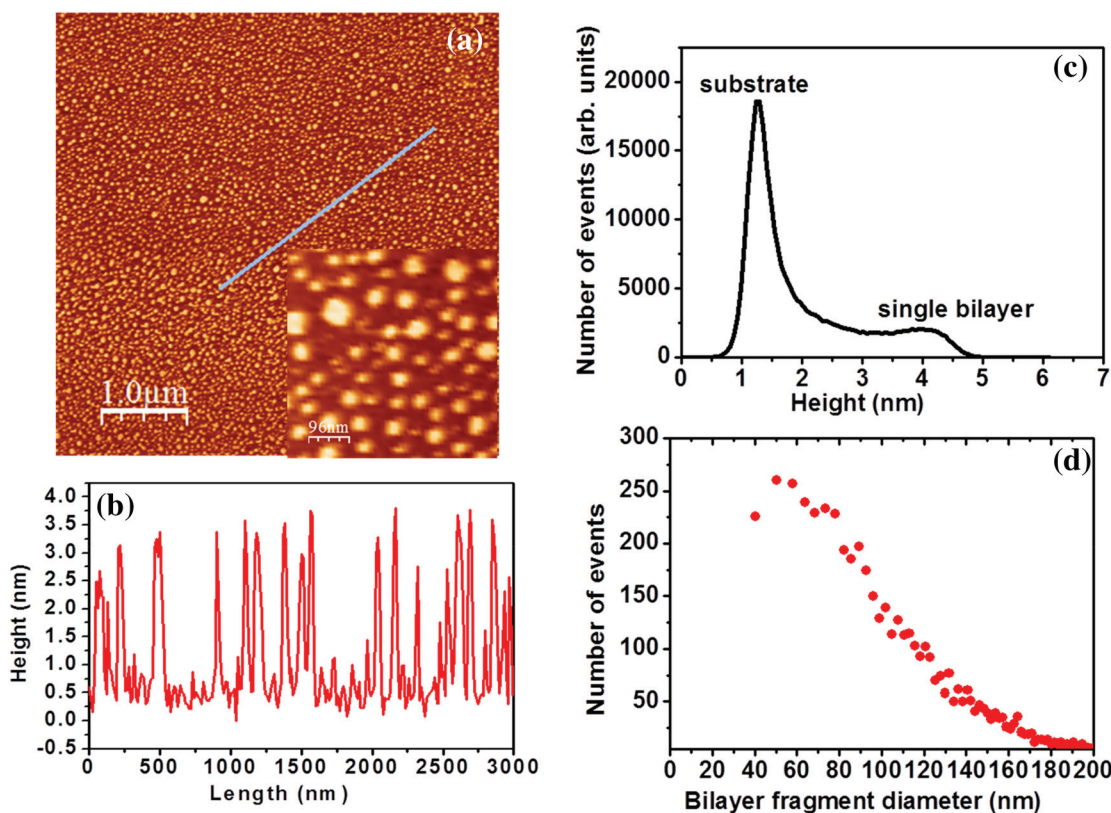

Fig. 2 **a** AFM image of DOPC bilayer fragments on mica surface after 15 min incubation with 10 µl solution and subsequent rinse with water, **b** line profile along the marked line, **c** height distribution of the surface, and **d** lateral size distribution of the bilayer fragments (Color figure online)

interaction between the vesicle and mica surface (Israelach-vili 2011; Takáts-Nyeste and Derényi 2014a, b). At finite temperature, pores of a vesicle membrane appear stochastically and reseal transiently. The pore opening is driven by the membrane tension, whereas its closure is guided by the pore's line tension (Karatekin et al. 2003). It was assumed that the vesicles in the solution are spherical in shape. Mui et al. (1993) showed that if contamination-free Millipore water is used, the vesicles will swell to spherical shape after extrusion. When the vesicles are in contact with the flat hydrophilic surface, their shapes are deformed to maximize its contact area with the adhering surface (Takáts-Nyeste and Derényi 2014a, b). On considering a cap-shaped deformed adsorbed vesicle on a mica surface (Fig. 3) as described by Takáts-Nyeste and Derényi (2014a, b, the surface tension of the membrane can be described by the force balance equation of Young Dupre (Seifert and Lipowsky 1990) in thermal equilibrium condition: $\sigma = \frac{w}{1+\cos\varphi} = w\frac{A_{\parallel}-\pi R^2}{2\pi R^2} \approx w\frac{A_0-\pi R^2}{2\pi R^2}$, where w is the adhesion energy per unit area between the membrane and the surface, φ is the contact angle between surface and the vesicle, R is the radius of the contact area of the vesicle with the surface, $A_{\parallel}$ is the projected area of the vesicle when thermally induced undulations of the membrane are averaged, and A_0 is the total area of the vesicle. A critical value of w for rupture of the vesicle of radius R_0 can be estimated by balancing the energy gain due to adhesion and the energy cost of the free edge of the final bilayer patch of radius $2R_0$, i.e.,$4\pi R_0^2 w_{\mathrm{crit}} = 4\pi R_0 \lambda$, or $w_{\mathrm{crit}} = \lambda/R_0$, where λ is the line tension of the bilayer edge. The w_{crit} obtained from this thermodynamic criterion does not guarantee the rupture of vesicle. It occurs only for significant larger value of w than w_{crit} (Takáts-Nyeste and Derényi 2014a, b). This can be understood from the pore opening kinetics and the consequent change of surface tension.

Pore opening in the membrane is a stochastic process and can occur anywhere along the membrane. Pore formation leads to a decrease of energy $(-\pi r^2\sigma)$ due to the relaxation
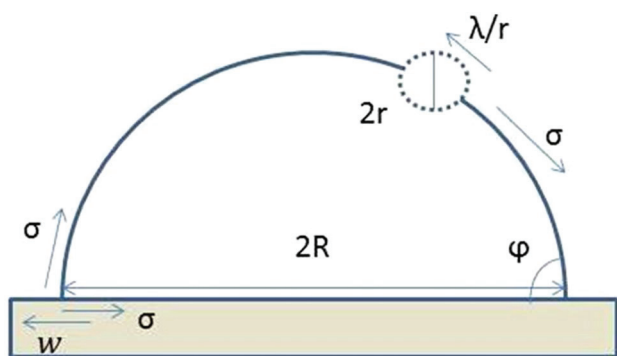

Fig. 3 Schematic diagram of pore formation and adsorption of vesicle on a solid substrate (Color figure online)

of stress and increase of energy $(2\pi r\lambda)$ due to pore boundary formation (Helfrich and Servuss 1984), where r is the radius of pore and λ is the line tension. The energy of the pore can be written as $\Delta E \cong 2\pi r\lambda - \pi r^2\sigma$. Now the maximum energy of the pore is given as $\Delta E_{\mathrm{max}} = \frac{\pi\lambda^2}{\sigma}$ at $r = \frac{\lambda}{\sigma}$ which can be considered as the activation energy of pore formation. Thus, pore opening rate can be written as $K_{\mathrm{d}} = K_0 \frac{A_{\mathrm{c}}}{a^2} \exp\left[-\frac{\pi\lambda^2/\sigma}{K_{\mathrm{B}}T}\right]$, where $A_{\mathrm{c}} = A_0 - \pi r^2$ is the non-adhering surface area of the vesicle, a^2 is the surface area of the lipid molecule of linear size $a \approx 0.8$nm, K_0 is the local attempt rate of pore nucleation, and $k_{\mathrm{B}}T$ is the thermal energy. Thus, to open a pore on the membrane, the value of surface tension has to exceed $\sigma_{\mathrm{crit}} = \frac{\pi\lambda^2}{K_{\mathrm{B}}T\ln\left(\frac{K_0 A_{\mathrm{c}}}{K_{\mathrm{d}}a^2}\right)}$. At the initial stage of vesicle adsorption, the non-adhering area A_{c} is very small, and therefore, surface tension is larger than this threshold value. As a result, the pore opens easily, but if pore reseals and adhering area increases, the surface tension drops below this threshold value. The situation is worst when vesicle is almost flat, i.e., $\varphi = 0$ and $\sigma = w/2$ (Fig. 3). Pore opening for adsorbed vesicle of any arbitrary shape is therefore ensured only when adhesion is larger than $w_{\mathrm{crit}}^{\mathrm{pore}} = 2\sigma_{\mathrm{crit}}$ (Takáts-Nyeste and Derényi 2014a, b). Thus, vesicle rupture is not guaranteed when $w > w_{\mathrm{crit}}$, but it is assured when $w = w_{\mathrm{crit}}^{\mathrm{pore}} > 2\sigma_{\mathrm{crit}}$. It indicates very high adhesion energy which confirms spontaneous vesicle rupture. High adhesion energy between DOPC vesicle and mica surface in the present experiment leads to the instantaneous rupture of vesicles and formation of isolated bilayer patches of area equivalent to individual vesicles.

Earlier, quartz crystal microbalance resonant frequency and dissipation (QCM-D) combined with surface plasmon resonance (SPR) spectroscopy revealed that the vesicle rupture occurs only after a critical vesicle coverage (Keller et al. 2000). It is found that DOPC vesicles of all size rupture on mica and form bilayer patches as soon as they adhere to the surface. Reviakine and Brisson (2000) also studied SLB formation on mica. They found both supported vesicular layers, as well as isolated bilayer patches, by varying vesicle size, lipid concentration, and presence of Ca^{2+} ions. Recently, Andrecka et al. (2013) observed spontaneous rupture of DOPC vesicle similar to the present experiment, as well as wave-like bilayer spreading on silica, mica, and plasma-modified mica surface. They wet the surface by buffer solution (10 mM HEPES, pH 6.8, 200 mM NaCl, 2 mM $CaCl_2$) first and then added the vesicle solution. They concluded that the individual vesicle rupture or wave-like cascade rupture depends on the vesicle size and functionalization of the surface. Role of different ion containing buffer solution on SLB formation is complex; thus, the mechanism is not well understood. In this article, the authors, therefore, use ultrapure water for making DOPC vesicle solution. Isolated bilayer patch have been repeatedly observed,

but no supported vesicular layer has been found by AFM measurement. Leonenko et al. (2000) found similar isolated bilayer patch formation as well as double bilayer formation on unmodified and modified mica surface by deposition of DOPC solution with ultrapure water. It turns out that, if the interaction between the adsorbed vesicle and substrate surface is strong enough, the vesicles rupture spontaneously at adsorption as observed in the present case; otherwise, rupture of a seed vesicle is required to start a cascade or the nearby vesicles coalesce to grow larger to attain a critical size. The vesicle rupture may also take place if the adhesion property of the substrate surface is altered by deposition of polymer, chemical treatment or nanoparticles incorporation (Melcrova et al. 2016; Tanaka et al. 2009; Verma and Stellacci 2009). The distribution of fragment size (Fig. 2d) also illustrates that the possibility of vesicle fusion within the solution or on the substrate is rare. Anderson et al. (2009) also reported that a strong electrostatic attraction between the charged substrate and the uncharged vesicle helps adhere, deform, rupture, and spread as bilayer, but the vesicles do not adhere or fuse each other in solution. DLS measurement of the stock solution on different days also shows no considerable change in vesicle size distribution. However, few larger bilayer fragments with the size equivalent to multiple vesicles are also observed as shown in AFM image wherever the adsorbed vesicle density is more than average.

To explain the isolated patch formation instead of continuous or semi-continuous bilayer formation due to dilute DOPC solution deposition, the approximate number of DOPC vesicles in 10 µl of stock solution (0.05 mg/ml), deposited on 12 mm × 12 mm mica surface, have been estimated. 10 µl 0.05 mg/ml solution contains 0.5 µg DOPC which corresponds to 0.636 nmol. The number of DOPC molecule in 0.636 nmol is 38.3×10^{13}. On considering each DOPC molecule to cover 0.7 nm^2 (Kucerka et al. 2005), all the molecules will cover 134 mm^2 area in the form of bilayer out of 144 mm^2 mica surface if all the molecules are

assumed to be adsorbed and ruptured. Leonenko et al. (2000) stated that it is unlikely that every vesicle–surface interaction results in adhesion. They showed that out of 424 vesicles/µm^2 only 150 vesicles/µm^2 (approx. 35%) are adsorbed during 2 min deposition and a brief rinse. Therefore, formation of isolated bilayer patches are expected for 10 µl, 0.05 mg/ml DOPC solution deposition on 12 mm × 12 mm mica surface.

To verify the dynamic growth and stability of the bilayer patches during incubation with 10 µl stock solution (0.05 mg/ml), the AFM images of mica surface with the deposited DOPC solution have been recorded. At the initial stage of incubation, bilayer fragments are formed as observed in Fig. 2 (AFM after rinse with water). Appearance of additional patch or any considerable change of the existing bilayer fragments was not observed even after 30 min (Fig. 4). However, a slight lateral shift of the features is observed with time due to the thermal drift of AFM scanner (Wang et al. 2014). This dynamic imaging during incubation indicates that no further growth or lateral movement of bilayer fragments takes place with the increase of incubation time. It also confirms the strong adhesion of the first bilayer with the mica surface and immobility of the bilayer patches. Leonenko et al. also found immobility of the bilayer patches even after a long time.

In order to verify the merging of individual fragments, the same experiment was performed with double quantity (20 µl) of DOPC vesicle solution on the same area of mica substrate (12 mm × 12 mm, Fig. 5). It is observed that the average bilayer fragment sizes increase, and most of the fragments are larger than the individual vesicle size. It indicates that when the number of the adsorbed vesicles is twice on the same substrate area, the possibility of merging of the ruptured vesicles increases. The possibility of vesicle fusion in the solution is very rare; any change of DLS size distribution of the stock solution have not been seen even after a few days. Anderson et al. (2009) also predicted rare probability of merging in such diluted solution. Andrecka et al. (2013) never observed

Fig. 4 10 µl 0.05 mg/ml DOPC solution deposited on freshly cleaved mica and incubated for 15 min. Time-lapse AFM images taken in liquid mode immersed with the same solution, **a** at time 15–24 min and **b** at time 24–33 (Color figure online)
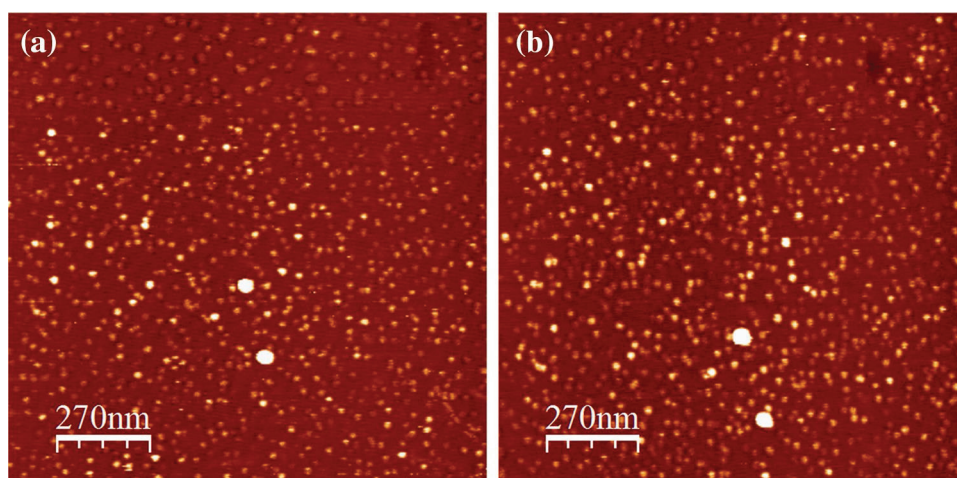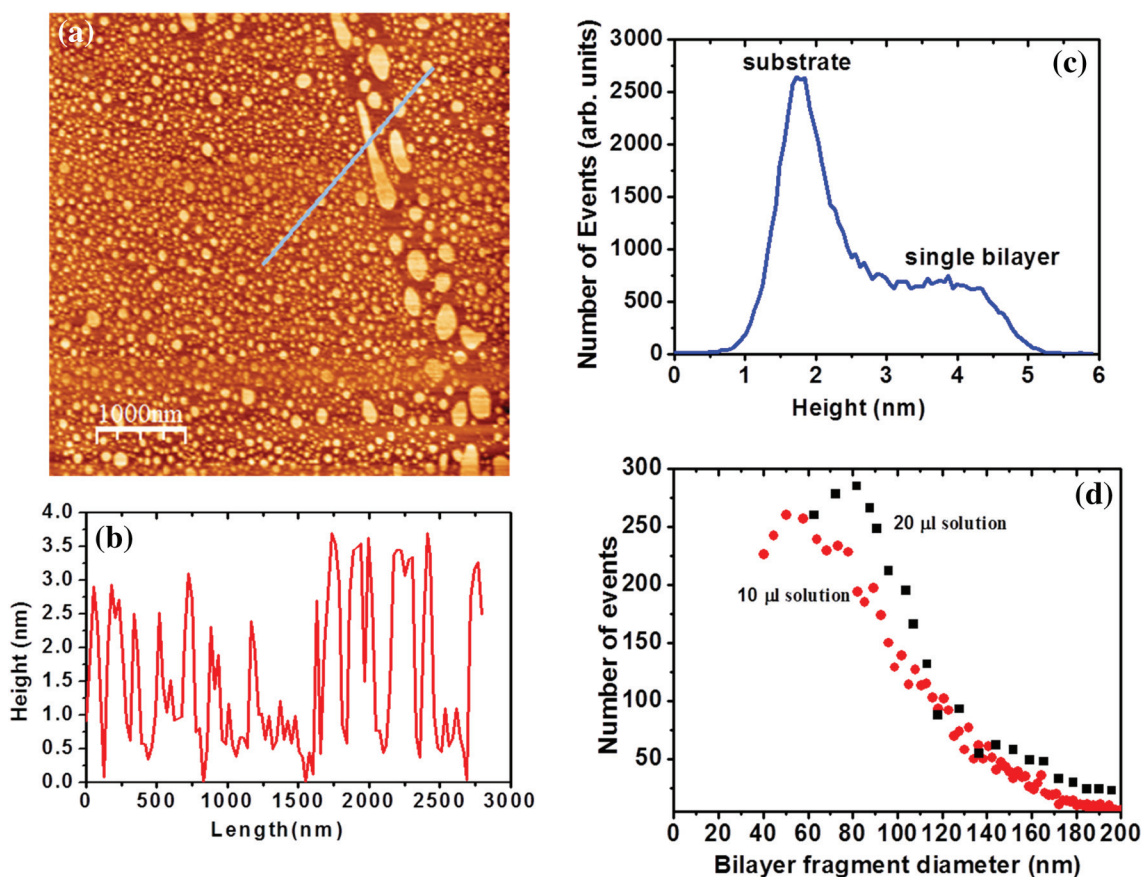
Fig. 5 a AFM image of DOPC bilayer fragments on mica surface after 15 min incubation with 20 µl solution and subsequent rinse with water, **b** 1D profile along the marked line, **c** height distribution of sur- face, and **d** lateral size distribution of bilayer fragments (red circles for Fig. 2a and black squares for **a**) (Color figure online)

signature of vesicle fusion during monitoring bilayer formation from different-size DOPC vesicles on different substrates by interferometric scattering microscopy. In some part of the mica surface where the adsorbed number of vesicles are sufficient to cover more area, a semi-continuous bilayer is formed due to the merging of individual bilayer fragments (Fig. 5a). A simi- lar type of semi-continuous bilayer is also reported for incuba- tion with 0.5 mg/ml concentrated vesicle solution (Attwood et al. 2013). Richter et al. (2006) described the formation of such extended bilayer patches as a result of cascade rupture of adsorbed neighboring vesicles on the surface. In the present case, DOPC on mica (Figs. 2, 4, 5), the isolated or extended bilayer patches are not formed by the sequential cascade rup- ture. Instead spontaneous rupture of individual vesicles on the mica surface and successive bilayer edge-guided merging take place. When the coverage of adsorbed vesicles is low, each vesicle forms isolated patches (Figs. 2, 4), but when the cover- age is more, semi-continuous bilayer patches are formed due to the merging of isolated patches. When bilayer fragments are in close proximity, the edges become energetically unfavorable and are expected to promote the interaction with the adjacent

lipid material. Such bilayer edges also play an important role to initiate the rupture of surface-bound or near-surface vesi- cles as in the case of wave-induced vesicle rupture (Andrecka et al. 2013). As the surface-bound vesicles are not available due to the instant rupture of the vesicle, the adjacent bilayer patches merge and minimize the energy. For example, if two equal patches of average radius R_1 merge, the resultant average radius would be $\sqrt{2}R_1$; therefore, edge energy will be reduced from $4\pi R_1 \lambda$ to $2\sqrt{2}\pi R_1 \lambda$ due to merging. Thus, the fragments coalesce and grow larger when the number of fragments are increased due to the increase in vesicle number. The increase of average bilayer size due to the increase of vesicle number is presented in Fig. 5d. Only the merging of fragments is found but not any lateral mobility of bilayer fragments.

Mechanism of Bilayer Edge-Guided Vesicle Rupture and Co-existence of Double and Single Bilayers

In order to establish the instant rupture effect without cas- cading or wave-induced bilayer formation (Andrecka et al. 2013; Keller et al. 2000; Reviakine and Brisson 2000), the

number of DOPC vesicle is increased on the same surface area by increasing the solution quantity (30 µl and incubation time 15 min). Any continuous single bilayer is not found. Instead, the co-existence of single and double bilayers have been observed (Fig. 6). If cascading or wave-induced bilayer formation applies to the present case, double bilayer formation should be forbidden until the continuous single bilayer is completely formed. The presence of immobile isolated first bilayer patches leads to the second bilayer formation on it.

The adsorbed vesicle on the first bilayer may not rupture spontaneously because bilayer--bilayer adhesion is weaker than bilayer mica adhesion. However, it is stronger than the two free-standing bilayers because of the entropy loss of the surface-bound bilayer (Jass et al. 2000; Takáts-Nyeste and Derényi 2014a, b). Nevertheless, spontaneous rupture of adsorbed vesicle on the first bilayer and the formation of the second bilayer are rare if the first bilayer is continuous. But, if the first bilayer patches are small and isolated, bilayer edges play the main role in rupturing the adsorbed vesicle

on it. Bilayer edge-guided rupture and stacking of double bilayer due to immobility of DOPC bilayer on mica surface can be described as follows:

In Fig. 3, it have been shown that the energy of a pore $\Delta E \cong 2\pi r \lambda - \pi r^2 \sigma$. Now it is considered that a vesicle is adsorbed on an already formed bilayer patch and a portion of the vesicle touches the edge of the patch. Further, a pore of radius r is assumed on the vesicle, and a section of its boundary merges with the bilayer edge. Now the energy of the pore will be $\Delta E \cong 2\pi r \lambda - \pi r^2 \sigma - \chi \times 2\pi r \lambda = 2\pi r \lambda (1 - \chi) - \pi r^2 \sigma$, where χ is the fraction of the pore boundary, which merges with the bilayer edge. Maximum energy $\Delta E_{max} = \frac{\pi \lambda^2}{\sigma}(1 - \chi)^2$ at $r = \frac{\lambda(1-\chi)}{\sigma}$. Therefore, activation energy ΔE_{max} required for pore formation is reduced with the share of pore boundary with the bilayer edge. In case of single bilayer fragment formation, instant and spontaneous rupture of vesicle on mica surface due to strong adhesion $w = w_{crit}^{pore} > 2\sigma_{crit}$ and thereby decrease of activation energy have been seen. In case of bilayer edge-guided vesicle rupture, the activation energy is decreased due to the overlap of pore boundary with the bilayer
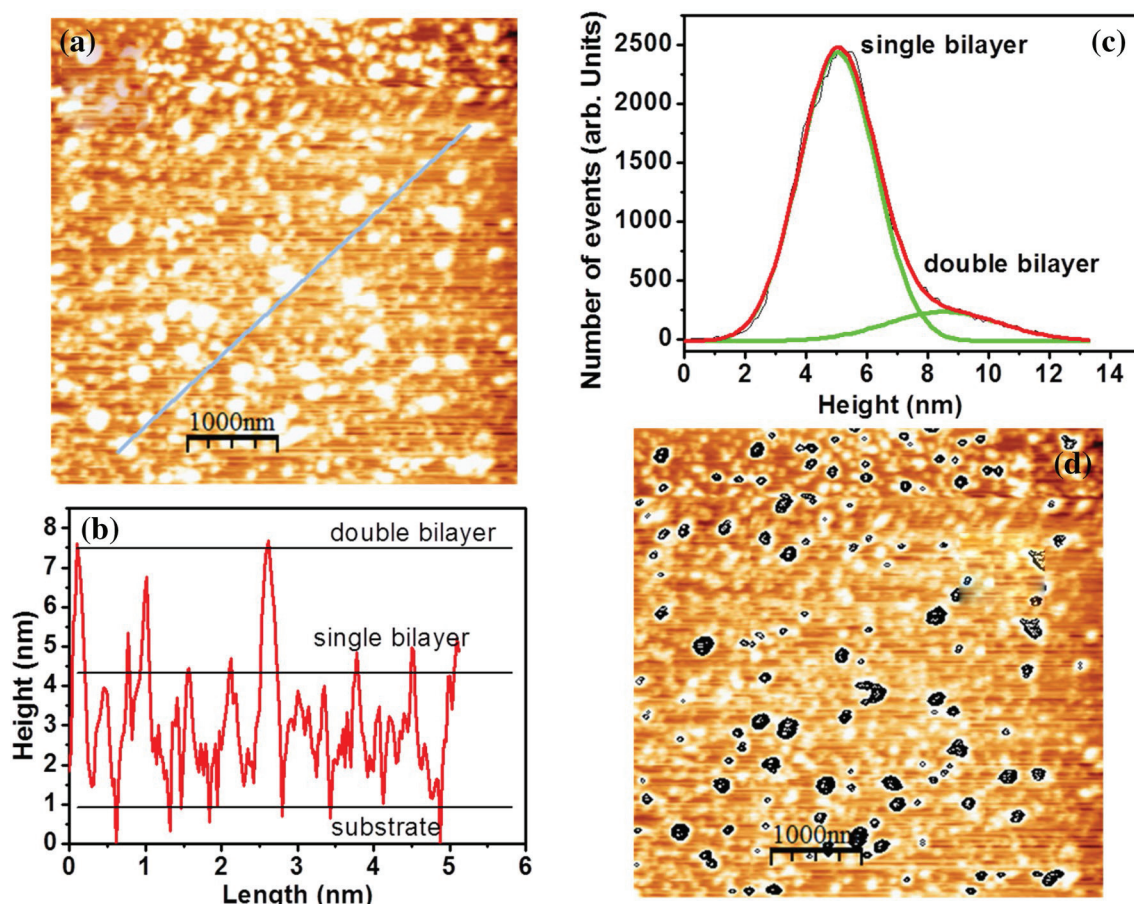

Fig. 6 Bilayer and double bilayer formation with the increase of incubation time (15 min) and solution (3 times). **a** AFM image, **b** height profile along the marked line, **c** height distribution, and **d** contour plot between 4.5 and 8 nm heights of AFM image shows the second bilayer of thickness ~3.5 nm (Color figure online)

edge. Although the adhesion energy of bilayer patch is not strong enough as mica substrate, the reduction of activation energy and thereby the reduction of required $\sigma_{crit} = \dfrac{\pi[\lambda(1-\chi)]^2}{K_B T \ln\left(\frac{K_0 A_c}{K_d a^2}\right)}$ favors the vesicle rupture. Egawa and Furusawa (1999) found the single and double bilayers for successive injection of stock solution. The presence of double bilayer was also reported on silica surface; however, with time, it formed continuous single bilayer because of the mobility of the first bilayer (Jass et al. 2000). Double bilayer may also form by hat-shaped adsorption of the vesicle as modeled by Takáts-Nyeste and Derényi (2014a, b. The existence of the double bilayer indicates again the immobility of the first bilayer and edge-induced rupture of the vesicle adsorbed on it.

Sequential Deposition and Multi-Bilayer Formation

Stimulated by this double bilayer formation, 10 µl stock DOPC solution was deposited successively three times with 15 min interval on the same area of mica substrate. Figure 7 shows the co-existence of single, double, and triple bilayers by 3 consecutive dropping of 10 µl DOPC solution at 15 min interval and subsequent gentle rinse with water.

Figure 7a shows the AFM height image, Fig. 7b shows the height distribution of the entire image, and Fig. 7c presents the line profile along the marked line shown in Fig. 7a. Mainly, there are four groups of distributed heights corresponding to (1) mica substrate with water layer, (2) first bilayer, (3) second bilayer, and (4) third bilayer which are clearly detected. An AFM phase image of the same is also presented in Fig. 7d where the phase is inversely proportional to the height of lipid layers.

The sequential dropping and sufficient incubation time allow the vesicles to form single, double, as well as triple bilayers. Landing of vesicles on the already formed first or second bilayer fragments lead to double/triple layer formation by the edge-guided rupture as discussed above. AFM topographic 3D image and contour plot of co-existing multilayers are presented again in Fig. 8. Figure 8a shows 3D AFM image and Fig. 8b presents the contour plot of the AFM image. To show the different layers, Fig. 8b is sliced correspondence to substrate (0–1.5 nm), first bilayer (1.5–5 nm), second bilayer (5–8.5 nm), and third bilayer (8.5–12 nm), respectively, and is presented in Fig. 8c.

Further, for continual increase in vesicle number by the sequential dropping of stock solution and longer incubation time, the formation of the third bilayer as well as the
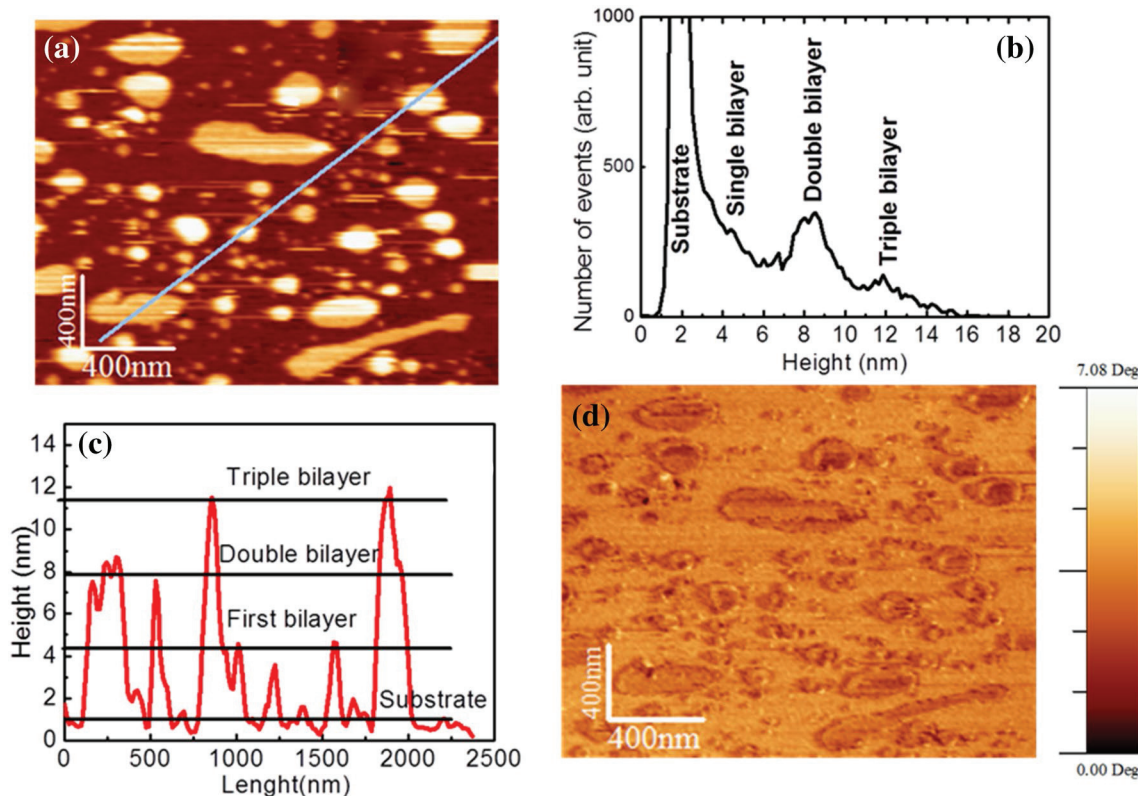

Fig. 7 Bilayer, double bilayer, and triple bilayer formation by sequential deposition of total 30 µl DOPC solution (10 µl in every 15 min for 3 times and rinse after total 45 min incubation time) on mica surface. **a** AFM image, **b** height distribution, **c** height profile along the marked line and **d** phase imaging of the same area (Color figure online)
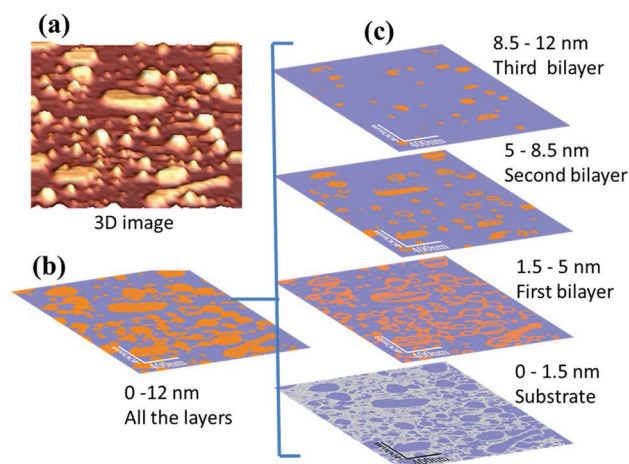
Fig. 8 a 3D topography image of Fig. 6a, **b** contour plot of the topography, and **c** contour plot of sliced layers show single, double, and triple bilayer zones separately (Color figure online)

coexistence of double and single bilayer is confirmed. Figure 9 demonstrates such co-existence of single, double, and triple bilayers for 75 min incubation with 50 μl solution on the same area of mica surface. 10 μl DOPC solution was added for 5 times at a regular interval of 15 min and finally rinsed gently with Millipore water. The stacking of multibilayer is confirmed by the measurement of height profile of AFM images. Figure 9b shows the height profile along the marked line on the AFM image where three groups of height ranges 1.5–5.0 nm, 5.0–8.5 nm, and 8.5–12.0 nm are observed corresponding to the single, double, and triple bilayers, respectively. Usually, multiple bilayer formation by vesicle rupture process is rare. Sironi et al. (2016) set up a large number of bilayer stacking by drop casting and drying of aqueous liposome solution. Heath et al. (2016) developed a layer after layer methodology to form multiple bilayers by vesicle rupture using PLL as an electrostatic polymer linker. Jensen et al. (2007) also fabricated multilamellar membrane by spin coating. In general, most of the reported multiple

bilayers are either formed by drying the aqueous solution or by using linker between the bilayers (Heath et al. 2016; Jensen et al. 2007; Sironi et al. 2016). In the present case, the third bilayer formation by sequential addition of vesicle solution is possible when the first bilayer is strongly bound with the substrate and the cohesive force exists between the successive bilayers formed by the edge-induced rupture mechanism.

Figure 10 shows the contour plot of AFM image recorded after sequential dropping of 50 μl solution and total 75 min of incubation. It clearly shows the co-existence of single, double, and triple bilayers. It distinguishes the bare substrate zones of height 0 to 1.5 nm (Fig. 10a), single bilayer patches of height between 1.5 and 5.0 nm (Fig. 10b), double bilayer patches of height between 5.0 and 8.5 nm (Fig. 10c), and triple bilayer patches of height between 8.5 and 12.0 nm (Fig. 10d). Strong adhesion between mica surface and vesicle leads to the first bilayer formation, whereas multi-bilayer arrangement is observed due to bilayer edge-guided rupture and physisorption of bilayer on bilayer. Third bilayer formation is possible only for soft landing of vesicle on second bilayer and rupture by the edge of the second bilayer. The stability of the third bilayer is very low. It was observed that the third bilayer is stable on gentle rinse, but it is washed out even by moderate rinsing by water. Fourth or more bilayer is not observed by sequential addition technique because bilayer–bilayer adhesion is supposed to decrease with the increase of stacked bilayer numbers.

In Situ Vesicle Deposition and Time-Lapse AFM

Instead of imaging the surface after incubation and rinse, the isolated single bilayer formation as well as the second and third bilayer formation have been monitored due to in situ injection of DOPC solution and time-lapse AFM measurements. Figure 11 shows time-lapse AFM images of mica surface incubated with 10 μl 0.05 mg/ml DOPC solution as well as successive injection of additional vesicle of same

Fig. 9 a AFM image in aqueous medium shows the multibilayer formation due to longer incubation time (75 min) and sequential addition of total 50 μl DOPC solution (10 μl in every 15 min) on mica surface, **b** height profile on marked line (Color figure online)
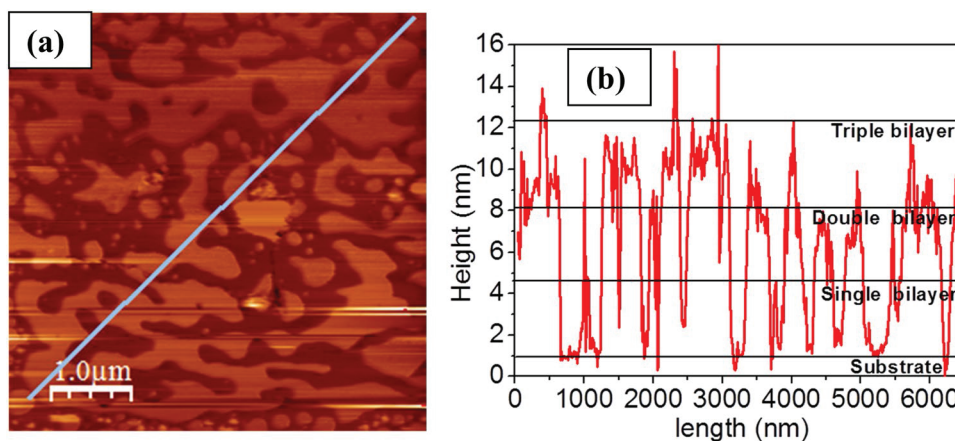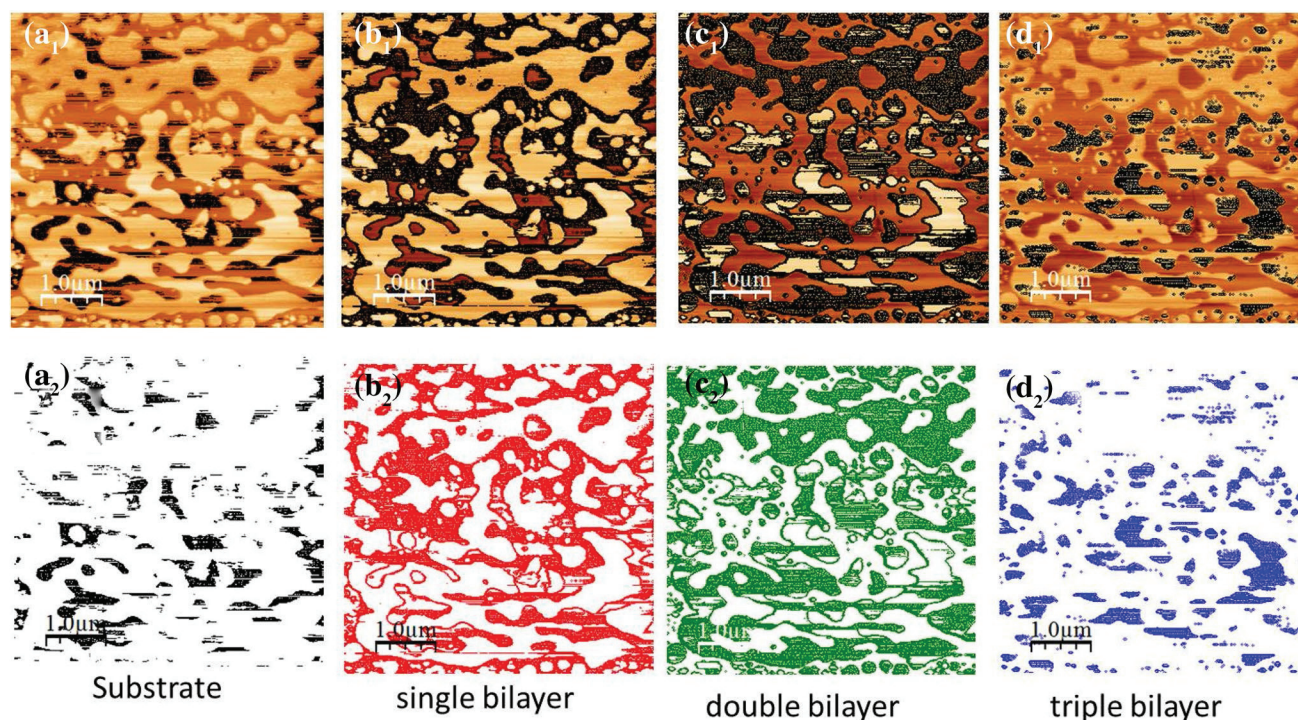
Fig. 10 *Top row* contour plot (black) of AFM image Fig. 9a shows a_1 bare substrate zones (height between 0 and 1.5 nm), b_1 single bilayer patches (height between 1.5 and 5.0 nm), c_1 double bilayer patches (height between 5.0 and 8.5 nm), and d_1 triple bilayer patches (height between 8.5 and 12.0 nm). *Bottom row* the same is represented by different colors a_2 bare substrate zones (black), b_2 single bilayer patches (red), c_2 double bilayer patches (green), and d_2 triple bilayer patches (blue) (Color figure online)

concentration during imaging. Figure 11a shows the AFM image in DOPC solution after 15 min incubation. Additional 10 µl vesicle solution was injected into the liquid cell at $t = 42$ min, and time-lapse AFM images were recorded. Figure 11b shows the image taken at 42–61 min, after in situ injection of additional vesicle solution. Figure 11c and d shows the images at $t = 61$–70 and 70–79 min, respectively. The time-lapse AFM measurements are consistent with the earlier final-state (after incubation and rinse) data where isolated bilayer patches as well as second and third bilayer patches are observed.

Figure 12 shows the contour plot of sliced first, second, and third bilayers for in situ DOPC solution deposition and time-lapse AFM measurements (Fig. 11). Figure $12a_1$–d_1, shows the dynamics of the first bilayer only. Similarly, Fig. $12a_2$–d_2 and a_3–d_3 shows the development and dynamics of the second and third bilayers, respectively. It is observed that the coverage by isolated bilayer increases with time after in situ injection of DOPC solution as well as the second and third bilayers appear and increase in number. However, the numbers of second and third bilayer patches are few compared to the first bilayer. Adsorbed vesicle on the mica surface is rarely observed, either by deposition and rinse with water or by time-lapse measurement with successive deposition of DOPC solution. Reviakine and Brisson (2000)

reported SLB formation on mica, but in some cases, they reported the patches as adsorbed vesicle. In the present case, adsorbed vesicles (~60 nm diameter) can be easily distinguished from the ruptured bilayer(s). Leonenko et al. (2000) also mentioned that the observation of adsorbed vesicles (Reviakine and Brisson 2000) may be due to the difference in sample preparation (Leonekko et al. 2000). In case of non-rinse time-lapse AFM images (Figs. 11, 12), the heights of severely flattened intact vesicle on mica and on first bilayer are equivalent to second and third bilayers, respectively. It is believed that severely flatten adsorbed vesicles will be unstable and will result in the formation of second or third bilayer by rupture at the edge. Leonenko et al. (2000) also concluded that the observed patches having height equivalent to two bilayers were actually the double bilayer.

Formation of single, double, and triple bilayers on mica due to DOPC vesicle adsorption is schematically summarized in Fig. 13. It shows the selection of strong adhesive mica substrate and diluted DOPC stock solution (0.05 mg/ml) where total number of vesicles in 10 µl is insufficient to cover the entire substrate area (12 mm × 12 mm) and forms random isolated patches (Fig. 13a). Figure 13b shows the addition of DOPC solution of same concentration increases the bilayer coverage area as well as forms a second bilayer due to adsorption and rupture of vesicle at the edges of

Fig. 11 In situ sequential deposition and time lapse AFM scan. 10 μl of 0.05 mg/ml, DOPC solution deposited on mica at $t=0$ and incubated for 15 min, **a** AFM image with DOPC solution without rinse ($t=33$–42 min). At $t=42$ min, additional 10 μl solution injected into the liquid cell without stopping the scan, **b** AFM image at $t=52$–61 min. **c** AFM image $t=61$–70 min. **d** AFM image $t=70$–79 min (Color figure online)

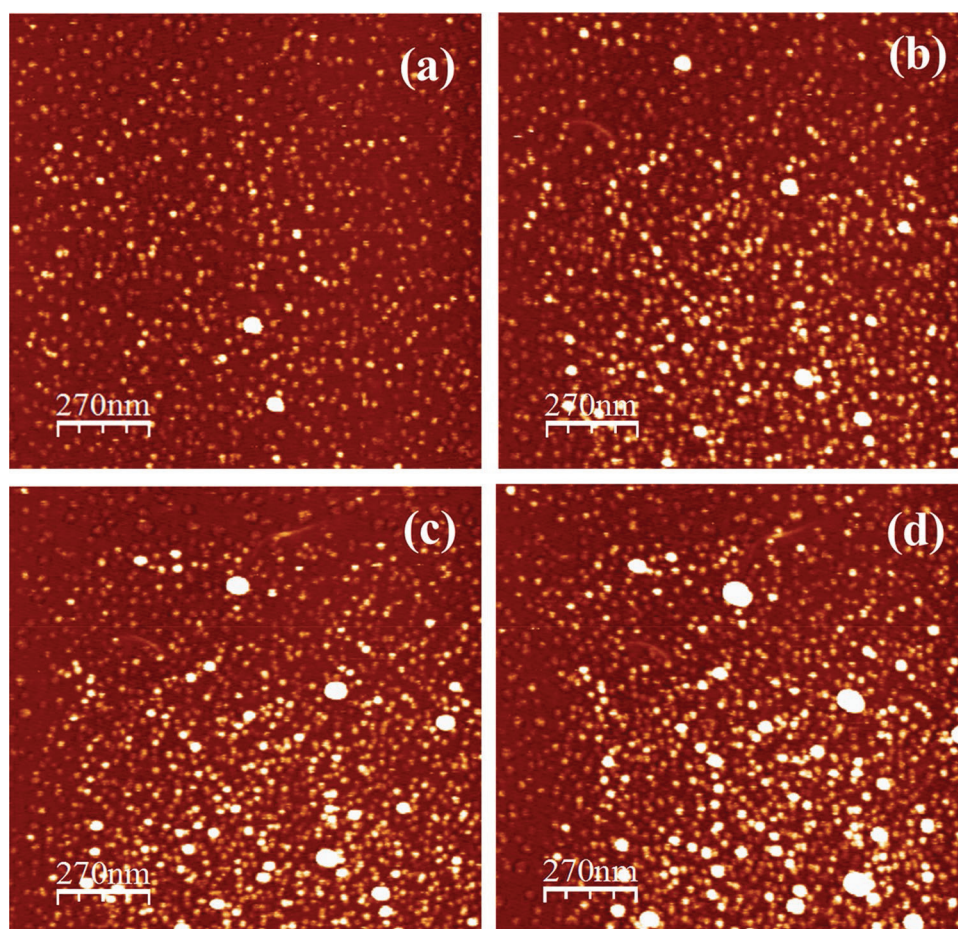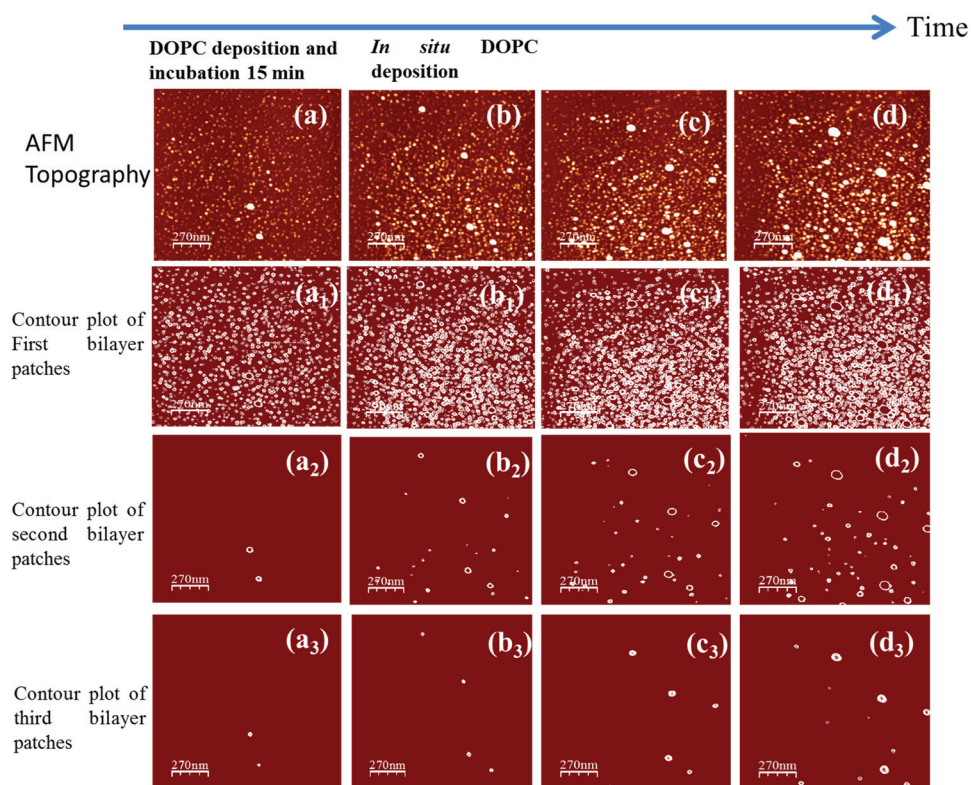**Fig. 12** In situ sequential deposition and time-lapse AFM scan. *Top row* the b–d of Fig. 11, corresponding to (a, b, c, d), a_1–d_1 are the contour plot of sliced first bilayer (height between 1.5 and 5.0 nm) patches only, a_2–d_2 are the second bilayer (height between 5.0 and 8.5 nm) patches only, and a_3–d_3 are the third bilayer (height between 8.5 and 12.0 nm) patches only (Color figure online)

previously formed bilayer patches. Due to immobility of the first bilayers, the ruptured vesicle piles partially or fully on first bilayer and forms the second bilayer. The third bilayers (Fig. 13c) are observed by sequential addition of droplets from the stock solution during incubation. The added vesicles are gently adsorbed on the already formed single or double bilayer patches and are ruptured when they find the bilayer edge. Although the adhesion between second and third bilayers is assumed to be weak, immobility of first and second bilayers allows part of the ruptured vesicle to stay on the second bilayer. Thus, vesicles in the first deposited diluted solution are depleted and form isolated bilayer patches. Successive addition of stock solution increases again the number of vesicles on the same surface. Thus, in addition to increasing first bilayer coverage area, the presence of bilayer edges of previously formed bilayer patches aids to form second and third bilayers due to sequential deposition of diluted DOPC solution on mica surface. No requirement of special substrate treatment or linker addition, second or third bilayers formation by sequential dilute solution dropping, is consistent and simple as well as more close to the natural multilayer system.

The instant rupture of adsorbed vesicle, observed isolated bilayer patch formation, as well as coexistence of second and third bilayers is due to strong adhesion between mica surface and DOPC lipid molecules. The adhesion between mica and vesicle can be understood through the interaction force between mica surface and lipid vesicles in aqueous media. The total interaction force acting between the support and lipid bilayer in water media can be divided into two major parts: The first one is the attractive force between zwitterionic DOPC molecule and negatively charged freshly cleaved mica surface, whereas the other is the repulsive hydration force, originated due to the tendency of bulk water to fill the space between bilayer and support (Anderson et al. 2009; Pertsin and Grunze 2014). The charge density on the substrate surface strongly influences the vesicle adhesion and rupture process (Anderson et al. 2009). It is shown that the presence of external ions modifies the interaction by screening the charge as well as directly interact with the support and lipid molecules (Hennesthal and Steinem 2000; Raedler et al. 1995). The influence of divalent ions like Ca^{2+} shows surprising effect on vesicle adsorption and rupture (Richter et al. 2006). Mica has layered structure, where negatively charged aluminosilicate layers are interconnected by positively charged K^+ ions as described before. The freshly cleaved mica surface shows super hydrophilic behavior. At the time of cleavage, top K^+ layer is disrupted and expose the basal negatively charged aluminosilicate layer. If the cleaved mica surface is kept in air, the surface charge is compensated by the bulk lattice charge (Balmer et al. 2008). In the present case, the strong adhesion of mica surface is not fully understood; however, strong negative surface charge of freshly cleaved mica is the major source of strong adhesion. Cha et al. (2006) also reported that adhesion increases with increase of surface charge density. They showed that charge neutral (zwitterionic) vesicles readily rupture and form supported phospholipid bilayers when the density of surface charge is high. It have been seen that the water contact angle of freshly cleaved mica is lowest, and it increases with time as the surface charge is slowly compensated by the bulk charge. Isolated bilayer patches as well as coexistence of second and third bilayers for dilute DOPC solution deposition is observed without the addition of ionic solution; however, uniform patch distribution is observed in local (Jharkhand, India) mica, whereas both large and small bilayer patches are observed on MTI mica. This indicates mobility of bilayer patches on MTI mica is little more, which increases merging

Fig. 13 Schematic representation of vesicle adsorption, rupture, and **a** single, **b** double, and **c** triple bilayer formation (Color figure online)
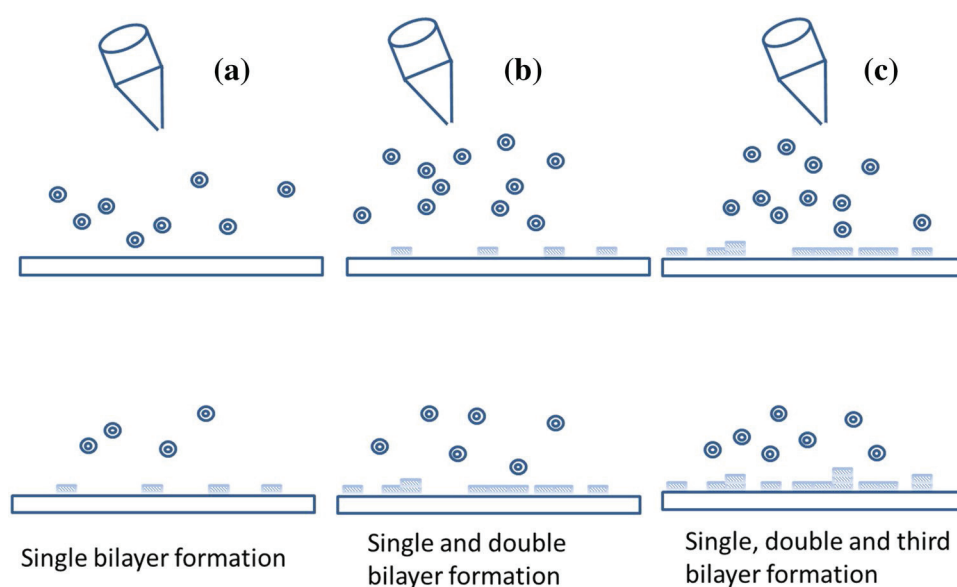
(a)	(b)	(c)

Single bilayer formation	Single and double bilayer formation	Single, double and third bilayer formation

probability and creates larger bilayer patches. Second and third bilayer patches are also found to form on MTI mica and, however, are less in number due to less available bilayer edges (data not shown). This observation indicates the adhesion property of Jharkhand mica is slightly more than the MTI mica. Markedly difference in bilayer formation was also reported for different silica surfaces (Richter et al. 2006).

Conclusion

The growth of single as well as multiple bilayers of DOPC vesicle on highly hydrophilic mica surface was examined by simple vesicle fusion method without any complex preparation of the substrate or incorporation of external reagent. AFM measurements of water-rinsed bilayer surface show no movement, cascading or wave-like vesicle rupture, rather the vesicles are ruptured spontaneously at the contact of strong adhesive mica surface. The interaction between the edges of adjacent isolated bilayer fragments plays the role of merging. Multi-bilayers are formed by further adsorption of vesicle on the already formed bilayer and rupture by the edge of the supported bilayer patches.

The direct observation of co-existence of single, double, and triple lipid bilayers by quantitative AFM measurement shows excellent prospect not only for easy preparation of single and multiple lipid bilayer but also for the study of the interaction of proteins or drugs with single and multiple DOPC bilayers in a single system.

Further study of such system by X-ray, cryo-TEM, and other complimentary techniques as well as selection of other substrate–lipid combinations with strong adhesion property may reveal more information and way out to increase the layer beyond the third bilayer. Formation of coexisted bilayer and stacked multiple bilayers in natural aqueous solution will open up possibilities for new biophysical studies on interaction between membranes as well as membrane associated proteins with co-existed single and multiple bilayers.

Compliance with Ethical Standards

Conflict of interest The authors declare that they have no conflict of interest.

Ethical Approval This article does not contain any studies with human participants or animals performed by any of the authors.

References

Åkesson A, Lind T, Ehrlich N, Stamou D, Wacklin HP, Cárdenas M (2012) Composition and structure of mixed phospholipid supported bilayers formed by POPC and DPPC. Soft Matter 8:5658–5665

Anderson TH, Min YJ, Weirich KL, Zeng HB, Fygenson D, Israelachvili JN (2009) Formation of supported bilayers on silica substrates. Langmuir 25:6997

Andrecka J, Spillane KM, Ortega-Arroyo J, Kukura P (2013) Direct observation and control of supported lipid bilayer formation with interferometric scattering microscopy. ACS Nano 7:10662

Attwood SJ, Choi Y, Leonenko Z (2013) Preparation of DOPC and DPPC supported planar lipid bilayers for atomic force microscopy and atomic force spectroscopy. Int J Mol Sci 14:3514

Balmer TE, Christenson HK, Spencer ND, Heuberger M (2008) The effect of surface ions on water adsorption to mica. Langmuir 24:566–1569

Bernchou U, Brewer J, Midtiby HS, Ipsen JH, Bagatolli LA, Simonsen AC (2009) Texture of lipid bilayer domains. J Am Chem Soc 131:14130

Bhowmik D, Karmakar P (2018) Physicochemical variation of mica surface by low energy ion beam irradiation. Nucl Inst Methods Phys Res B 422:41–46

Bhowmik D, Karmakar P (2019) Tailoring and investigation of surface chemical nature of virgin and ion beam modified muscovite mica. Surf Interface Anal 51:667–673

Blodgett KB (1935) Films built by depositing successive monomolecular layers on a solid surface. J Am Chem Soc 57:1007

Cha T, Guo A, Zhu X-Y (2006) Formation of supported phospholipid bilayers on molecular surfaces: role of surface charge density and electrostatic interaction. Biophys J 90:1270–1274

Egawa H, Furusawa K (1999) Liposome adhesion on mica surface studied by atomic force microscopy. Langmuir 15:1660–1666

Gimeno A, Ares P, Horcas I, Gil A, Gomez-Rodriguez JM, Colchero J, Gomez-Herrero J (2015) Flatten plus: a recent implementation in WSxM for biological research. Bioinformatics 31:2918–2920

Han X, Achalkumar AS, Cheetham MR, Connell SDA, Johnson BG, Bushby RJ, Evans SD (2010) A self-assembly route for double bilayer lipid membrane formation. Chem Phys Chem 11:569

Heath GR, Li M, Polignano IL, Richens JL, Catucci G, O'Shea P, Sadeghi SJ, Gilardi G, Butt JN, Jeuken LJC (2016) Layer-by-layer assembly of supported lipid bilayer poly-L-lysine multilayers. Biomacromolecules 17:324

Helfrich W, Servuss R-M (1984) Undulations, steric interaction and cohesion of fluid membranes. Il Nuovo Cim D 3:137–151

Hennesthal C, Steinem C (2000) Pore-spanning lipid bilayers visualized by scanning force microscopy. J Am Chem Soc 122:8085–8086

Hope MJ, Bally MB, Webb G, Cullis PR (1985) Production of large unilamellar vesicles by a rapid extrusion procedure: characterization of size, trapped volume and ability to maintain a membrane potential. Biochim Biophys Acta 812:55

Israelachvili JN (2011) Intermolecular and surface forces. Academic, Waltham

Jass J, Tjärnhage T, Puu G (2000) From liposomes to supported, planar bilayer structures on hydrophilic and hydrophobic surfaces: an atomic force microscopy study. Biophys J 79:3153

Jensen MH, Morris EJ, Simonsen AC (2007) Domain shapes, coarsening, and random patterns in ternary membranes. Langmuir 23:8135–8141

Kang M, Tuteja M, Centrone A, Topgaard D, Leal C (2018) Nanostructured lipid-based films for substrate-mediated applications in biotechnology. Adv Funct Mater 28:1704356

Karatekin E, Sandre O, Brochard-Wyart F (2003) Transient pores in vesicles. Polym Int 52:486

Kataoka-Hamai C, Higuchi M, Iwai H, Miyahara Y (2010) Detergent-mediated formation of polymer-supported phospholipid bilayers. Langmuir 26:14600

Keller CA, Glasmästar K, Zhdanov VP, Kasemo B (2000) Formation of supported membranes from vesicles. Phys Rev Lett 84:5443

Kucerka N, Tristram-Nagle S, Nagle JF (2005) Structure of fully hydrated fluid phase lipid bilayers with monounsaturated chains. J Membr Biol 208:193–202

Leonenko ZV, Carnini A, Cramb DT (2000) Supported planar bilayer formation by vesicle fusion: the interaction of phospholipid vesicles with surfaces and the effect of gramicidin on bilayer properties using atomic force microscopy. Biochim Biophys Acta 1509:131–147

Lind TK, Wacklin H, Schiller J, Moulin M, Haertlein M, Pomorski TG, Cárdenas M (2015) Formation and characterization of supported lipid bilayers composed of hydrogenated and deuterated *Escherichia coli* lipids. PLoS ONE 10:e0144671

Lv Z, Banerjee S, Zagorski K, Lynbchenko YL (2018) Supported lipid bilayers for atomic force microscopy studies. Methods Mol Biol 1814:129–143

Melcrova A, Pokorna S, Cwiklik L (2016) The complex nature of calcium cation interactions with phospholipid bilayers. Sci Rep 6:38035

Mornet SP, Lambert O, Duguet E, Brisson A (2005) The formation of supported lipid bilayers on silica nanoparticles revealed by cryoelectron microscopy. Nano Lett 5:281–285

Mui BL-S, Cullis PR, Evans EA, Madden TD (1993) Osmotic properties of large unilamellar vesicles prepared by extrusion. Biophys J 64:443

Müller K, Chang CC (1969) Electric dipoles on clean mica surfaces. Surf Sci 14:39

Okamoto Y, Tsuzuki K, Iwasa S, Ishikawa R, Sandhu A, Tero R (2012) Fabrication of supported lipid bilayer on graphene oxide. J Phys Conf Ser 352(01):2017

Perino-Gallice L, Fragneto G, Mennicke U, Salditt T, Rieutord F (2002) Dewetting of solid-supported multilamellar lipid layers. Eur Phys J E 8:275

Pertsin A, Grunze M (2014) Possible mechanism of adhesion in a mica supported phospholipid bilayer. J Chem Phys 140:184707

Raedler J, Strey H, Sackmann E (1995) Phenomenology and kinetics of lipid bilayer spreading on hydrophilic surfaces. Langmuir 11:4539–4548

Reviakine I, Brisson A (2000) Formation of supported phospholipid bilayers from unilamellar vesicles investigated by atomic force microscopy. Langmuir 16:1806

Richter R, Berat R, Brisson AR (2006) Formation of solid-supported lipid bilayers: an integrated view. Langmuir 22:3497

Richter R, Mukhopadhyay A, Brisson A (2003) Pathways of lipid vesicle decomposition on solid surfaces: a combined QCM-D and AFM study. Biophys J 85:3035

Richter RP, Brisson AR (2005) Following the formation of supported lipid bilayers on mica: a study combining AFM, QCM-D, and ellipsometry. Biophys J 88:3422–3433

Schonherr H, Johnson JM, Lenz P, Boxer SG (2004) Vesicle adsorption and lipid bilayer formation on glass studied by atomic force microscopy. Langmuir 20:11600

Seifert U, Lipowsky R (1990) Adhesion of vesicles. Phys Rev A 42:4768

Sironi B, Snow T, Redeker C, Slastanova A, Bikondoa O, Arnold T, Kleine J, Briscoe WH (2016) Structure of lipid multilayers via drop casting of aqueous liposome dispersions. Soft Matter 12:3877

Takáts-Nyeste AA, Derényi I (2014) Development of hat-shaped liposomes on solid supports. Langmuir 30:15261

Takáts-Nyeste A, Derényi I (2014) Rupture of lipid vesicles near solid surfaces. Phys Rev E 90:052710

Tanaka M, Tutus M, Kaufmann S, Rossetti FF, Schneck E, Weiss IM (2009) Native supported membranes on planar polymer supports and micro-particle supports. J Struct Biol 168(2009):137–142

Tero R, Fukumoto K, Motegi T, Yoshida M, Niwano M, Hirano-Iwata A (2017) Formation of cell membrane component domains in artificial lipid bilayer. Sci Rep 7:17905

Tristram-Nagle SA (2007) Preparation of oriented, fully hydrated lipid samples for structure determination using X-ray scattering. In: Dopico AM (ed) Methods in membrane lipids. Humana Press, Totowa, pp 63–75

Verma A, Stellacci F (2009) Effect of surface properties on nanoparticle–cell interactions. Small 6:1–10

Vogel M, Münster C, Fenzl W, Salditt T (2000) Thermal unbinding of highly oriented phospholipid membranes. Phys Rev Lett 84:390

Wacklin HP (2011) Composition and asymmetry in supported membranes formed by vesicle fusion. Langmuir 27:7698

Wacklin HP, Thomas RK (2007) Spontaneous formation of asymmetric lipid bilayers by adsorption of vesicles. Langmuir 23:7644

Wang Y, Wang H, Bi S (2014) Real time drift measurement for colloidal probe atomic force microscope: a visual sensing approach. AIP Adv 4:057130

Weirich KL, Israelachvili JN, Fygenson DK (2010) Bilayer edges catalyze supported lipid bilayer formation. Biophys J 98:85

Zhu Y, Negmi A, Moran-Mirabal J (2015) Multi-stacked supported lipid bilayer micropatterning through polymer stencil lift-off. Membranes 5:385–398

Preparation of Giant Unilamellar Vesicles and Solid Supported Bilayer from Large Unilamellar Vesicles: Model Biological Membranes

Amrita Basu[1], Pabitra Maity[1], Prasanta Karmakar[2] and Sanat Karmakar[1]*

[1]Department of Physics, Jadavpur University, Kolkata- 700032, India
[2]Variable Energy Cyclotron Centre, Kolkata -700064, India; sanat@phys.jdvu.ac.in

Abstract

Giant Unilamellar Vesicles (GUV) and supported planar membranes are excellent model biological systems for studying the structure and functions of membranes. We have prepared GUV from Large Unilamellar Vesicles (LUV) using electroformation and Supportedplanar Lipid Bilayer (SLB) by vesicle fusion method. LUV was prepared using an extrusion method and was characterized using Dynamic Light Scattering (DLS) and zeta potential measurements. The techniques for obtaining GUV as well as SLB from LUV have been demonstrated. We have directly observed the formation of GUV under phase contrast microscopy. This study will provide some insights into the physico-chemical properties of both nano and micron size vesicles. We believe that this method could be extremely useful for reconstituting various bio-molecules in GUV. We have presented one example where an antimicrobial peptide NK-2 was reconstituted in GUV prepared from LUV. SLB formation was monitored and characterized using Atomic Force Microscopy (AFM).

Keywords: AFM, Dynamic Light Scattering, Model Membranes, Optical Microscopy, Solid Supported Bilayer, Vesicles

1. Introduction

Lipid bilayers are the basic building blocks of all biological membranes [1]. Phospholipids are their major constituents. Therefore, phospholipids bilayer serves as an excellent model system of bio-membranes. The complexity of biomembrane has led to the development of a wide variety of simpler model systems. As model systems, unilamellar vesicles and solid SLB are widely used for studying structure and function of membranes at physiological condition. SLB is popularly described in terms of physiological matrix and are useful to study the surface chemistry of the cell and the membrane-protein interaction [2]. A variety of experimental techniques were employed to study the fundamental as well as applied aspects of membrane structure, dynamics in the presence of various bimolecular, such as proteins, cholesterol, receptors etc. [3, 4]. AFM is one of the well-established techniques for imaging SLBs at nanometer resolution. A unique feature of AFM is its ability to monitor dynamic processes, such as the interaction of membranes with proteins and other bio-active molecules [5]. Besides SLB, unilamellar vesicles are also widely used bio-mimetic systems. Vesicles are basically microscopic sac that encloses a volume with molecularly thin biomembrane. These are formed by self assembly of amphiphilic molecules, such as phospholipids, diblock co polymer etc. [6, 7]. Phosphatidylcholines (PCs) are the most abundant phospholipids in all eukaryotic cells, whereas, phosphatidylglycerols (PGs) and phosphatidylethanolamines (PEs) are found in bacterial cell [1] as well as eukaryotic cell. The phospholipids, when suitably mixed with water or similar solvent, form bilayers, commonly known as Multilamellar Vesicles (MLV). However, MLV do not serve as a good model system of biological membranes, as cellular membrane is a single bilayer of lipid molecules. Therefore, one needs to prepare model membrane containing single bilayer, known as unilamellar vesicles.

MLV can form unilamellar vesicles whose size ranging from tens of nanometers (small unilamellar vesicles, large unilamellar vesicles) to tens of micrometers (giant unilamellar vesicles) depending on the preparation methods used. GUV, owing to their large size, can directly be observed under optical microscopy and therefore, they serve as an excellent model system to study many biological phenomena [8-10].

Biological membranes are complex, regulated by various membrane components. Therefore, it is often useful to study model membranes in order to understand the physical mechanisms of many biological phenomena occurring on the cell surface. For examples, lipid-peptide interaction is one of the most important systems in order to get some insight into the structure and functions of membrane proteins [11]. Study of antimicrobial activity of an antimicrobial peptide on the model membrane has drawn lots of attention due to their potential for bio-medical applications, such as antibiotics [12]. Model membranes can also be used to study the structure and formation of cholesterol-rich domains know as 'raft'. These rafts has been proposed to exist on the cell surface [13, 14]. Giant vesicles are used as microreactors for enzymatic RNA synthesis [15] and also to form nanoparticles of controlled size distributions [16]. Aqueous phase separation, biomineralization and many other phenomena which mimic biological compartmentalization can be studied using GUV [17, 18]. Vesicles are also extensively used as carriers of bioactive agents, including drug, vaccines and cosmetics [19, 20].

In the present paper, we have discussed the preparation of LUV using extrusion method. Zeta potential and the size distribution of LUV made from different phospholipids and lipid mixtures are also presented. The aim of the present study is to prepare GUV and SLB from the well characterized LUV. There are several protocols for the preparation of GUV available in the literature [21]. However, electroformation is the most popular and widely used protocol as it gives more yields for GUV [22]. Here, we have prepared GUV from LUV based on electroformation. We have also prepared solid supported bilayer from vesicle fusion method which also serves as a model system of biological membranes. The usefulness of these methods and importance of GUV and solid supported bilayer has also been discussed. We have also shown that an antimicrobial peptide. NK-2 can be reconstituted in GUV, if prepared from LUV.

2. Materials and Methods

Phospholipids, dioleoylphosphatidylcholine (DOPC), dioleoylphosphatidylgylcerol (DOPG) and dioleoylphosphatidylethanolamine (DOPE) were purchased from Sigma Aldrich and were used for vesicle preparation without further purification.

2.1 Preparation of LUV

LUV was prepared using an extrusion technique as described by Hope et al. [23]. An appropriate amount of lipid solution in chloroform (stock solution of concentration of 10 mg/ml) was transferred to a 10 ml glass bottle. Organic solvent was removed by gently passing nitrogen gas. The sample was then placed for couple of hours in a desiccator connected to vacuum pump to remove the traces of the solvent. 2.5 ml of 1 mM HEPES (pH 7.4) was added to the dried lipid film. The lipid film with the buffer was kept overnight at 4^0C to ensure better hydration of the phospholipid heads. Vortexing of hydrated lipid film for about 30 minutes produced Multilamellar Vesicles (MLV). In the present experiments, we have prepared MLV of concentration ~ 1.2 mM. Sometimes long vortexing is required to make uniform lipid mixtures. LUV was prepared by extrusion method using LiposoFast from AVESTIN (Canada). MLV suspension was extruded successively through polycarbonate membranes having pore diameters of 400 , 200 and 100 nm. This resulted in the formation of well defined size of LUV. This method produced vesicles of diameter ~ 100 nm measured by dynamic light scattering. LUV composed of DOPC-DOPG mixture was used for reconstituting antimicrobial peptide NK-2 in GUV.

2.2 Zeta Potential and Dynamic Light Scattering

Zeta potential and size distribution were obtained at a temperature (~ 30^0 C) with Zetasizer Nano ZS (Malvern Instruments, UK). Zetasizer Nano uses 4 mWHeNe Laser of wavelength 632.8 nm. The detector was positioned at scattering angle 173^0. The detected scattered light was sent to signal processing correlator.

The rate of decay of intensity-intensity autocorrelation function was measured which was used to calculate size distributions of LUV using Stoke-Einstein relation.

Zeta potential was measured from electrophoretic mobility (μ) by Laser Doppler Velocimetry [24, 25]. ζ is now obtained from the model described by Smolushovski-Huckel equation, $\zeta = \dfrac{2\mu\eta}{3\epsilon\epsilon_0 f(\kappa a)}$, where ϵ and ϵ_0 are the relative permittivity of the medium and permittivity of the free space, respectively and η is the coefficient of viscosity of the aqueous solution. The Henry function is the function of vesicle radius *a* and the inverse Debye length κ. The μ provides information about the effective charges, Q_{eff}, of the vesicles. The Q_{eff} per vesicle has also been estimated from the measured electrophoretic mobility, according to the equation, $Q_{eff} = 6\pi\eta a_{eff}\mu$, where, Q_{eff} is the effective radius of the vesicle including stern layer.

Average ς and the size distribution were obtained from 3-4 successive measurements.

2.3 Preparation of GUV

GUV were formed in 100 mM sucrose prepared in 1 mM HEPES (pH 7.4) buffer using electrofomation, as described by Pott et al. [26]. We have modified the method. Instead of dried lipid film, we have used LUV suspension to deposit onto the Indium Tin Oxide (ITO) glass. In brief, two to four drops (each ~ 2- 4 μl) of LUV (~ 1 mM) suspension, prepared using an extrusion method, was deposited onto both the ITO glasses. These droplets were allowed to dry overnight in a closed chamber containing saturated solution of NaCl. This was to avoid complete drying of the droplets. The hydration of these droplets facilitates electroformation process. Electroformation chamber for vesicle preparation consists of two ITO coated glasses separated by a Teflon spacer of thickness ~ 2 mm. An alternating voltage of 1-2 volts (peak to peak amplitude) and 10 Hz frequency was applied to the chamber for a couple of hours. For best result we have gradually increased the alternating voltage starting from 0.7 volts to 1.5 volts in the interval of 15 minutes. Similarly, at the end of 1-2 hour, voltage was gradually decreased before we switched off the alternating field. This procedure help to detach vesicles from the substrate. It is important to note that one needs to keep temperature of the electroformation chamber above the chain melting transition temperature (T_m) of lipid. For DOPC (T_m = -18 ^{0}C), the temperature was kept constant at room temperature (~ 27^{0}C) during the electroforamtion process. The diameter of the GUV was found to be in the range of 20-100 μm. After the formation of GUV, vesicle solution was transferred to a glass vial for storage. For better contrast in phase contrast microscopy, GUV solution was diluted in 100 nm glucose prepared in 1 mM HEPES (pH 7.4) for observation. Both glucose and sucrose solution were kept same osmolarity in order to balance the osmotic pressure between the interior and the exterior of the GUV. Production of GUV in the present protocol very much reproducible as we have prepared GUV several times and obtained a fairly good amount of GUV always. For the reconstitution of peptide NK-2, GUV was prepared from LUV containing NK-2. Aqueous solution of NK-2 (1 mg/ml) was added to the LUV and kept it for 2 hours. The final concentration of NK-2 in the solution containing LUV was kept at 10 μM. The rest of the procedure was the same as described above.

2.4 Phase Contrast Microscopy

Conventional optical microscopy will not be able to produce sufficient contrast to observe GUV, as the refractive indices between interior and exterior of vesicles are very similar. Therefore, phase contrast microscopy was employed to visualize GUV. Microscopic observation was performed with an Axiovert 135 inverted microscope from Zeiss. Electroformation chamber was directly placed on the microscopy sample base for observation during vesicle formation. Figure 2 shows the electroformation of GUV. Images were captured using CCD Camera. We have also transferred the 10-100 μl of GUV solution from the electroformation chamber to an O ring pasted on a glass side for observation. In this case GUV was diluted 10 times with glucose solution, as mentioned before. This is to mismatch and enhance the refractive index contrast of the interior and the exterior of GUV leading to better contrast of the phase contrast micrographs.

2.5 Preparation of Solid Supported Planar Lipid Bilayer

Solid supported bilayer was prepared by the well known vesicle fusion method [27]. The supported bilayer on a mica surface was prepared from DOPC LUV. Our aim was to obtain the defect free uniform bilayer. Large unilamellar vesicles (~ 1 mM) were prepared using an extrusion technique, as described above. 1-2 drops (each 2 μl) of freshly prepared LUV were deposited onto the freshly cleaved mica substrate. After 5 minutes, the vesicle deposited mica was thoroughly rinsed with deionised water (Millipore grade) for several times. Few drops of

millipore water were then introduced to avoid dewetting of the sample. The vesicle deposited mica sheet was carefully placed onto the atomic force microscope stage for scanning the sample.

2.5.1 Atomic Force Microscopy

All AFM images were taken using a Bruker made Multi mode and Catalyst Scanning Probe Microscope equipped with a Nanoscope V controller. AFM scanning was done in contact or tapping mode using SNL10 probe with spring constant k = 0.7 N/m. The contact mode allows us an excellent control in a liquid environment and is ideally suitable for imaging soft supported bilayer surfaces.

3. Results and Discussions

We have chosen phospholipids, such as, DOPC, DOPG and DOPE, due to their low chain melting transition temperature (T_m = -18^{0}C) so that vesicles can be prepared at room temperature (25 ^{0}C). At room temperature, vesicles prepared from above mentioned phospholipids are in fluid lamellar (L_α) phase. Before preparing GUV, size distribution and zeta potential have been measured. Size distributions of the LUV have been confirmed by dynamic light scattering. Typical size distribution of DOPC LUV is shown in Figure 1(a). Average size in terms of effective hydrodynamic diameter was found to be ~ 100 nm. The size distribution reveals that LUV is mainly mono-dispersed. The extrusion method provides fairly mono-disperse vesicles as evidenced from the Polydispersity Index (PDI) measured from the width of the distribution. Average size in terms of the effective hydrodynamic radius of LUV, PDI of the size distribution and the summary of zeta potential results have been presented in Table 1. It is known that PDI greater than 0.7 usually indicates that the sample is highly polydisperse
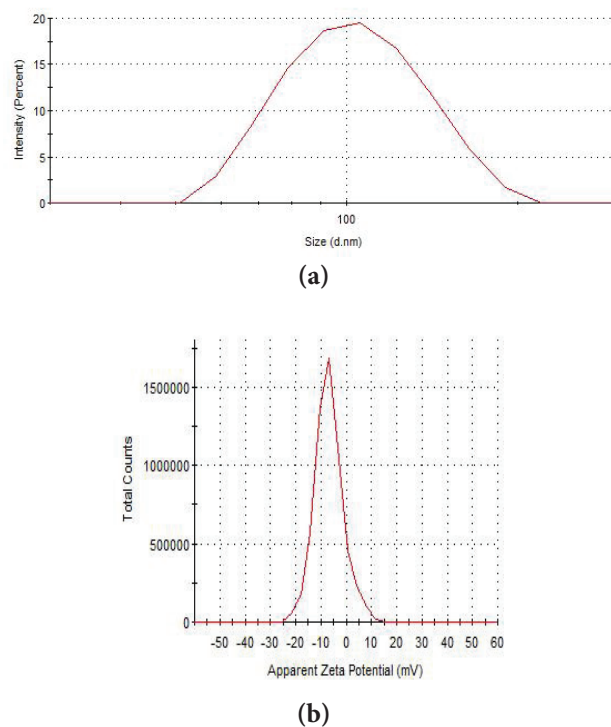
(a)

(b)

Figure 1. **(a)** and **(b)** show size and zeta potential distributions obtained from LUV composed of DOPC. These are captured images from the software provided by Malvern Instrument.

and probably not suitable for the DLS measurement. LUV was found to be stable for several days.

Zeta potential can be used to study the physico-chemical properties of the membranes and it can provide a good approximation of surface potential at low and moderate electrolyte concentrations (<100mM). Detailed studies on zeta potential measurement in the presence of various electrolyte concentrations have been discussed in our previous paper [28]. Although zeta potential usually appears with respect to charged surface, a negative zeta potential

Table 1. Summary of size distribution and zeta potential results. PDI: the polydispersity index. μ: electrophoretic mobility, Q_{eff}: effective elementary charges per vesicle in the unit of electronic charge. Errors are calculated from 3 consecutive measurements. As κ is a function of ionic composition, f(κa) alters significantly [25]. However, in the present experiment, zeta potential was estimated from the Smoluchowski approximation with f(κa) = 1.5

Phospholipids	Size (d nm)	PDI	μ (cm²/Vs) 10⁻⁴	Zeta Potential (mV)	Q_{eff}(e)
DOPC	98 ± 2	0.06	-0.5 ± 0.1	- 6 ± 2	65
DOPC-DOPE (4:1)	99 ± 3	0.07	-1.3 ± 0.1	-16 ± 3	66
DOPC-DOPG(4:1)	98 ± 3	0.06	-4.0 ± 0.2	-52 ± 3	205
DOPE-DOPG (4:1)	100 ± 4	0.10	-4.4 ± 0.2	-56 ± 4	225
DOPG	99 ± 3	0.08	-4.8 ± 0.3	-61 ± 3	245

of neutral DOPC obtained from the experiment is thus intriguing. The orientation of hydration layers of the membranes, head group, water polarization as well as presence of impurity may be the possible origin of non-zero zeta potential in DOPC. The low negative zeta potential of DOPC is consistent for independent measurements of the different batches of the sample. As expected zeta potential for DOPG was found to be ~ - 61 mV. Zeta potential of LUV obtained from a mixture of DOPC-DOPG and DOPE-DOPG was found to decrease, as shown in Table 1. This is expected as the amount of charge decreases in the membrane surface when LUV is prepared from a mixture of charge lipid (DOPG) and neutral lipid (DOPC). Larger zeta potential obtained from DOPC-DOPE mixture as compared to pure DOPC could be a consequence of increasing the rigidity in the presence of DOPE. As the zeta potential is sensitive to pH of the aqueous solution, we have kept the pH fixed at 7.4 for all measurements. DOPE alone cannot form vesicles. This is due to fact that the DOPE head group forms hydrogen bonds with the water molecules making the bilayer very stiff. We have used a mixture of DOPC-DOPE (4:1) to form LUV. Size and zeta potential distributions were found to be very similar to that of DOPC. We have also estimated effective charges per vesicle from the zeta potential (Table -1). This information would be useful in the context of electrostatic behavior of the membranes.

Although LUV can serve as model systems of biological membranes to study the interaction with ions or different bio-molecules, there are few major disadvantages. LUV often displays broad size distribution. Therefore, properties such as permeability, spectra, etc may not be identical for different LUV. Curvature of the membrane also plays an important role in governing lipid packing, phase separation and many other phenomena occurring in the membrane surface. Small sizes LUV possess a high curvature, compared to the much flatter cellular membrane. As LUV cannot be observed under an optical microscope, much information, such as shape deformation or fluctuation, phase separation etc. cannot be visualized directly. We can overcome the above disadvantages, by preparing GUV. In this article, we discuss the preparation of GUV as well as SLB from DOPC only.

After characterizing LUV from DOPC, we have successfully obtained giant unilamellar vesicles from large unilamellar vesicles as shown in Figure 2. Similar results were found for DOPG and DOPC-DOPE mixture also. The present work is an innovative approach of preparing GUV
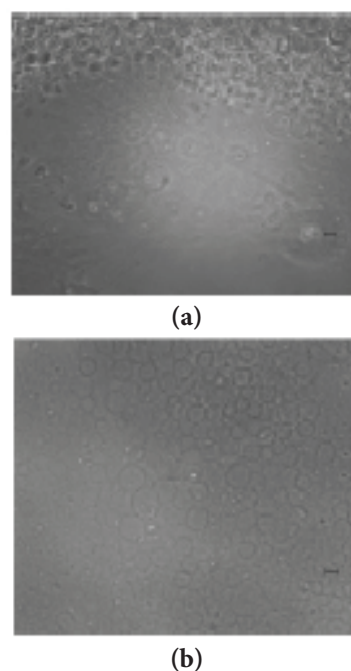

(a)

(b)

Figure 2. Phase contrast micrograph of GUV made from DOPC during their formation from LUV. Fig (a) and (b) show the formation of GUV 10 minutes and one hour later from the application of alternating field, respectively. Images were taken from two different regions of the sample. Scale bar 5 μm.

from LUV using electroformation. Although LUV can be prepared at high salinity and physiologically relevant conditions [28], GUV cannot be obtained in the presence of high salt (>100 mM NaCl) concentrations using conventional parameters (10 Hz, ~700 V/m) of electroformation [29]. Therefore, it is necessary to change the experimental parameters. For example, at 100 mm NaCl, we need to increase the alternating voltage to 1300 V/m and frequency 500 Hz. In the present study, we have not explored the GUV preparation in the presence of salt. It is important to note that the small osmotic stress of the oriented membranes, resulting from LUV deposition, can lead to better yield of electroformation. This is done by controlling the dehydration of aqueous LUV to form oriented membranes on the electrodes, as discussed in the material method section. Concentration of LUV also plays a crucial role in GUV formation process. After evaporation of excess water in LUV deposition, it is necessary to have ~ 50-100 bilayers for optimum yield. It is important to mention that the electric field must be applied as soon as the chamber is filled with aqueous medium to avoid the spontaneous swelling. In the present study, we have not looked at the effect of electroformation parameters on the size distribution of GUV.

However, it is known from the previous literature [26] that by increasing the strength of the electric field slowly and reaching to the maximum value of the electric field after 20 to 30 minutes during the electroformation process one can control the final size of the GUV. This procedure seems to work for any lipid mixture or lipid-cholesterol mixture provided the electroformation chamber is maintained at temperature above the chain melting transition (T_m) of lipid of the highest T_m [30].

There are several advantages of this protocol over conventional electroformation [29]. Once we prepare LUV, in organic solvent such as chloroform will no longer be required. Therefore, the process of preparing a lipid solution and solvent evaporation after coating onto an ITO glass can be avoided. A major advantage of our method is the use of LUV for experiments prior to the preparation of GUV. For example, we have measured size distribution and zeta potential of LUV prepared from charged as well as neutral phospholipid vesicles. In fact, we could study the interaction of various divalent and monovalent ions, drugs, antimicrobial peptide with LUV prior to the preparation of GUV. Therefore, if we prepare GUV from LUV, it would be a good protocol to reconstitute various biomolecules in GUV. This is also useful to envisage the influence of curvature and size on the bilayer properties of the vesicles. It is important to mention that an inappropriate choice of voltage or electrode material could lead to both lipid hydrolysis and oxidation reactions. However, use of ITO glass or platinum electrode did not seem to have such effect on the electroformation.

For electroformation of GUV from lipid deposit on a conducting substrate, it is essential to achieve well oriented and partially dehydrated membrane stacks. LUV deposit seems to provide these conditions much better than lipid deposition through organic solvent, as reported from small angle x-ray scattering [26]. Unlike all previous studies which have used small unilamellar vesicles (SUV) for GUV formation, we have used LUV which is much easier to obtain by extrusion method. Although, previous literatures have discussed similar protocol, they have not presented any characteristic information on SUV [30, 31].This information may be useful when we reconstitute peptide or proteins in GUV to form proteoliposome. Characteristic information on SUV will also help us to decide the lipid compositions to be used in GUV formation. For example the binding affinity of the proteins or peptides to the membranes is necessary to prepare proteoliposome. We have already done some preliminary experiments to show NK-2 (an antimicrobial peptide) has stronger binding affinity to negatively charged membranes (unpublished result). Therefore we have used mixture of DOPC and DOPG to form LUV and hence GUV. This result will be discussed later.

We now discuss the formation of supported bilayer on a mica substrate. Figure 3 describes the AFM images showing the bilayer formation as a function of time. Figure 3 (a). shows the AFM image of virgin mica. When LUV was adhered to the substrate, the lipid bilayer was formed instantly (Figure 3 (b)). We have observed the growth of bilayer on the mica surface with the increase of incubation time (Figure 3c-e). The entire process required about 40 to 60 minutes obtaining the uniform bilayer on the mica substrate. However, bilayer was not formed on the entire mica substrate. The bare regions of mica substrate (black patches) were visible in between the bilayers. We have also shown the height profiles of all AFM images starting from 5 minutes incubation. Height profile of 3.0 ± 0.5 nm clearly indicated the presence of bilayer on the mica substrate which was in agreement with the previous literature [32].

A variety of substrates, such as fused silica, borosilicate glass, mica and oxidized silicon were used for the formation of robust and stable supporting phospholipid bilayers. However, for high quality defect free membrane, the surface must be hydrophilic, smooth, and clean [27]. There are three general methods for the formation of lipid bilayers. First method involves the transfer of bilayer in Langmuir Blodgett (LB) and Langmuir Schaefer (LS) techniques [33]. The second method is the adsorption and fusion of vesicles from an aqueous suspension to the substrate surface [34]. A combination of the above
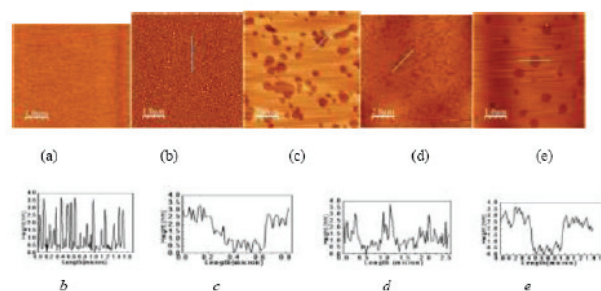

Figure 3. Lipid bilayer formation on mica surface from DOPC LUV. AFM topography of **(a)** virgin mica **(b)** after 5 minutes, **(c)** 15 minutes, **(d)** 30 minutes, **(e)** 45 minutes incubation with LUV. Height profiles of corresponding AFM are shown below the AFM images. All images were taken in contact mode.

two methods can also be used to prepare supported lipid bilayers. We have prepared bilayers by fusion of DOPC vesicles on a mica substrate. The schematic diagram of different steps of vesicle fusion and bilayer formation is shown in Figure 4. The bilayer formation process begins with the adsorption of LUV to the substrate. At the early stages vesicles may deform or fused. Eventually the vesicles rupture and fuse to form supported bilayers. The vesicle fusion method is very useful for the incorporation of membrane protein, whereas LB and LS techniques, it is difficult to transfer protein to the bilayers. Although computer simulations, such as Monte Carlo method, were used to understand the mechanism of the formation of supported bilayers, the exact mechanism of bilayer formation via vesicle fusion is still poorly understood [33].

Here we report an example, how an antimicrobial peptide, NK-2, can be reconstituted in GUV. Figure 5(a) shows GUV prepared from LUV without the presence of NK-2. NK-2 is a highly cationic (+10 at physiological pH) peptide and known to display antimicrobial activity against invading pathogens, such as viruses, fungi, bacteria etc [35]. They target the bacterial membrane, especially negatively charged surface, and create defects, such as pores, leading to disruption of the membrane by targeting the negatively charged bacterial membranes. Therefore, we have chosen LUV composed of DOPC-DOPG mixture to form GUV. In the present method we were able to reconstitute NK-2 in GUV. Interestingly, evidence of pores in GUV can be envisaged from the phase contrast images without introducing any fluorescence probe (Figure 5(b)). Hallow region of the phase contrast image was due to the presence of sucrose in the interior
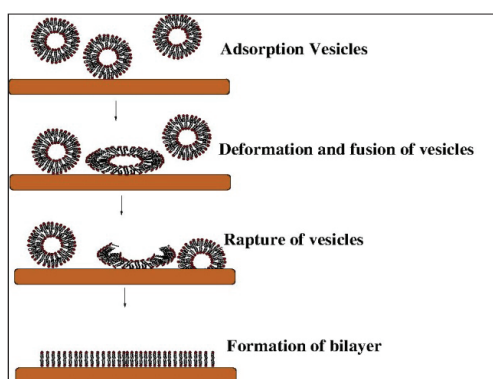

(a)

(b)

Figure 5. A phase contrast micrograph of GUV made from LUV composed of DOPC and DOPG mixture at 4:1. Figs (a) and (b) show GUV in the absence and presence of antimicrobial peptide NK-2, respectively. The size of these GUVS is ~ 20μm.

Figure 4. Schematic diagram of the mechanism for the formation of supported lipid bilayers. Vesicles in solution adsorb and spontaneously fuse to the mica surface to form a solid supported lipid bilayer.
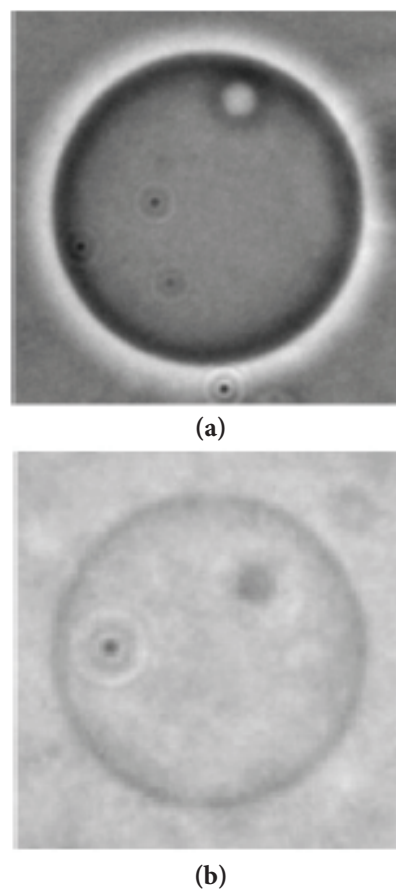
and glucose in the exterior of GUV. In the absence of hallow region in Figure 5(b) exhibits no contrast between the interior and exterior fluids of the membranes. Therefore, it was conceived that there are some pores on the GUV surface induced by NK-2 leading to the exchange of interior and exterior fluids through the pores. This process led to decrease in contrast in the hallow region of the image of GUV. Therefore, the image of GUV in the presence of NK-2 was very similar to the image when GUV were prepared with the aqueous solution and diluted with the same solution.

GUVS are excellent model systems to determine binding and stretching modulus of lipid bilayer using either micropipette aspiration techniques or Fourier analysis of fluctuation spectra. GUVS are also useful to introduce molecules, such as DNA using microinjection techniques.

4. Conclusion

Preparation and characterization of lipid membranes are the key steps for understanding the properties and functions of cellular membrane. In the present study, we have discussed the formation and characterization of phospholipid bilayer, an excellent model system of biological membranes, in the form of LUV, GUV and SLB. We have successfully obtained GUV from LUV using electroformation. We have also measured size distribution and zeta potential of LUV using dynamic light scattering. The several advantages of the present approach to prepare GUV over the conventional electroformation were also discussed. GUV provides the possibility to directly visualize certain interactions in a small but optically resolvable volume encapsulated by the vesicle membrane. We have presented an example, where an antimicrobial peptide NK-2 was reconstituted in GUV prepared from LUV. Formation of SLB was described using AFM study. The present study provided us an important insight into the physico-chemical properties of membranes in terms of their size and geometry. Therefore, GUV and SLB could be excellent and simple model systems whose size, geometry, and composition could be tailored with great precision.

5. Acknowledgment

6. References

1. B. Alberts, D. Bray, J. Lewis, M. Raff, K. Roberts and J. D. Watson, '*Molecular Biology of the Cell*', Garland publishing, Tayor and Francis Group (1994).

2. D. W. Lee, X. Banquy, K. Kristiansen, Y. Kaufman, J. M. Boggs and J. N. Israelachvili, *Prog. Natl. Acad. Sc.*, USA, 111, 768 (2014).

3. R. P. Richter, R. Bérat, and A. R. Brisson, *Langmuir*, 22, 3497 (2006).

4. G. J. Hardy, R. Nayak, S. Zauscher, *Curr.Opin. Coll. Int. Sc.*, 18, 448 (2013).

5. M. Mingeot-Leclercq, M. Deleu, R. Brasseur and Y. F Dufrêne, *Nature Protocols*, 3, 1654 (2008).

6. D. E. Discher and A. Eisenberg, *Science*, 297, 967 (2002).

7. J. R. Howse, R. A. L. Jones, G. Battaglia, R. E. Ducker, G. J. Leget and A. J. Ryan, *Nature Materials*, 8, 507 (2009).

8. S. F. Fenz, K. Sengupta, *Integr. Biol.*, 4, 982 (2012).

9. R. Dimova, S. Aranda, N. Bezlyepkina, V. Nikolov, K. A. Riske and R. Lipowsky and J. *Phys: Condens. Matter,* 18, S1151 (2006).

10. P. Walde, K. Cosentino, H. Engel and P. Stano, *Chem. Bio. Chem.*, 11, 848 (2010).

11. S. Galdiero, A. Falanga, M. Cantisani, M. Vitiello, G. Morelli and M. Galdiero, *Int. J. Mol. Sci.*, 14, 18758 (2013).

12. K. A. Brogden, *Nature*, 4, 238 (2005).

13. S. Karmakar and V. A. Raghunathan, *Physics Express,* 4,6 (2014).

14. S. Karmakar and V. A. Raghunathan, *Phys. Rev. Lett.*, 91, 098102 (2003).

15. Fischer, A. Franco and T. Oberholzer, *Chem. Bio.Chem.,* 3, 409 (2002).

16. J. B. Song, L. Cheng, A. P. Lin, J. Yin, M. Kuang and H. W. Duan, *J. Am. Chem. Soc.,* 133, 10760 (2011).

17. P. Yang and R. Dimova. *Biomimetic Based Application*, Edited by A Georg, In Tech, 523 (2011).

18. Y. Li, R. Lipowsky and R. Dimova, *J. Am. Chem. Soc.,* 130, 12252 (2008).

19. M. N. Holme, I. A. Fedotenko, D. Abegg, J. Althaus, L. Babel, F. Favarger, R. Reiter, R. Tanasescu, P.L Zaffalon, A. Ziegler, B. Muller, T. Saxer and A. Zumbluehl, *Nature Nanotech*, 7, 536 (2012).

20. V. P. Torchilin, *Nature Rv. Drug. Discov.*, 4, 145 (2005).

21. F. M. Menger and K. D. Galrielson, *Angew Chem. Ed. Engl.,* 34, 2091(1995).

22. M. I. Angelova, S. Soleau, Phmeleard, J. F. Faucon and P. Bothorel, *Progr. Coll. Pol. Sci.,* 89, 127 (1992).

23. M. J. Hope, M. B. Bally, W. Webb and P. R. Cullis, *Biochim. Biophys. Acta*, 812, 55 (1985).

24. R. Hunter, *Zeta potential in colloid Science*, Academic Press, New York (1981).

25. B. Klaszyk, V. Knecht, R. Lipowsky and R. Dimova, *Langmuir,* 26, 18951 (2010).

26. T. Pott, H. Baurrais, and P. Meleard. *Chem. phys. Lipids,* 154, 115 (2008).

27. C. Scomparin, S. Lecuyer, M. Ferreira, T. Charitat and B. Tinland. *Eur. Phys. J. E.*, 28, 211(2009).

28. P. Maity, B. Saha, G. Suresh Kumar, S. Karmakar, *Biochim. Biophys. Acta,* 1858, 706 (2016)

29. M. I. Angelova, S. Soleau, P. Meleard, J.F Faucon and P. Bothorel, *Prog. Colloid Polym. Sci.*, 89, 127 (1992).

30. T. Bhatia, P. Husen, J. Brewer, L. A. Bagatolli and P. L. Hansen, *Biochim. Biophys. Acta.*, 1848, 3175 (2015).

31. P. Meleard, L. A. Bagatolli, T. Pott, *Methods Enzymol.*, 465, 161 (2009).

32. W. Hanke, W. R. Schulue, '*Planar Lipid Bilayers: Methods and Applications*', Academic Press (2012).

33. L. K. Tamm and H. M. McConnell, *Biophys. J.*, 47, 105 (1985).

34. E. Kalb, S. Frey and L. K. Tamm, *Biochim. Biophys. Acta*, 1103, 307 (1992).

35. M. Zasloff, *Nature*, 415, 389 (2002).